CHARACTERIZATION OF THE CATALYTIC MECHANISMS OF 'ESCHERICHIA COLI' FUMARATE REDUCTASE AND UBIQUINAL OXIDASE CYTOCHROME-BD

Alan Donaldson Moodie

A Thesis Submitted for the Degree of PhD
at the
University of St Andrews

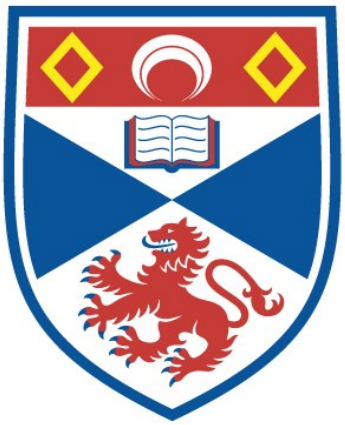

1991

Characterization of the Catalytic Mechanisms of *Escherichia coli* Fumarate Reductase and Ubiquinol Oxidase Cytochrome-*bd*

Alan Donaldson Moodie

1990

University of St.Andrews,
Department of Biochemistry and Microbiology,
North Street,
ST. ANDREWS,
Fife,
U.K.

DECLARATION

I Alan Donaldson Moodie hereby certify that this thesis has been composed by myself, that it is a record of my own work, and that it has not been accepted in partial or complete fulfilment of any other degree of professional qualification.

Signed ..... Date 7/6/90

I was admitted to the Faculty of Science of the University of St.Andrews under Ordinance General No. 12 in January 1987, and as a candidate for the degree of Ph.D. in October 1987.

Signed ..... Date 7/6/90

CERTIFICATE

I Dr.W.J. Ingledew hereby certify that the candidate has fulfilled the conditions of the Resolution and Regulations appropriate to the Degree of Ph.D.

Signature of Supervisor..... Date.....

COPYRIGHT DECLARATION

In submitting this thesis to the University of St.Andrews I understand that I am giving permission for it to be made available for use in accordance with the regulations of the University Library for the time being in force, subject to any copyright vested in the work not being affected thereby. I also understand that the title and abstract will be published, and that a copy of the work may be made and supplied to any bona fide library or research worker.

ACKNOWLEDGEMENTS

I would like to thank my supervisor W. John Ingledew for his help and guidance throughout my period of study in St. Andrews. Thanks are also due to Richard A. Rothery, Mark Bacon, John C. Salerno and Bob Mitchell for many helpful discussions, and to Alex Houston for technical assistance. I would also like to thank Jackie for her support and understanding throughout my time in St. Andrews.

ABSTRACT

Escherichia coli respiratory enzymes fumarate reductase and ubiquinol-oxygen oxido-reductase cytochrome-*bd* have been investigated with the aim of determining their catalytic mechanisms.

A rapid-freeze quench apparatus was developed for discontinuous pre-steady state spectral analysis of fumarate reductase prosthetic group electron transfer. The ram system includes the application of stainless steel HPLC parts for mixing. The novel feature of the apparatus is the cryostat which is safer and more convenient to use than its predecessors. The cryostat was designed for application to electron paramagnetic resonance studies but could easily be modified for use with other spectroscopic techniques. Test reactions determined the resolution of the apparatus in the low millisecond range.

Reduction/oxidation events for the iron-sulphur centres FR1 and FR3 of fumarate reductase were not kinetically resolved in the low millisecond range (internal equilibration rapid). From data presented, FR1 and FR3 are thought to be kinetically competent for the predicted maximum turnover of the fumarate reductase benzyl viologen assay ($30s^{-1}$, Simpkin, 1985). E.p.r. signals for FR2, the low potential iron-sulphur centre, were not observed in the pre-steady state or steady state and the role of this centre

in electron transfer remains ambiguous. The data is consistent with a sequential model of electron transfer from menaquinol----->FR3----->FR1----->flavin----->fumarate. A dual, high potential/low potential, pathway for fumarate reductase (Cammack *et al.*, 1986a,b) is not consistent with available data.

Ligand binding studies for cytochrome-*bd* demonstrate carbon monoxide and nitric oxide ligation to both haem-d and haem-b595. Photodissociation affects for the carbon monoxide inhibited oxidase (oxygen electrode) and time dependent haem-NO formation (optical and e.p.r.), suggest a bimetallic site with two haems in close proximity. The catalytic mechanism for dioxygen reduction is proposed as a single dioxygen ligation between haem-b595 and haem-d with subsequent reduction by haem-b558 and quinol. A stabilized (bound) semiquinone in close proximity to haem-b558 is also detected.

CONTENTS

Chapter 1

Chapter 2

Chapter 3

Chapter 4

Chapter 5

Chapter 6

ABBREVIATIONS

ATP -adenosine 5'triphosphate

BES -N,N-bis[2-Hydroxyethyl]-2-aminoethanesulphonic acid

DNP -2,4-dinitrophenol

EDTA -ethylenediaminetetraacetic acid (disodium salt)

E.p.r. -electron paramagnetic resonance

etp -electron transport particle (membrane preparation)

EXAFS -extended X-ray absorption fine structure

FAD -flavin adenine dinucleotide

FR -fumarate reductase

FR1, FR2, FR3 -iron-sulphur clusters of fumarate reductase

HOQNO -2-n-heptyl-4-hydroxyquinoline N-oxide

MES -2-[N-Morpholino]ethanesulphonic acid

MQ -menaquinone

NADH -nicotinamide adenine dinucleotide (reduced)

Q -quinone

Δp -proton gradient

$\Delta\mu_{H^+}$ -proton-electrochemical gradient

SDH -succinate dehydrogenase

S1, S2, S3 -iron-sulphur clusters of succinate dehydrogenase

SDS -sodium dodecyl sulphate

TE -tris-EDTA buffer

TES -(N-tris[Hydroxymethyl]methyl-2-aminoethanesulphonic acid

Tris -tris(hydroxymethyl)aminomethane

TTFA -thenoyl trifluoroacetone

Chapter 1

GENERAL INTRODUCTION

Chapter 1

1.1. Preface.

This work concentrates on the biophysical characterization of *Escherichia coli* respiratory enzymes fumarate reductase and the ubiquinol-oxygen oxido-reductase cytochrome-*bd*; both of these enzymes catalyze terminal electron reductions for respiration, fumarate reductase reducing fumarate to succinate in a two-electron transfer and cytochrome-*bd* reducing dioxygen to water in a four-electron transfer. The relative advantages and limitations of growth, anaerobically with fumarate or utilizing oxygen, have been discussed (Moodie and Ingledew, 1990).

The aim herein was to test presently proposed model systems for catalysis in these enzyme systems and stress thermodynamic and kinetic limitations for these models with a view to presenting improved models.

Fumarate reductase was last extensively reviewed in 1984 and 1985 (Ingledew and Poole, 1984; Cole *et al.*, 1985) concentrating mainly on the genetic and structural aspects of the enzyme. The biophysical aspects of the enzyme, identification and characterization of the prosthetic groups, have not been recently reviewed. Section 1.2. is an introduction to fumarate reductase concentrating on the biophysical characterization of the enzyme in relation to structural data. Section 1.3. outlines the rapid-freeze quench technique to be used when studying fumarate reductase (chapters 3 & 4), and briefly gives an overview of this

technique and its contributions to our present understanding of some of the classic electron transfer complexes.

Cytochrome-*bd* has been extensively reviewed (Poole and Ingledew, 1987; Anraku and Gennis, 1987; Rothery, 1989) and so only a brief introduction to this oxidase will be given (Section 1.4.). Sections on carbon monoxide and nitric oxide binding to haem centres are reviewed as an introduction to chapters 5 and 6, respectively. The final chapter of this thesis correlates the available data to present models for electron transfer and catalysis in fumarate reductase and cytochrome-*bd*.

1.2. Escherichia coli Fumarate Reductase.

1.2.1. The enzyme.

Escherichia coli, when grown under anaerobic conditions using a non-fermentable substrate and fumarate as electron acceptor, produces fumarate reductase (FR) as the terminal respiratory enzyme (Spencer and Guest, 1973). This enzyme *in vivo* catalyses the two electron reduction of fumarate to succinate:

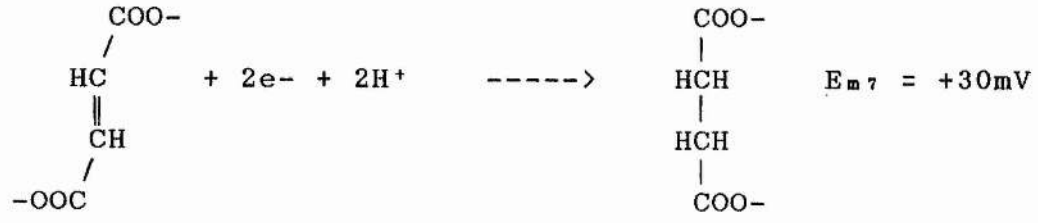

From the Nernst equation the reaction has a pH dependence of 59mV per pH unit. The major dehydrogenases utilized by fumarate reductase are those for formate, NADH, lactate and α-glycerophosphate (Ingledew, 1983). Genetic control of fumarate reductase production, under anaerobic growth conditions, is at the transcriptional level via an *fnr* gene product acting on the *frd* gene for fumarate reductase expression (Jones and Gunsalus, 1987). Fumarate reductase is membrane bound but not proton translocating, $\Delta\mu_{H^+}$ (proton electrochemical gradient) and therefore ATP synthesis and growth is supported at a dehydrogenase proton translocating site (site 1) (Hellingwerf *et al.*, 1981; Gutowski and Rosenberg, 1976, 1977). Miki and Lin (1973, 1975) have shown ATP synthesis and generation of Δp (proton gradient) to be coupled to glycerol 3-phosphate oxidation (fumarate reduction). Glycerol 3-phosphate dehydrogenase has a cytoplasmic catalytic site and does not generate protons in the periplasm (not proton translocating). There is therefore a discrepancy as to how Δp is generated in this case (see later). Succinate dehydrogenase (SDH), catalysing the reverse reaction of the above couple, is closely related to fumarate reductase in subunit number, molecular weight and prosthetic group composition (Fig. 1.1). However, the two enzymes are genetically distinct, with the fumarate reductase operon at minute 94 of the *E. coli* genomic map (Hirsch *et al.*, 1963; Spencer and Guest, 1973; Guest and Nice, 1978) and the succinate dehydrogenase operon at minute 16 (Spencer and Guest, 1982). Succinate dehydrogenase

Figure 1.1

A schematic representation of fumarate reductase in the membrane.

The four-subunit holoenzyme, as it is thought to be arranged in the membrane, is presented. The catalytic A + B subunits have a cytoplasmic aspect and are anchored to the membrane by the C + D subunits. The prosthetic groups, FAD and the three iron-sulphur clusters, are shown in their respective subunits (see Simpkin, 1985). Dimensions were obtained from electron microscopy studies (Lemire *et al.*, 1983). MQ is menaquinone within the membrane bilayer.

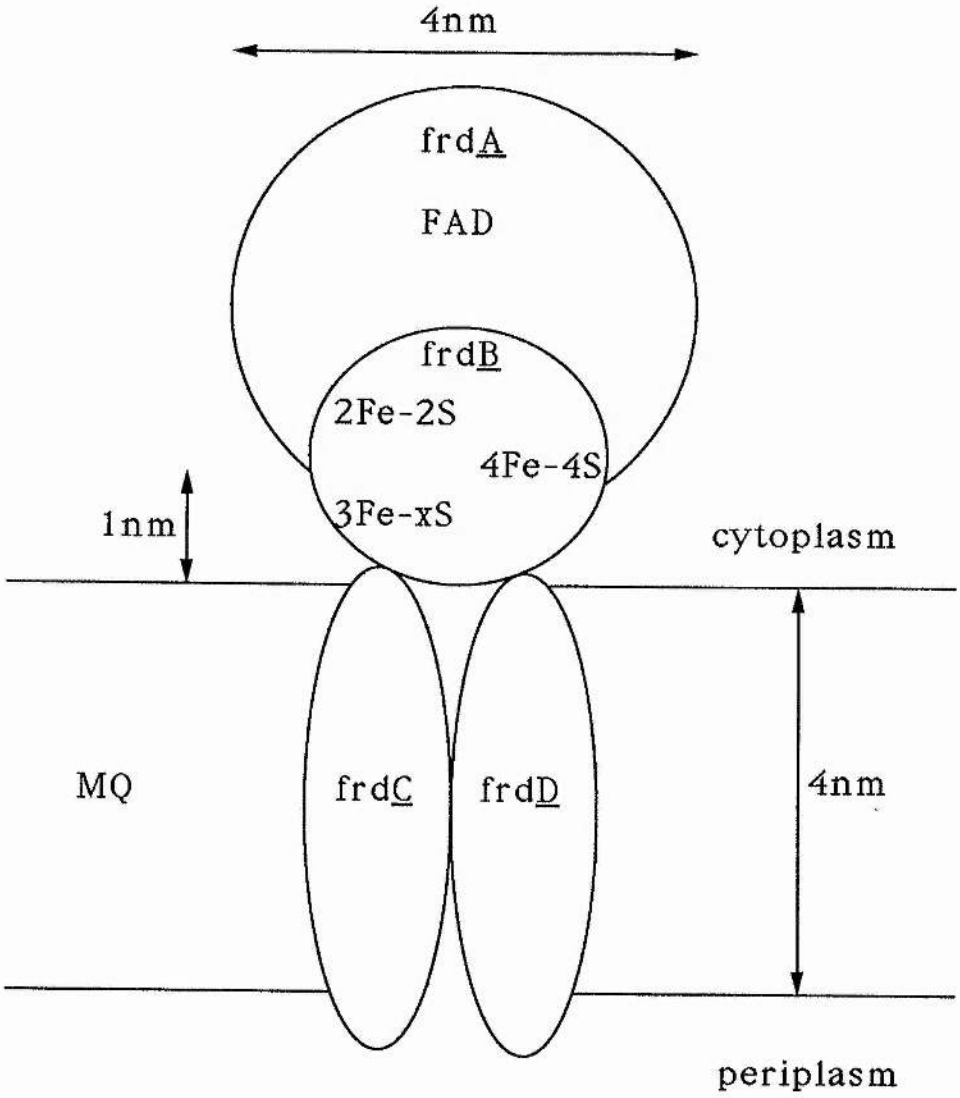
4nm
frdA
FAD
frdB
2Fe-2S
4Fe-4S
3Fe-xS
1nm
cytoplasm
MQ
frdC
frdD
4nm
periplasm

synthesis in *E. coli* is promoted by aerobic growth but repressed under anaerobic conditions. This is the reverse of fumarate reductase control where synthesis is repressed by aerobic growth, or anaerobically in the presence of nitrate, but expressed anaerobically in the presence of fumarate (Iuchi *et al.*, 1986; Cole and Guest, 1979a). Fumarate reductase and succinate dehydrogenase can catalyse the fumarate/succinate couple in either direction (Dickie and Weiner, 1979; Robinson and Weiner, 1981; Hirsch *et al.*, 1963). The enzymes can substitute for each other depending on enforced conditions (Guest, 1981). Fumarate and succinate are cytoplasmic substrates transported across the cell membrane by C_4-dicarboxylic acid carriers (Kay and Kornberg, 1971). These carriers are rate limiting for whole cell fumarate reductase activity in strains overproducing fumarate reductase, but are not rate limiting for wild-type levels of the enzyme (Simpkin and Ingledew, 1984). Within the respiratory chain the direct electron donor for fumarate reductase is menaquinol-8 (E_{m7}=-74mV) (Guest, 1977) whereas the electron acceptor for succinate dehydrogenase is ubiquinone-8 (E_{m7}=+65mV); the quinone species present being dependent on growth conditions (Ingledew and Poole, 1984).

Both enzymes are flavo-iron-sulphur proteins consisting of four nonidentical subunits. The fumarate reductase operon has a promoter/operator region, four cistrons, *frd*A,B,C and D, and a transcriptional terminator. *Frd*A encodes subunit A (MW 69000) containing 602 amino acids, this subunit also binds the single flavin

(8α-[N(3)-histidyl]FAD) group which is the active site for fumarate (Weiner and Dickie, 1979; Cole, 1982). *Frd*B encodes subunit B (MW 27000), 244 amino acids (Cole *et al.*, 1982), this subunit contains three iron sulphur clusters FR1, FR2 and FR3 (Ingledew, 1983). These clusters were later characterised by various research groups as FR1 a $[2Fe\text{-}2S]^{+1,+2}$ centre (Ingledew, 1983; Johnson *et al.*, 1985; Simpkin and Ingledew, 1985), FR2 a $[4Fe\text{-}4S]^{+1,+2}$ centre (Johnson *et al.*, 1985a; Cammack *et al.*, 1986b) and FR3 a $[3Fe\text{-}xS]^{0,+1}$ centre (where x is probably equal to 4). The determination of FR3 as a 3Fe and not a 4Fe cluster (as originally thought) involved the accumulated data of various biophysical techniques including electron paramagnetic resonance (e.p.r.) spectroscopy, magnetic circular dichroism (MCD), electron spin-echo envelope modulation (ESEEM), and linear electric field effect e.p.r. (LEFE-EPR) (Johnson *et al.*, 1985a; Morningstar *et al.*, 1985; Cammack *et al.*, 1988; Johnson *et al.*, 1988). FR1 and FR2 are paramagnetic (and e.p.r. detectable) in the reduced 1+ state (Johnson *et al.*, 1985b). In FR1 the 2Fe's are antiferromagnetically coupled as +2 and +3 (S=1/2 reduced, S=0 oxidised) giving the classic [2Fe-2S] g-values of $2.03g_z$ and $1.94g_{xy}$ peak with a trough at 1.92 (Fig.1.2). FR2 has 4Fe's coupled to give a net S=1/2 with this e.p.r. signal showing as an increase in signal height at g_{av}=1.94 (see later) and additional wings in the spectra at 2.19, 2.06, 1.82 and 1.65 (Fig.1.2). FR3 is paramagnetic and e.p.r. detectable in the oxidised 1+ state (S=1/2) (peak at g=2.012, Fig.1.2) but e.p.r. silent

Figure 1.2

Electron paramagnetic resonance spectra of the three iron-sulphur clusters of Escherichia coli fumarate reductase.

The upper spectra show the dithionite reduced spectra (FR1 + FR2) of a membrane preparation (strain HB101/pFRD84, 28mg.ml^{-1}, 50mM BES, 5mM EDTA, pH7.0). The g-values are shown above the spectra. The gain required to observe the winged features of the spectra are shown to the side of each of the upper spectra. E.p.r. conditions were: temperature, 10K; microwave power, 6.9mW; modulation amplitude, 0.2mT. The lower spectra gives the peroxide oxidized spectra (FR3) of membranes under the same e.p.r. conditions. The g-value assignments are explained in the text.

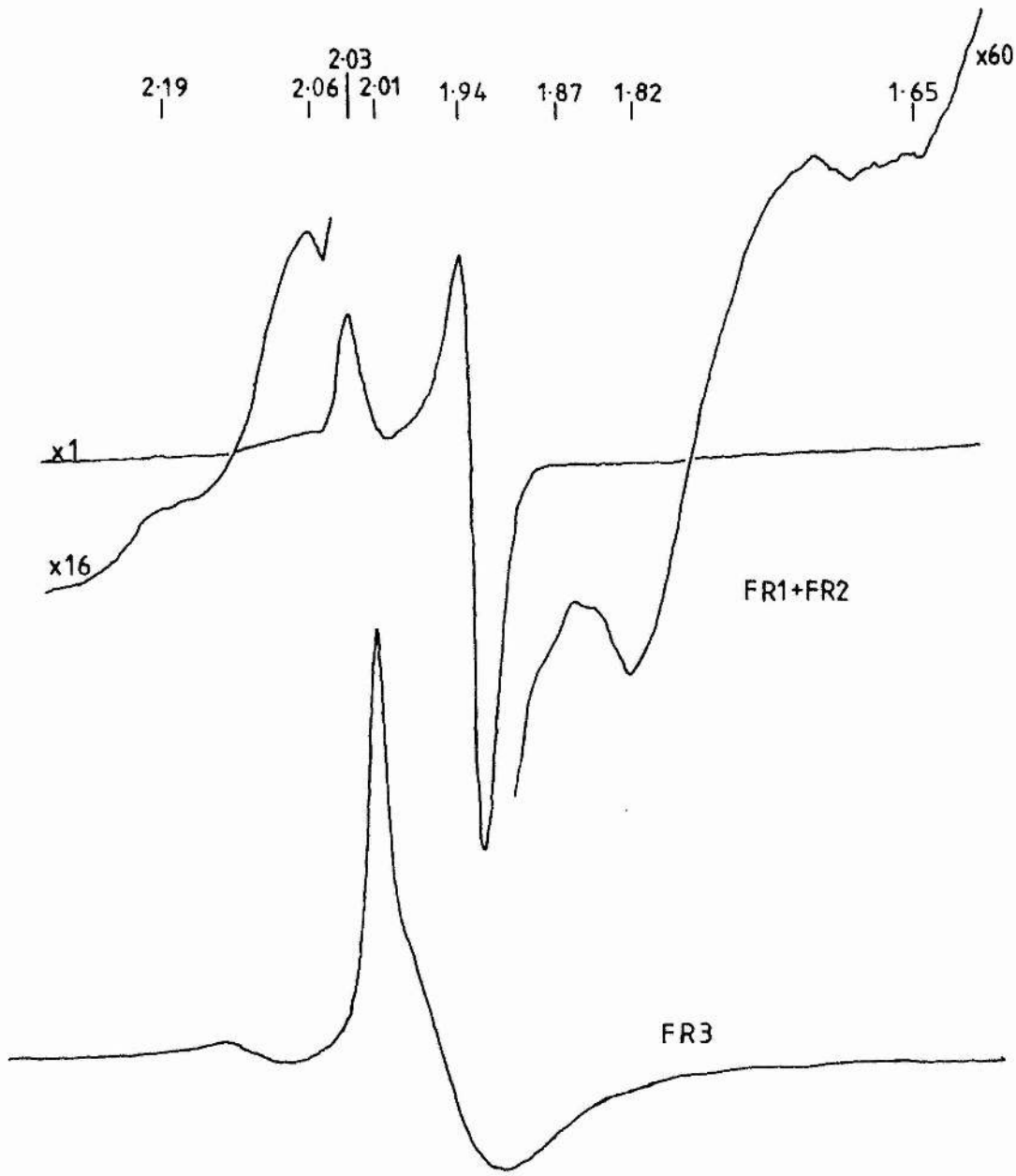
2·03
2·19
2·06
2·01
1·94
1·87
1·82
1·65
x60
x1
x16
FR1+FR2
FR3

in the reduced but paramagnetic S=2 ground state. The FR3 e.p.r. signal (air or peroxide oxidized) and FR2 wings (dithionite reduced) are only observed at low temperatures (<20K). FR1 unlike FR2 can be reduced by physiological substrates and is more easily saturated than either FR2 or FR3, giving maximal e.p.r. signals at around 30K.

The fumarate reductase and succinate dehydrogenase enzymes are unique in having one each of the three types of iron-sulphur centres. They are ligated by cysteine residues. The prosthetic groups FR1, FR2, FR3 and flavin are present in 1:1:1:1 ratios in the holoenzyme (Simpkin, 1985; Johnson *et al.*, 1985a,b; Morningstar *et al.*, 1985; Johnson *et al.*, 1988). Subunits C and D of fumarate reductase (MW 15000 and 13000 respectively) encoded by *frd*C and D contain no reported prosthetic groups but act to anchor the catalytic A and B subunits to the cytoplasmic aspect of the membrane. These subunits span the membrane and are hydrophobic with relatively basic amino acids (Lemire *et al.*, 1982; Van der Plas *et al.*, 1983). Both of the anchor subunits are required in a 1:1 ratio if the catalytic subunits are to bind (Cecchini *et al.*, 1986; Latour and Weiner, 1987; Condon and Weiner, 1988). The anchor proteins are assembled into the membrane before the catalytic domain is added (D.J.Latour and J.H.Weiner, personal communications).

Electron microscopy studies for fumarate reductase-overproducing strains have shown the catalytic A and B subunits to be cytoplasmic and bound to the anchor subunits (Lemire *et al.*, 1983) (as shown in Fig.1.1).

Subunit A appears as a knob like structure of 4nm diameter attached to the membrane via a short stalk, presumably subunit B, of approximately 1nm. Chymotrypsin treatment of the membrane removes the 69000 subunit leaving only the iron-sulphur B subunit bound to the membrane subunits. Both catalytic subunits can be stripped from the anchor subunits with 6M urea. These stripped membranes can be reconstituted to form the membrane bound holoenzyme by adding back the purified two subunit complex (A+B) (but not the denatured urea stripped A and B subunits) (Lemire *et al.*, 1983; Dickie and Weiner, 1979). This selective removal of subunits can give flexibility to the composition of the enzyme studied.

The electron microscopy study of Lemire *et al.* (1983) observed helical tubule formations of fumarate reductase in the cytoplasm, these occur when the membrane becomes saturated with fumarate reductase. Elmes *et al.* (1986) showed the tubule formations to have a lower lipid/protein ratio than the cytoplasmic membrane with fumarate reductase accounting for 90% of the tubule protein; the cytoplasmic membrane increases the total amount of lipid to maintain the same lipid/protein ratio (Weiner *et al.*, 1984). The cytoplasmic tubules are linear cylinders covered with 5nm spherical proteins in a regular helical arrangement of 10 units per turn. The anchor proteins are buried in the tubule lipid with the catalytic subunits protruding at the surface, subunit ratios are as for the membrane bound enzyme at 1:1:1:1. The helical structure of the tubules is due to a direct association with amplified levels of cardiolipin

compared to wild-type (Elmes *et al.*, 1986). The tubules formed by the strain carrying the multicopy plasmid are more stable than the tandem duplication ampicillin hyperresistant mutant (see later) (Cole and Guest, 1979a), although cardiolipin levels are high in both strains. The reason for this variation in stability between overproducing strains is not known. Membrane saturation by fumarate reductase is reached when the membrane protein doubles compared to wild-type and approximately 50% of the protein is fumarate reductase (Weiner *et al.*, 1984). Fumarate reductase amplification does not diminish the levels of other membrane bound proteins. Amplified strains of *E. coli* give fumarate reductase specific activities 30-40 times that of wild-type (approximately 10μmol fumarate reduced.mg protein^{-1}.min^{-1} compared to approximately 0.3μmol fumarate reduced.mg protein^{-1}.min^{-1} for electron transport particles after anaerobic growth in the presence of fumarate (Simpkin, 1985; Cole *et al.*, 1985).

Escherichia coli succinate dehydrogenase also contains subunits A, B, C, and D in 1:1:1:1 ratio with molecular weights of 71,000, 26,000, 17,000 and 15,000 respectively; these subunits are encoded by the *sdh* gene region in the order C,D,A, then B (Condon *et al.*, 1985). The succinate dehydrogenase catalytic subunits (A+B) have a large degree of sequence homology with fumarate reductase but the two sets of hydrophobic anchor proteins show little sequence homology (Wood *et al.*, 1984). Succinate dehydrogenase has recently been amplified in *E. coli* to at

least 6 times the level of wild-type strains by inserting the *sdh* gene region in a low-copy plasmid (Kita *et al.*, 1989). Succinate dehydrogenase contains the same prosthetic group types as reported above for fumarate reductase but in addition a *b*-type haem has been identified in the anchor protein subunits. No *b*-type cytochrome has been identified for fumarate reductase in *E. coli* although there are reports of cytochrome affiliation in the fumarate reductases of *Bacillus subtilis* and *Wollinella succinogenes* (Hederstedt *et al.*, 1987; Unden and Kroger, 1981). A point mutation in the His-82 (—>arg) of *E. coli* fumarate reductase subunit C prevents transfer of electrons from quinones to fumarate, this may be due to a lack of a *b*-type cytochrome if this histidine is acting as one of the 5th or 6th coordinate ligands for the cytochrome or it may be due to a structural change at the quinol binding site (Weiner *et al.*, 1986). Possibly the use of amplified fumarate reductase strains has not facilitated the identification of the *b*-cytochrome if haem synthesis or insertion cannot be maintained at the high level necessary to bind all of the fumarate reductase. Succinate dehydrogenase of *Bacillus subtilis*, beef heart mitochondria and *E. coli* have similar subunit compositions with *b*-type cytochrome association (Hederstedt *et al.*, 1979; and as reviewed by Hederstedt and Rutberg, 1981). The *E. coli* succinate dehydrogenase *b*-cytochrome has been identified as b_{556} and is part of the succinate dehydrogenase operon encoded by *sdh*C (Murakami *et al.*, 1985).

In *E. coli* fumarate reductase the identified prosthetic groups FR1, FR2 and FR3 have reported pH7.0 midpoint potentials of -50mV (-20mV), -285mV (-320mV) and -50mV (-70mV) respectively (Simpkin and Ingledew, 1985; and in brackets Cammack *et al.*, 1986b) with succinate dehydrogenase S1, S2 and S3 at +10mV, -175mV and +65mV respectively (Condon *et al.*, 1985). The mitochondrial E_{m7} values for S1, S2 and S3 are 0mV, -260mV and +60mV, respectively (Ohnishi *et al.*, 1976a,b). The flavin in fumarate reductase has a reported midpoint potential for its two-electron transfer of -12mV by e.p.r. redox titration (Simpkin,D., Moodie,A.D., Salerno,J.C. and Ingledew,W.J., 1990, submitted) and -55mV by substrate studies with the inhibitor oxaloacetate (Ackrell *et al.*, 1989). Mitochondrial succinate dehydrogenase flavin has a midpoint potential of -79mV (Ohnishi *et al.*, 1981), the midpoint potential of *E. coli* succinate dehydrogenase flavin has not been determined. The difference in midpoint potentials between fumarate reductase and succinate dehydrogenase prosthetic groups is probably a functional one.

The FR3 and S3 clusters have, as mentioned above, different donor acceptors in the form of menaquinone and ubiquinone, respectively. The electron donor to FR3 is probably through direct interaction with menaquinol (E_{m7}=-74mV) i.e. a positive redox drop to FR3. The electron acceptor for S3, ubiquinone has a midpoint potential in the same potential region as S3 if the mitochondrial value of +110mV for Q is taken (Salerno and Ohnishi, 1980). The

b-type cytochrome in mitochondrial succinate dehydrogenase has a midpoint potential of -185mV (Yu *et al.*, 1987), this cytochrome, not S3, may be the direct electron donor to ubiquinone although its low potential means it is difficult to reduce with succinate. Interestingly, the b-type cytochrome of *E. coli* succinate dehydrogenase has a much higher midpoint potential (E_{m7}=+36mV) and is reduced by succinate (Kita *et al.*, 1989).

Fig.1.3 illustrates the currently proposed mechanism for fumarate reductase (Fig.1.3a) and succinate dehydrogenase (Fig.1.3b) internal electron transfer (Cammack *et al.*, 1986a,b). This model is not based on available e.p.r. data for the redox state of the centres but on midpoint potential values. The model is most easily explained by considering the succinate dehydrogenase model (Fig.1.3b) and comparing with the dehydrogenase function of the reductase. For this condition, in the presence of succinate, S1, S3 and flavin are all reduced as found from e.p.r. data (FR1, FR3, and flavin for fumarate reductase). If an electron is to be transfered to the semiquinone ($QH\cdot$) then the quinone (Q) must first have been reduced by the *b*-type cytochrome; this quinone cannot be reduced if the reduced flavin ($FADH_2$) cannot first reduce the high potential pathway then reduce the low potential pathway (S2 and cytochrome-*b*), S1 and S3, however, are already reduced! (consult Fig.1.3). In Fig.1.4 an electron pocket arrangement of the proposed model would fail to be primed, even ignoring the available e.p.r. data, this is because S1 must first be

Figure 1.3

Models previously proposed for fumarate reductase and Succinate dehydrogenase (Cammack et al., 1986a,b).

a) The high potential / low potential pathways for *E. coli* fumarate reductase are presented with midpoint potential values taken from the work of Ingledew and co-workers (see text). The transfer of reducing equivalents from menaquinol (MQH_2, menaquinone-8) through the iron-sulphur centres (FR1, FR2 and FR3) and an, as yet, unidentified *b*-type cytochrome to flavin (FAD), and eventually fumarate, involves transfer of electrons through all centres shown. The menaquinone and flavin free radicals are shown as the neutral species.
b) The equivalent model presented for mitochondrial succinate dehydrogenase is shown. The electron transfer direction is the reverse of fumarate reductase. The iron-sulphur centres S1, S2 and S3 with the positively identified *b*-type cytochrome are shown. Midpoint potentials are taken from Ohnishi *et al.*, 1976a,b, 1981 and Salerno & Ohnishi, 1980.

The catalytic cycle for these models are explained in the text.

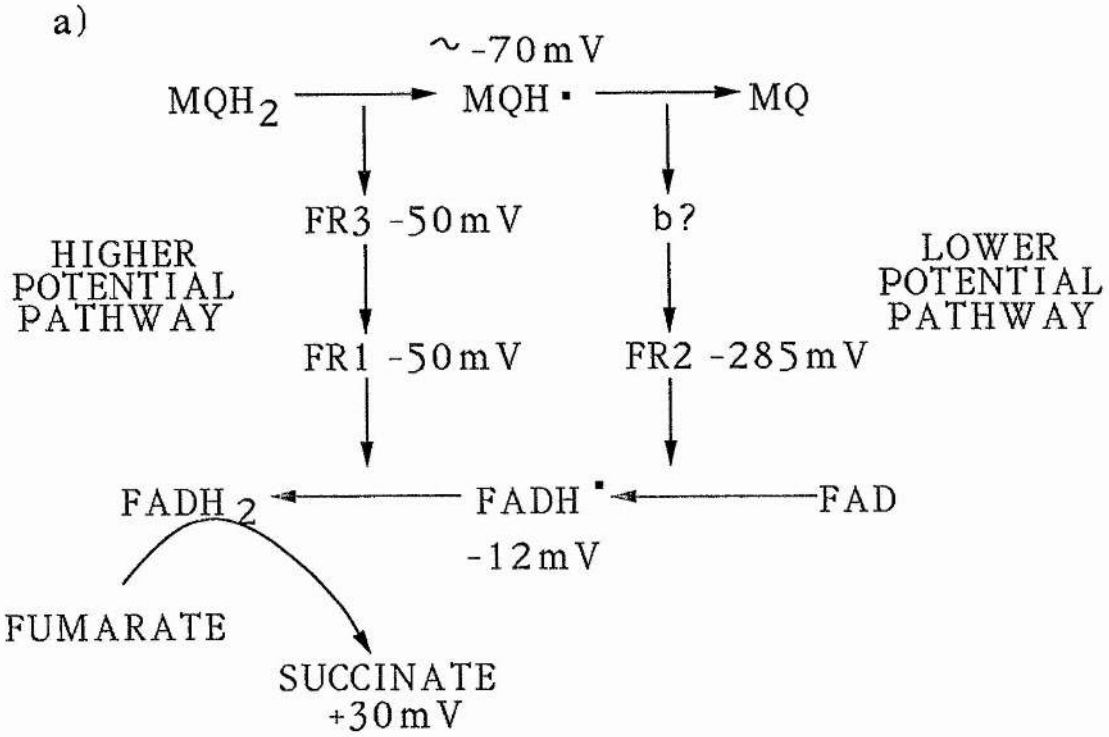
a)
~ -70mV
MQH2
MQH·
MQ
FR3 -50mV
b?
HIGHER POTENTIAL PATHWAY
LOWER POTENTIAL PATHWAY
FR1 -50mV
FR2 -285mV
FADH2
FADH·
FAD
-12mV
FUMARATE
SUCCINATE
+30mV

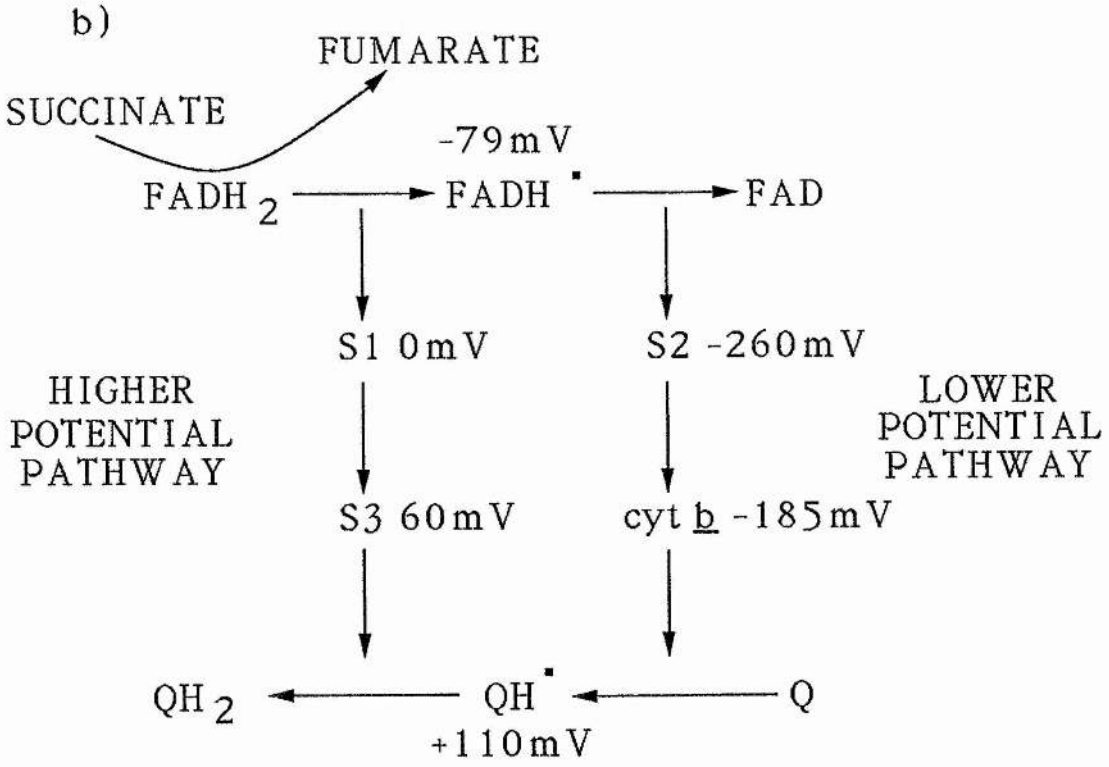
b)
FUMARATE
SUCCINATE
-79mV
FADH2
FADH·
FAD
S1 0mV
S2 -260mV
HIGHER POTENTIAL PATHWAY
LOWER POTENTIAL PATHWAY
S3 60mV
cyt b -185mV
QH2
QH·
Q
+110mV

Figure 1.4

Electron pocket arrangement of Figure 1.3.

An electron pocket diagram of the proposed succinate dehydrogenase model is presented. The arrangement shows electron transfer through the enzyme in eight individual steps. Reduced centres are shown with star symbols (*). Reduction of quinone (Q) at steps 7 and 8 can be followed from step 1. The system will turnover assuming S1 is initially reduced (as shown).

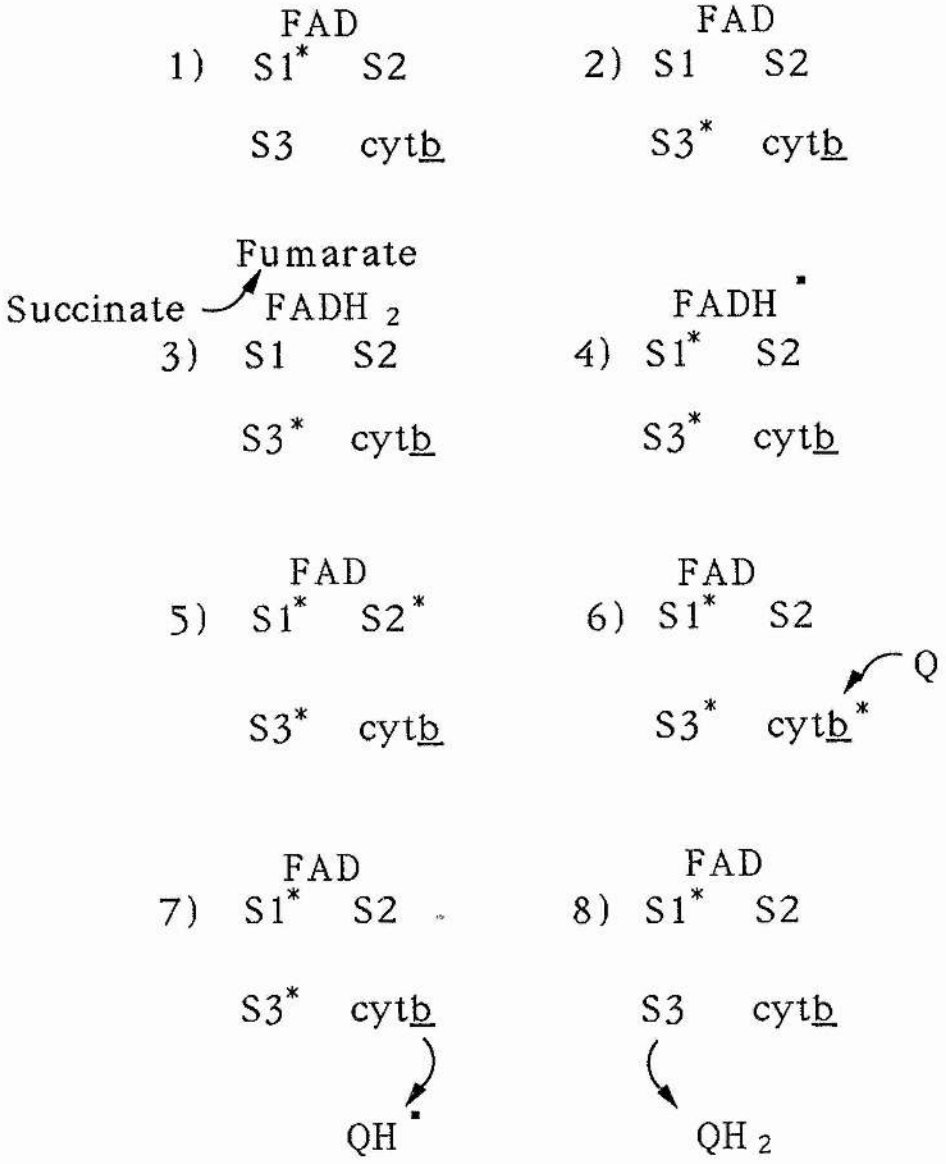
FAD
1) S1* S2
S3 cytb
FAD
2) S1 S2
S3* cytb
Fumarate
Succinate
FADH 2
3) S1 S2
S3* cytb
FADH
4) S1* S2
S3* cytb
FAD
5) S1* S2*
S3* cytb
FAD
6) S1* S2
Q
S3* cytb*
FAD
7) S1* S2
S3* cytb
QH
FAD
8) S1* S2
S3 cytb
QH 2

reduced in the absence of substrate by an, as yet, unidentified donor. A low potential pathway for the associated b-type cytochrome of *E. coli* succinate dehydrogenase seems even more unlikely as this centre has an E_{m7} value of +36mV.

Furthermore, it is unlikely that two separate pathways for electron transfer would exist within an enzyme which has close proximity of centres as shown by S1/S2, S2/S3, S1/S3, FR1/FR2, FR2/FR3 and FR1/FR3 spin-spin interaction (see later). From the measured midpoint potentials of the prosthetic groups it would appear that FR1 and FR3 (or S1 and S3) would be capable of electron transfer through the enzyme from donor to acceptor. The function of the very low potential FR2 and S2 remains an enigma: they can only be reduced chemically and not by substrate. However, it should be remembered that FR2 and S2 potentials can only be measured when centre 1 is already reduced: if, in the steady-state, centre 1 is normally oxidized when centre 2 is reduced then the actual midpoint potential of centre 2 may be less negative. The measured midpoint potential of FR2 would then constitute the interaction energy between FR1 and FR2 as well as the actual potential. This could give the actual midpoint potential value of FR2 as >100mV less negative (Ohnishi and Salerno, 1982).

Centre 1/centre 2 electronic interaction have been shown in both mitochondrial succinate dehydrogenase (Ohnishi *et al.*, 1976a) and *E. coli* fumarate reductase (Simpkin, 1985; Johnson *et al.*, 1985b). This interaction was

demonstrated in fumarate reductase as a spin-spin interaction when the g=1.93 signal relaxes faster on dithionite reduction (when both FR1 and FR2 are reduced) compared with succinate reduction (only FR1 reduced). The FR1 signal in the succinate sample is more easily saturated. The distance between FR1 and FR2 is given as 10-16A (Simpkin, 1985). Simpkin also determined a FR1/FR3 interaction as an increase in signal height (relaxation) of FR3 (g=2.01) when poised at -50mV compared to the fully oxidised sample at +150mV; a distance of 8-12Å between these two centres was given. Interaction between centres in all distance estimations are assumed to be predominantly dipolar and not due to an overlap of spins as in isotropic exchange coupling. No FR2/FR3 interaction was observed in Simpkin's study and the FR2 e.p.r. signal wings were not assigned. The additional wings of this complex reduced spectra have been assigned by other research groups (Johnson *et al.*, 1985b; Cammack *et al.*, 1986) and by the author as shown, Fig.1.2. The S2/S3 interaction of mitochondrial succinate dehydrogenase is thought to be wholly responsible for the complicated wings observed in spectra of dithionite reduced preparations. The spin-coupling is due to an interaction between the paramagnetic and e.p.r. detectable S2 (S=1/2) and the paramagnetic but e.p.r. undetectable S3 (S=2, ground state) (Ohnishi, 1987).

Oriented multilayer studies of iron-sulphur clusters are well documented in *E. coli* (Blum *et al.*, 1980). A specific study of *E. coli* fumarate reductase (Simpkin, 1985)

has shown the iron-sulphur centres to have a significant difference in g-tensors orientation compared to the equivalent centres in succinate dehydrogenase; this may be important for the functional difference between these enzymes. Interestingly fumarate reductase overexpressing strains show 3-dimensional orientation in multilayers (normally 2D), this may be due to a crystalline nature of the enzyme in amplified membranes.

The quinone binding site in mitochondrial succinate dehydrogenase has been shown to be associated with the anchor protein subunits in the membrane. This is a double quinone binding site which, when in the semiquinone form, gives a split e.p.r. signal around g=2.0. (Ruzicka *et al.*, 1975; Ingledew and Ohnishi, 1975; Ohnishi *et al.*, 1977; Salerno and Ohnishi, 1980). The split semiquinone radical signal is due to a dipolar interaction of which it was originally thought S3 was interacting with a single QH· semiquinone (Ruzicka *et al.*, 1975). Reinterpretation of the data gave a better simulated fit of the e.p.r. spectra if another QH· semiquinone was the interacting species, with a noninteracting but overlapping S3 signal. The split free radical signal is only observed at low temperatures (<15K) when S3 overlaps the semiquinone e.p.r. signal (S3 E_{m7} +60mV; Q E_{m7} +110mV). From the data of Salerno *et al.* (1977) it was concluded that the quinone pair is oriented with the quinone ring planes perpendicular to the membrane plane, as well as the line between the two quinones being perpendicular to the membrane plane. The two quinones are

thought to associate with the anchor subunits near the internal phase of the mitochondrion.

Menaquinone association for fumarate reductase anchor subunits may also be towards the inner phase if electron transfer is to occur between MQ and FR3. Succinate dehydrogenase and fumarate reductase will therefore take-up and release protons in the inner phase. If menaquinone releases protons into the cytoplasm, not the periplasm, fumarate reductase will not contribute to Δp generation. As mentioned above, growth utilizing glycerol 3-phosphate dehydrogenase and fumarate reductase generates a Δp. Glycerol 3-phosphate dehydrogenase is not intrinsically coupled however, so Δp generation would then appear to be dependent on a charge separation at fumarate reductase. A possible explanation for generation of Δp would then need to involve the anchor subunits acting as a proton-well for H^+ release into the periplasm. The apparent lack of a b-type cytochrome to act as a possible bridging centre between MQ and FR3 would suggest that electron transfer from a periplasmic MQ binding site to FR3 would not occur (inter-centre distances being too far for electronic transfer).

It is thought that menaquinone binds to one (either C or D) or both of the fumarate reductase anchor subunits (Cecchini *et al.*, 1986; Weiner *et al.*, 1986). E.p.r. evidence shows a single, not a double, MQ binding site (Simpkin, 1985). This difference, compared to the double binding site of mitochondrial succinate dehydrogenase, is

probably a function of complex III (bc_1-complex), it would therefore be interesting to compare the radical signals of *E. coli* succinate dehydrogenase with those of mitochondria (*E. coli* has no bc_1-complex). For e.p.r. observation of menaquinone radical, with little spectral overlap from flavin, the sample can be poised at -100mV pH7.0, at this potential FR3 and FR1 signals will also be present and the radical has a central g-value of 2.003. The flavin semiquinone can be observed, with little interference from the MQ radical, when the sample is poised at 0mV, this gives a peak at g=2.006. The flavin peak/trough linewidth is slightly narrower (1.0-1.1mTesla, pH7.0) than the MQ radical (1.25mTesla, pH7.0), although the flavin is a broader signal overall due to winged features in the spectra (Simpkin,D., Moodie,A.D., Salerno,J.C. and Ingledew,W.J., 1990, submitted). A possible menaquinone/FR3 interaction is tentatively assigned from the titration curve of MQ, suggesting a close proximity for these two centres (cytoplasmic aspect?). A flavin/FR1 interaction has been determined although under the conditions for observing FR1 the flavin is saturated. The flavin/FR3 interaction is very weak indicating a larger distance between these two centres. The flavin semiquinone can be observed independently from menaquinone by purifying the two catalytic subunits A and B from the anchor subunits (Dickie and Weiner, 1979; Robinson and Weiner 1982; Lemire and Weiner, 1986). The two subunit form of the enzyme has less activity than the membrane bound enzyme but is stimulated by the presence of anions which are

thought to stabilize the enzyme by conformational changes (Robinson and Weiner, 1981). The two subunit form of the enzyme is also alkali sensitive (pH8.6) and more thermolabile than the membrane bound holoenzyme (Lemire *et al.*, 1982). At pH12 the holoenzyme, rather than forming a random coil structure, through denaturation, forms a β-sheet structure. The significance of this, as far as folding and assembly, is not known (Fronticelli *et al.*, 1986).

The topological and e.p.r. data published for fumarate reductase has been greatly facilitated by the use of *E.coli* strains which are amplified in the enzyme. Three amplified fumarate reductase strains have been constructed:

a). a chromosomal duplication mutant, where amplification is linked to ampicillin concentration due to an *ampC* overlap (β-lactamase) with *frdD*; this gives ampicillin hyper-resistance to 800μg/ml (Cole and Guest,1979b; Grundstrom and Jaurin, 1982);

b). a replicating λ*frd* phage (Cole and Guest 1980a,b);

c). and a multicopy hybrid plasmid (Guest, 1981; Lohmeier *et al.*, 1981). These plasmids have ampicillin resistance which is not linked to the *frd* operon.

A variety of fumarate reductase mutant strains lacking individual subunits have been constructed (Condon and Weiner, 1988). Recently strains of *E. coli* overproducing succinate dehydrogenase have been developed (Kita *et al.*, 1989).

1.2.2. Experimental objectives for fumarate reductase.

Section 1.2.1. gave an insight into the depth of knowledge which has been accumulated within the last 10 years for the iron-sulphur protein, fumarate reductase. This well characterized enzyme has many similarities with succinate dehydrogenase. The bacterial enzyme can be manipulated genetically for experimentation and is often mechanistically compared to mitochondrial complex II. Prosthetic group midpoint potential values are consistent with a positive redox drop for electron flow in the two enzymes. The role of the three iron-sulphur centres, the quinone binding site and the flavin in electron transfer from menaquinone to fumarate has not been conclusively determined. The internal transfer pathway for electrons, in the pre-steady state, are to be determined. The time resolved studies of rapid-freeze quenching, when used in conjunction with electron paramagnetic resonance spectroscopy, may present information not only for this enzyme but will suggest future experimentation for iron-sulphur proteins as a whole.

Freeze-quench studies with fumarate reductase may determine the reduction sequence for the prosthetic groups. A linear sequence or an apparent sequence dependent on the individual midpoint potentials depends on the rate of internal electron transfers. These studies may also help to elucidate the role of the low potential centre FR2 (E_{m7}=

-285mV). If all three clusters are involved in electron transfer to fumarate it must be shown that the oxidation-reduction of each centre occurs at rates compatible with the catalytic event. *Escherichia coli* fumarate reductase, from the benzyl viologen/fumarate assay, has a maximal turnover of $30s^{-1}$ (from extrapolated steady-state data) (Simpkin, 1985). This value is compatible with the kinetic resolution of the freeze-quench technique.

From the early mitochondrial succinate dehydrogenase quenched flow studies of Beinert *et al.* (1975) kinetic resolution may be obtained with fumarate reductase.

1.3. Rapid-freeze quench studies and their contribution to our understanding of enzyme structure/function.

The analysis of pre-steady state kinetics for enzyme reactions can yield information on the biochemistry of these enzymes. Some forms of spectroscopy can be applied to these studies in actual time, but for other spectroscopic techniques the reaction has to be stopped at known lapsed times after initiation so that the enzymatic state can be analysed. E.p.r., when applied to many metalloproteins cannot be used in actual time because the spectra have to be obtained at low temperature. The study of enzymes in the "frozen" pre-steady state by rapid-freeze quenching was first reviewed in 1964 (Bray, 1964; Palmer and Beinert, 1964). This technique was originated, and has since been developed, principally by R.C.Bray and coworkers (Bray,

1961; Olson *et al.*, 1974; Bray and George, 1985). The time resolution of this method is in the low millisecond range.

The basic rapid-freeze quench apparatus consists of two pieces of equipment; a ram system, which actuates two syringes at a constant speed for a given period of time, and a cryostat. The syringe outputs are mixed and the mixed reactants travel down a specified length of tube, at a known velocity, before the reaction is terminated. Termination is either by denaturing the enzyme in acid then analysing the product formed (chemical quench) or freezing the enzyme mixture in pre-cooled iso-pentane (-140°C). After freeze-quenching, the enzyme, and its prosthetic groups, can be analyzed for time dependent ligand bound states or redox changes. By varying either the flow rate, or the length of tubing along which the reactant mixture travels, a time course of the reaction is obtained. As with other rapid reaction techniques, such as stopped-flow, the resolution limit for the apparatus is the dead-time, which, for freeze-quenching, will not only involve the mixing time for the reactants but also the freezing time. Iso-pentane is used for freezing because as a low molecular weight hydrocarbon it is less likely to chemically affect biological reactions, and experience bears this out (Bray and George, 1985). It is also convenient to use as it is a liquid at room-temperature (bp 28°C) with a very low freezing point (mp -160°C).

The oxidation of xanthine to uric acid by xanthine oxidase has been extensively studied using the rapid

freezing technique (see Bray and George, 1985; Olson *et al.*, 1974). The reduction sequence for the prosthetic groups (Molybdenum, iron-sulphur and FAD) has been determined as xanthine-->Mo-->Fe-S-->FAD-->O_2. Molybdenum was found to exist in various oxidation states during catalysis and these were named "very rapid" and "rapid" from freeze-quench observations of the $\underline{\overline{V}}$ oxidation state. A recent adaptation of the freeze-quench principle has been applied to extended X-ray absorption fine structure (EXAFS) analysis by Bray (George *et al.*, 1986; Turner *et al.*, 1989). Their initial EXAFS studies have been concerned with the xanthine oxidase "very rapid" molybdenum signal in the $\underline{\overline{IV}}$ oxidation state (approximately 85% of the Mo) whereas e.p.r. can only detect the $\underline{\overline{V}}$ oxidation state which is 1-2% of the total molybdenum present. An almost homogeneous state is preferential for EXAFS studies and this is found in the Mo(IV) signal of these preparations. Bray's findings suggest some reinterpretation of the structural data obtained from e.p.r. is needed although the electron transfer scheme remains unchanged. The molybdenum e.p.r. signal of xanthine oxidase can be detected at room-temperature (slow relaxation) which has led to the development of a continuous-flow/stopped-flow quartz cell for observing transient signals. The use of the flow cell arrangement has eliminated the possibility of the "very rapid" molybdenum signal being an artifact of freezing (Bray and George, 1985).

De Vries and coworkers (Van Hoek *et al.*, 1987; De Vries *et al.*, 1979, 1982, 1983) have studied the

bc$_1$-complex of mitochondria with rapid-freeze quenching and postulated complex modelling schemes for electron transfer within this complex. De Vries includes a hypothesised double *bc*$_1$-complex (dimer) to explain their kinetic data in relation to a Q-cycle. Their studies have been used in conjunction with HPLC for analysis of quinone turnover.

Initial rapid kinetic studies using mitochondrial succinate dehydrogenase (complex II) observed centre S3 reduction in the presence of succinate at a slower rate than S1 reduction (Beinert *et al.*, 1975). These preparations were under anaerobic conditions with SDH (or complex II) originally oxidized in the presence of the quinone binding site inhibitor thenoyltrifluoroacetone (TTFA), this inhibitor was necessary if reduction was to be observed. From the midpoint potentials known for S3 (Em_7=+60mV) and S1 (Em_7=0mV) the above observation is thermodynamically the reverse of what may have been expected if internal electron transfers are not rate limiting. Electron transfer within this enzyme may then be in a linear sequence from donor to acceptor, although the data given is not conclusive. Not all of the centres 1 and 3 were reduced within the turnover time of the enzyme.

An interesting paper by Beinert *et al.* (1976) showed the oxidation/reduction of haem and copper components of cytochrome oxidase to be time resolvable by freeze-quenching techniques. Their study included ligand binding observations which will be more fully discussed in Chapter 7, with direct implications to cytochrome-*bd* and cytochrome-*bo* of *E. coli*.

1.4. Echerichia coli ubiquinol-oxygen oxido-reductase cytochrome-bd: ligand binding.

1.4.1. Ubiquinol-oxygen oxido-reductase cytochrome-bd.

Escherichia coli can produce two functional terminal respiratory oxidases under specified growth conditions. Anaerobic growth or low oxygen tension induces cytochrome-*bd* with reduced levels of cytochrome-*bo* and early aerobic growth induces cytochrome-*bo*. Both oxidases are present if aerobic growth proceeds to the stationary phase (Castor and Chance, 1959; Reid and Ingledew, 1979; Ingledew and Poole, 1984). The two oxidases of *E. coli* have been reviewed by Poole and Ingledew (1987), Anraku and Gennis (1987) and Gennis (1987). Although optical properties of cytochrome-*bd* have been well characterized (see Poole and Ingledew, 1987), ligand binding perturbations caused to e.p.r. signals have received little attention (Kumar *et al.*, 1985; Hata-Tanaka *et al.*, 1987; Rothery and Ingledew, 1989; Meindhart *et al.*, 1989; Rothery 1989). E.p.r. studies have been further confused by uncertainties when assigning specific g-value regions to the three haem centres of cytochrome-*bd*.

Ligand binding studies, mainly on mammalian mitochondrial preparations, have greatly contributed to the elucidation of the catalytic mechanisms of dioxygen reduction in the cytochrome oxidase aa_3 system (Malmstrom, 1982; Naqui *et al.*, 1986; Hill *et al.*, 1986; Wikstrom,

1988). Cytochrome oxidase (aa_3) is known to bind many of the classic respiratory chain inhibitors (cyanide, azide, fluoride, sulphide, formic acid, carbon monoxide and nitric oxide), having the affect of eliciting changes in both the optical and e.p.r. spectra of the species (Wikstrom *et al.*, 1981).

Cytochrome-*bd* of *E. coli* has a high affinity for oxygen. Reported K_m values for oxygen are 0.23μM (Kita *et al.*, 1984) and 0.024μM (Rice and Hempling, 1978) which are lower than the cytochrome-*bo* values of 1.4μM and 0.2μM, respectively. The mitochondrial aa_3 system has a Km for oxygen of 0.5μM (Degn and Wohlrab, 1971). The values determined for Km are dependent on the technique applied. The Km for oxygen of cytochrome-*bd* is consistently 10 fold less than for cytochrome-*bo*. These results therefore show a higher oxygen affinity in cytochrome-*bd*.

Cytochrome-*bd* contains three haem centres, haem-b558, haem-b595 and haem-d. Haem-b558 is a low-spin, six coordinate, *b*-type haem (protoporphyrin IX) with an optical absorbance in the alpha region at 558nm and a β-band maxima at around 532nm, the Soret absorbance of haem-b558 is at 430nm (reduced minus oxidized spectra; Reid and Ingledew, 1979; Poole and Ingledew, 1987; Rothery and Ingledew, 1989). Haem-b595 is a high-spin, five coordinate, *b*-type haem (protoporphyrin IX) with an alpha region absorbance at 595nm and a large β-band contribution in the 560nm region, this haem also shows absorbance in the Soret region between 430nm and 440nm (Koland *et al.*, 1984). Haem-d (a chlorin

structure, Timkovich *et al.*, 1985) has a major peak-trough absorbance in the alpha region of reduced minus oxidized spectra at 630-647nm. The 630nm signal is attributed to unligated reduced haem-d with the 650nm region attributed to reduced haem-d ligated with dioxygen. A further trough at 680nm is attributed to peroxide ligated haem-d (Poole *et al.*, 1983a,b; Poole and Williams, 1988; Lorence and Gennis, 1989). Haem-d shows little absorbance in the Soret region. Unligated oxidized haem-d is not optically detected and is refered to as d* (Pudek and Bragg, 1974, 1975; Poole, 1983). Fig.1.5 shows reduced minus oxidized optical spectra for a membrane preparation of *E. coli* strain FUN4/pNG2 (deleted cytochrome-*bo*, amplified cytochrome-*bd*) in the wavelength region 400-700nm at 77K. Cytochrome-b556 of succinate dehydrogenase also contributes to the Soret and alpha regions of this spectrum.

Optical potentiometric titrations assign midpoint potential values (E_{m7}) for the n=1 electron transfers of +140mV for haem-b595, +280mV for haem-d and +250mV for haem-b558 in membrane preparations (Reid and Ingledew, 1979). Midpoint potentials for purified (soluble) cytochrome-*bd* have assigned E_{m7} values of approximately +140mV, +260mV and +150mV for haems b595, d and b558, respectively (Lorence *et al.*, 1984; Koland *et al.*, 1984). The midpoint potential values for the haems, especially haem-b558, and the activity of the enzyme, are susceptible to the solubilization detergent (Lorence *et al.*, 1984).

Figure 1.5.

Reduced minus oxidized spectrum of Escherichia coli amplified cytochrome-bd strain, FUN4/pNG2 (77K).

A dithionite reduced minus peroxide oxidized spectrum of a membrane preparation of FUN4/pNG2 (approximately 5mg.ml^{-1} etp, 50mM BES, pH7.0) is shown (77K). The major absorbance peak/troughs (nm) of the Soret and alpha regions are shown above the spectrum. The alpha region is amplified four fold compared to the Soret region. Assignment of peak and trough absorbance values are given in the text.

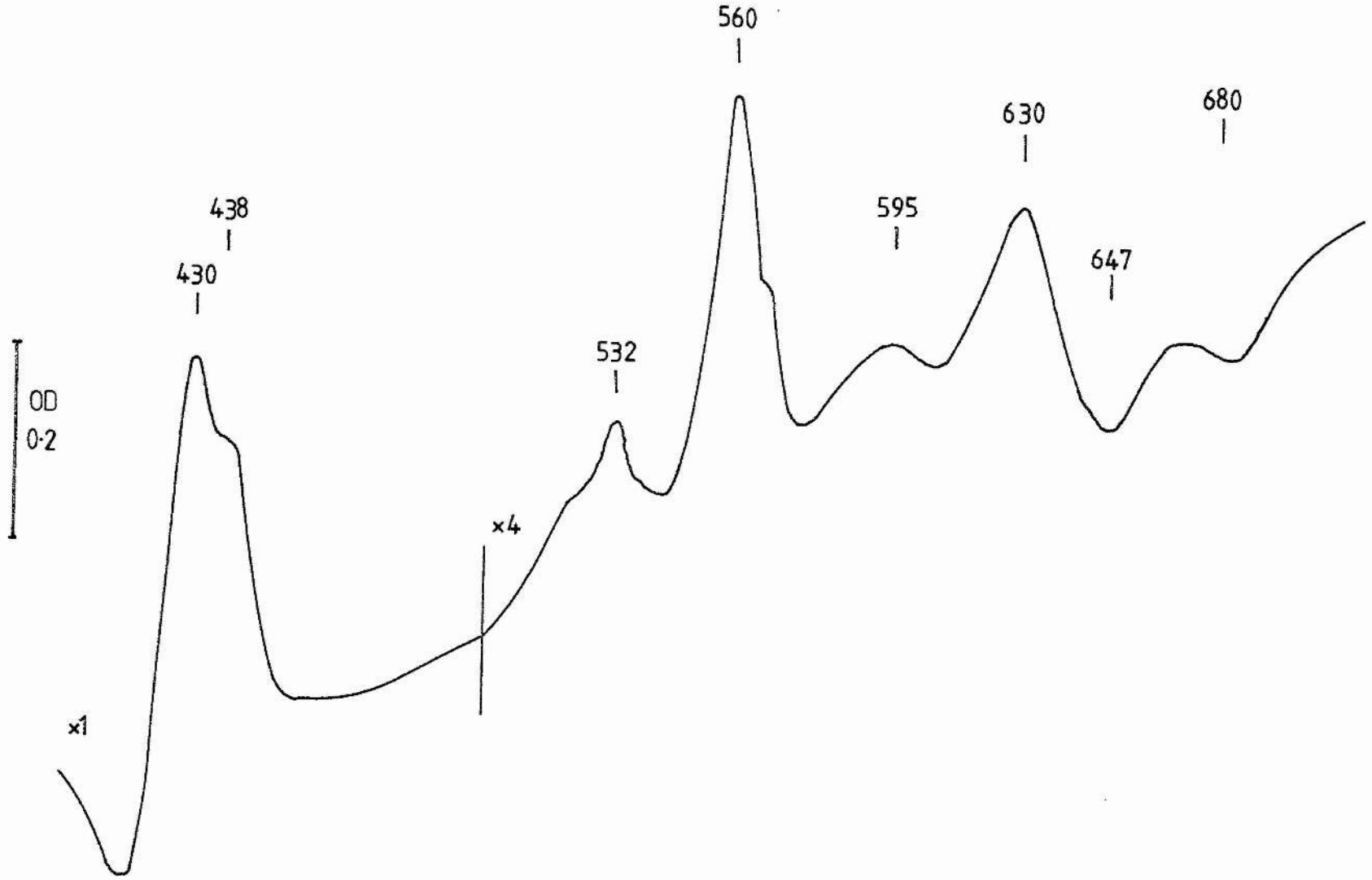
560
630
680
438
595
430
647
532
OD
0·2
×4
×1

Chapter 1

Cytochrome-*bd* has two membrane spanning subunits, subunits I and II (Fang *et al.*, 1989). From polyacrylamide gel electrophoresis of purified protein, and sequencing studies of the *cyd* locus, the holoenzyme has a molecular weight of 100000 (subunit I, 57000; subunit II, 43000) (Miller and Gennis, 1983; Green *et al.*, 1984a,b, 1986, 1988; Georgiou *et al.*, 1987; Miller *et al.*, 1988). Haem-b558 is located in subunit I; and haem-b595 and haem-d are associated with subunit II (Green *et al.*, 1984b). A report by Lorence *et al.* (1983) of two d-type haems per complex has been scrutinized by Rothery and Ingledew, and in conjunction with known e.p.r. data, only one d-haem is now thought to be present per complex (Rothery et al., 1987; Rothery and Ingledew, 1989; Rothery, 1989; Meindhart *et al.*, 1989).

Oxidized haem-d has been assigned a high-spin axial e.p.r. signal centred at g=6.0 and haem-b595 a high-spin rhombic signal at g_x=6.25 and g_y=5.54 in membrane preparations titrated potentiometrically in the absence of oxygen; both high-spin signals approach axial symmetry when oxidized by oxygen. Rhombic low-spin signals attributed to haem-d are present at g_z=2.5, g_y=2.3 and g_x=1.85 but these are at a much lower concentration than the axial g=6.0; a low-spin signal at g=3.3 is attributed to haem-b558 (Rothery and Ingledew, 1989; Rothery, 1989; Meindhart *et al.*, 1989)

Optical ligand binding studies have shown cyanide binding to the oxidized form of *E. coli* cytochrome-*bd* giving a d*-CN complex (Pudek and Bragg, 1974, 1975; Poole, 1983). Cyanide also elicits changes in the g=6.0 high-spin e.p.r.

region with the appearance of low-spin signals at g_z=2.96 and g_y around 2.10 although no g_x has been assigned (Rothery,1989, Rothery and Ingledew, 1989). Carbon monoxide binding to cytochrome-*bd* causes spectral line changes in the g=6.0 region when the sample is potentiometrically titrated to the oxidized form under an atmosphere of carbon monoxide (Rothery, 1989; Rothery and Ingledew, 1989). In the presence of CO the midpoint potential (E_{m7}) of haem-*d* is increased from +261mV to >+400mV, the haem-b595 signal has an E_{m7} value of +130mV which is unchanged in the presence of CO (Rothery and Ingledew, 1989; Meindhart *et al.*, 1989). Haem-b558 has a E_{m7} value of +180mV, also unchanged by CO. The E_{m7} values given here for the haem centres are taken from Rothery and Ingledew (1989) and are in close agreement with the values assigned by Meindhart *et al.* (1989). The midpoint potential values for haem-b558, haem-b595 and haem-d in membrane preparations are reported to be pH dependent by Meindhart *et al.* (1989) but pH independent by Rothery and Ingledew (1989; and personal communications), although Rothery and Ingledew observed lineshape changes at different pH values. The relative significance of possible pH dependence in these centres is refered to for the model systems presented in chapters 6 and 7.

Mitochondrial cytochrome oxidase has four prosthetic groups; two coppers, Cu_A and Cu_B; and two *a*-type haems, haem-*a* and haem-a_3; no copper is present in *E. coli* cytochrome-*bd*. *E. coli* cytochrome-*bo* has two b-type haems (one high-spin and one low-spin) and one copper, this has

led to a direct mechanistic comparisons between *E. coli* cytochrome-*bo* and mitochondrial cytochrome oxidase; the single copper in *E. coli* being associated with the high-spin oxygen binding haem in a similar fashion to Cu_B-a_3 interaction (Salerno *et al.*, 1989, 1990).

The data reported herein presents optical studies for CO (chapter 5) and NO binding, and e.p.r. studies for NO binding (chapter 6), in cytochrome-*bd* with the aim of presenting model systems for the catalytic reduction of dioxygen to water (chapter 7).

1.4.2. Nitric oxide.

The 'binding' of nitric oxide (NO) to reduced haemoproteins and copper-proteins has helped to elucidate the *in vivo* catalytic mechanisms for these proteins.

Nitric oxide binds and is e.p.r. detectable as a 6th coordinate ligand of high-spin haems (and synthesized inorganic haem complexes) when the iron is in the reduced (ferrous) state (Kon, 1969; Kon and Kataoka, 1969; Yonetani *et al.*, 1972; Henry and Banerjee, 1973; Yoshimura *et al.*, 1979; Morse and Chan, 1980; Tsubaki *et al.*, 1987). The optical spectra of reduced haems are bleached by NO and, unlike most other ligands, have e.p.r. signal associated with the unpaired electron of the ligand. This elicits spectral changes in the g=2.00 region. The electron is associated with the dz^2 orbital of the Fe and the NO orbitals (Kon and Kataoka, 1969). The unpaired electron of

NO is paramagnetic when associated with ferrous haem but e.p.r. silent when spin paired with the electron of oxidized ferric haem. Optical spectra of *E. coli* cytochrome-*bd* show a 438nm trough in the Soret region of the room-temperature reduced + nitrite minus reduced spectra with associated features at around 560nm in the alpha region. These signals have been attributed to the binding of NO to haem-b595. Bleaching of the optical spectra at 630nm was attributed to NO bound haem-d with no associated changes in the Soret region (Rothery *et al.*, 1987).

The work of Rothery *et al.* (1987) and Rothery (1989) showed a pH dependence for haem-NO formation, with both d-NO and b595-NO forming at low pH (pH6.0) but only an apparent d-NO formation at higher pH (pH8.5). Polarographic studies in the presence of nitrite have suggested cooperative kinetics for oxygen reduction by cytochrome-*bd*; the cooperative centres postulated as haem-d and haem-b595. The significance of this observed cooperativity is discussed in chapter 6 and is suggested to be a facet of nitrite reduction and competitive inhibition rather than true cooperativity for a double dioxygen binding site.

E.p.r. spectra of cytochrome-*bd* haem-NO in the g=2.00 region are complex with g-values being assigned to both d-NO and b595-NO by comparison to the time dependent haem-NO formation of optical spectra (b595-NO formation is much slower than d-NO formation) (Rothery, 1989). The d-NO e.p.r. signal is relatively rhombic and has been assigned a type-I NO configuration with g_x at 2.081, g_y at 1.984 and a g_z in

the 2.00 region, there is also a possible type-II resonance with a g_z of 2.047. The b595-NO signal is relatively axial with a type-II configurations (no type-I) and is assigned a peak at g=2.033 with a trough at around g=2.000 (Rothery, 1989).

The work of Rothery (1989) focussed on membrane particles and whole cells from a wild-type *E. coli* strain (prototroph, EMG2). The work presented in chapter 6 uses strain FUN4/pNG2 which is deleted in both cytochrome-*bo* and cytochrome-*bd* but carries expression of the *cyd* gene locus on a multicopy plasmid to give over-expression of cytochrome-*bd*. This strain will not contain cytochrome-*bo*, which was always a possibility with EMG2 even when grown anaerobically, and so any haem-NO signals (optical or e.p.r.) can be attributed to cytochrome-*bd*. Other centres which can bind NO in *E. coli*, such as nitrite reductase, catalase, peroxidase and iron-sulphur proteins, will be in much smaller relative concentration in the FUN4/pNG2 strain. A free radical signal observed by Rothery (1989) during time course experiments with nitrite reduction in cytochrome-*bd* at pH7.0 was thought to arise from either flavin or quinone. Chapter 6 further characterizes this radical by following the development of the signal at different pH values. Models are presented for cytochrome-*bd* based on the thermodynamic parameters of the haem centres and the assigned semiquinone.

From microwave power saturation (P1/2) profiles of the haem-NO complex (Blum et al., 1980), Rothery (1989) assigned a distance for haem-b595 of 12Å, and haem-d of 8Å,

below the surface of the protein on the cytoplasmic aspect of the membrane. The arrangement of the haem planes in the membrane is such that haem-b558 and haem-d are perpendicular to the membrane plane and haem-b595 is at 45° (Rothery, R.A., Salerno,J.C. and Ingledew,W.J. unpublished data). Haem-b595 and haem-d are in close proximity, as seen by haem-haem interaction (Rothery and Ingledew, 1989). This information is discussed in relation to NO binding, and therefore dioxygen binding. The hyperfine splitting of the haem-NO e.p.r. g_z region is discussed in relation to the recent work of Gennis and coworkers (Fang *et al.*, 1989).

1.4.3. Carbon monoxide.

The binding of carbon monoxide (CO) to reduced haemoproteins and the subsequent photolysis of the inhibited haem, at a specified wavelength of light, to allow dioxygen binding, is associated with an oxidase function (Castor and Chance, 1955). The first study of photochemical action spectra in *E. coli* clearly showed a functional d-type oxidase (previously a_2) and an o-type oxidase (Castor and Chance, 1959). Interestingly no photodissociable b595-CO was observed although this was probably because the larger haem-b595 B-band absorbance at 560nm was incorporated into the action spectra of cytochrome-*bo*.

The apparent low affinity of haem-b595 for CO as well as its other anomalous biophysical properties has led to often confusing analysis for this haem centre and its respective "oxidase" function (see, Ingledew, 1978).

However, a photochemical action spectra showing a distinct photodissociation wavelength of 595nm was shown by Edwards *et al.* (1981). An oxidase function cannot be assigned to haem-b595 in its own right because we know haem-d and haem-b595 are associated with the same oxidase complex. We can then define a photodissociable CO bound haem centre, which gives an action spectra, not necessarily as being dioxygen binding but as being involved in the catalytic cycle of dioxygen reduction for that oxidase (i.e. at the active site). This definition is important for the model of catalysis presented for cytochrome-*bd* in chapter 7.

Cytochrome-*bd* and cytochrome-*bo* of *E. coli* have been studied by the triple-trapping technique which was first used by Chance on mitochondrial preparations of cytochrome oxidase (Chance *et al.*, 1975; Poole and Chance, 1981; Poole *et al.*, 1982a, 1983a,b). The work of Poole and colleagues has assigned a CO bound haem-b595 (Poole *et al.*, 1981). Much of the triple-trapping work has been in the presence of both cytochrome-*bd* and cytochrome-*bo*, thus making it difficult to discern the overlap between the o-CO complex and the b595-CO complex. Indeed under growth conditions of low oxygen tension when little cytochrome-*bo* would be present a new o-type oxidase was postulated (o-436nm) which may equally have been assigned to haem-b595. Added confusion arises when oxidation of unligated low-spin b-type haems are considered.

The uncertainty in haem-b595 function, certainly as far as CO binding, suggests complex binding kinetics within the haem pocket. The low affinity of haem-b595 for CO and the much higher affinity of haem-d (Poole *et al.*, 1983b) is shown not only by triple-trapping and photochemical action spectra studies but also by potentiometric titrations, as outlined in section 1.4.1., where the midpoint potential of haem-d is increased in the presence of CO but that of haem-b595 remains unchanged.

The reduced + CO minus reduced optical spectra of cytochrome-*bd* show an alpha region trough at 623nm with a peak at 640nm and a Soret region trough at 445nm associated with d-CO; changes in the alpha region around 560nm and 595nm and in the Soret region at around 429nm are attributed

to b595-CO (Rothery, 1989). The Soret trough assigned to d-CO has previously been assigned to b595-CO (see Poole and Ingledew, 1987)

Chapter 5 deals with a photochemical apparatus based upon a Clarke-type oxygen electrode computer interfaced for rate analysis. Absorbance of light at wavelengths below 600nm gave increased rates of oxygen reduction and this is related to the role of haem-b595 in the catalytic cycle of dioxygen reduction to water.

1.5. Research project objectives.

The aims of this project were:-

1. To design and construct a rapid freeze-quench/continuous flow apparatus to be used in conjunction with electron paramagnetic resonance spectroscopy (Chapter 3).
2. To study the reduction/oxidation states of the prosthetic groups of *E. coli* fumarate reductase in the pre-steady state using the rapid-freeze quench apparatus (Chapter 4).
3. To observe photodissociable states of carbon monoxide bound *Escherichia coli* ubiquinol-oxygen oxido-reductase cytochrome-*bd* and relate these to the CO bound haem centres of this enzyme (Chapter 5).
4. To substantiate and expand on the work of Rothery (1989) showing the formation of nitric oxide bound haem-d and haem-b595 to be time dependent, haem-b595 having a lower affinity for NO (Chapter 6).

The data of chapters 4 and 5 & 6 are presented as models of enzyme catalysis for fumarate reductase and cytochrome-*bd*, respectively (Chapter 7). The available experimental data and their related controversies, as presented in this introduction, are considered for model systems.

Chapter 2

MATERIALS AND METHODS

Chapter 2

2.1. Organisms.

Escherichia coli strains used in this study were:-

Strain	Genotype	Source
EMG2	Wild-type	NCIB, Torry, Aberdeen.
GO103	F⁻, *rps*L, *gal*, *thi*, Δ*cyd*1::kan Phenotype:- kanamycin resistant deleted cytochrome-*bd* wild-type expression of cytochrome-*bo*	Professor R.B. Gennis, University of Illinois Urbana, U.S.A.
HB101/pFRD84	F⁻, *hsd*R, *hsd*M, *pro*, *leu*, *gal*, *lac*, *thi*, *rec*A, *rps*L. Amp^R multicopy plasmid containing the *frd* gene region expressing all four fumarate reductase subunits. Phenotype:- Ampicillin resistant. Fumarate reductase overexpressing.	Professor J.H. Weiner, University of Alberta, Edmonton, Alberta, Canada.

FUN4/pNG2	F⁻, *cyd*A2, *cyo*, *rec*A, *srl*, *rps*L, *gal*, *men*A401, *nad*A.	Professor R.B. Gennis, University of Illinois, Urbana, U.S.A.
	Tet^R multicopy plasmid containing the *cyd* gene region (cytochrome-*bd*). Phenotype:- cytochrome-*bd* overexpressing. cytochrome-*bo* deficient.	

2.2. Growth Media.

EMG2 and HB101/pFRD84 were grown anaerobically at 37°C in 20l bottles. GO103 was grown aerobically at 37°C in 20l bottles heavily sparged with air. FUN4/pNG2 was grown aerobically at 37°C in a 500l fermenter.

Strain EMG2 was grown anaerobically on glycerol-fumarate media to late exponential phase at 18hr . Strain HB101/pFRD84 was found to give a slightly higher growth yield when grown on a peptone media containing fumarate (as recommended by Prof.J.H. Weiner, personal communications) rather than a glycerol-fumarate media. This media still gave amplified levels of fumarate reductase and was harvested at late stationary phase after 48hr (Condon and Weiner, 1988). Strains GO103 and FUN4/pNG2 were grown aerobically on glucose to late exponential phase at 18hr .

Batch growths were innoculated with starter cultures

grown with appropriate antibiotic (concentrations as below). EMG2 and HB101/pFRD84 innocula were grown anaerobically in 500ml bottles of luria broth for 12hr (with appropriate antibiotic). GO103 and FUN4/pNG2 innocula were grown aerobically in shaker flasks (with appropriate antibiotic). The batch innocullum was 1%. All *E. coli* strains were maintained at -70°C in 20% DMSO/glycerol.

2.2.1. Glycerol-fumarate media (EMG2):-

7.9g.l^{-1} potassium dihydrogen phosphate; 6.1g.l^{-1} fumaric acid; 9.25g.l^{-1} potassium hydroxide; 2.1g.l^{-1} ammonium sulphate; 5.25ml.l^{-1} glycerol; 1.05g.l^{-1} acid hydrolysed casein; 1.05ml.l^{-1} 50mM/50mM sodium selenite/ammonium molybdate; 1.05ml.l^{-1} trace metals solution. pH7.4. Autoclave. After autoclaving add 0.21ml.l^{-1} magnesium sulphate 1M autoclaved separately.

2.2.2. Peptone media (HB101/pFRD84):-

4g.l^{-1} Peptone; 4g.l^{-1} yeast extract; 7.9g.l^{-1} potassium dihydrogen phosphate; 6.1g.l^{-1} fumaric acid; 9.25g.l^{-1} potassium hydroxide. pH7.4. Autoclave. After autoclaving add 100ml of 20% glucose filter sterilized and filter sterilized ampicillin to 100mg.l^{-1}.

2.2.3. Glucose media (GO103, FUN4/pNG2):-

5g.l^{-1} potassium dihydrogen phosphate; 1.5g.l^{-1} potassium hydroxide; 5g.l^{-1} D-glucose; 2g.l^{-1} tryptone; 2g.l^{-1} yeast extract; 0.5g.l^{-1} acid hydrolysed casein;

$1g.l^{-1}$ ammonium sulphate; $1ml.l^{-1}$ trace metals solution; $1.05ml.l^{-1}$ 50mM/50mM sodium selenite/ammonium molybdate; $2mg.l^{-1}$ iron nitrate. pH7.4. Autoclave. After autoclaving add $0.21ml.l^{-1}$ magnesium sulphate 1M autoclaved separately; plus filter sterilized vitamin B_1 $5mg.l^{-1}$.

Plus for Fun4/pNG2 only, nicotinic acid $50mg.l^{-1}$ and tetracycline to $10mg.l^{-1}$. (Although FUN4/pNG2 is not a *thi* mutant the addition of Vitamin B_1 appears to improve growth).

Plus for GO103 only, kanamycin at $30mg.l^{-1}$

2.2.4. Luria broth and Luria agar:-

$10g.l^{-1}$ tryptone; $5g.l^{-1}$ yeast extract; $10g.l^{-1}$ sodium chloride. pH7.5. For luria plates add 1% agar and Autoclave. When agar has cooled to 48°C add appropriate antiobiotic, at concentrations as above.

2.2.5. Trace metals solution:-

3mM iron(III) chloride; 2mM manganese(II) chloride; 2mM calcium chloride; 1.2mM cobalt sulphate; 4.5mM boric acid. 1l stock solution.

For GO103 only, 2mM copper sulphate was added to above solution.

2.3. Cell Harvesting.

Cells grown in 20l bottles were harvested to a pellet by continuous-flow centrifugation using a continuous-flow

rotor on an MSE High Speed 18 centrifuge, 18,000rpm. Cells grown in the 500l fermenter (University of Dundee) were filter harvested to a slurry of approximately 5l.

After harvesting cells were washed at least twice in 50mM phosphate buffer, pH7.2, 4°C, using a Sorvall RC-5B Superspeed centrifuge (DuPont), 9,000g, 15mins. Cells were suspended in 50mM BES, 5mM EDTA pH7.2, frozen in liquid nitrogen as pellets and stored at -30°C before membrane preparation.

2.4. Membrane preparation.

Electron transport particles (etp's) were prepared from cells by lysis, particles are not inverted vesicles but rather membrane fragments.

Cells in 50mM BES 5mM EDTA, pH7.2 were incubated at 4°C for 20-30mins with lysozyme ($2\mu g.ml^{-1}$) and deoxyribonuclease II ($2\mu g.ml^{-1}$, with magnesium sulphate for activation). The cells were broken by two passages through a French Press operating at 15MPa. Unbroken cells were removed by centrifugation at 9,000g for 15mins. Membrane fragments were pelleted by centrifugation at 100,000g for 1hr in a Prepspin 50 ultracentrifuge. The pellet was washed in 50mM BES 5mM EDTA pH7.2, and re-pelleted. The etp's were resuspended in the appropriate buffer (pH) for experimentation, concentration approximately $50mg.ml^{-1}$. The suspension was frozen as small pellets in liquid nitrogen and stored under liquid nitrogen until use. Samples were

stable for at least several months.

2.5. Assays.

2.5.1. Protein determination.

Protein concentrations were estimated by the method of Lowry *et al.* (1951) with the inclusion of 1% sodium dodecyl sulphate to solubilize membrane bound proteins. Bovine serum albumin was used as standard.

2.5.2. Oxygen electrode.

Oxygen electrode studies used a Clarke type oxygen electrode base purchased from Rank Brothers, Cambridge. The glass electrode vessel was made by Mr.C. Smith, Department of Chemistry, University of St.Andrews. The vessel was water jacketted sealed with a ground glass stopper which has a capillary portal for microsyringe additions, the internal volume was 2.55ml. A specialized oxygen electrode developed for photodissociation and subsequent analysis of data is described in chapter 5. At 30°C the aerated oxygen concentration of buffer is taken as 0.22mM, oxygenated buffer 1.121mM.

Data points for oxygen electrode progress curves were collected by interfacing to a BBC Microcomputer (Acorn Computers), as outlined by Rothery (1989). For analysis of single progress curves the data were applied to integrated Michaelis-Menten equations (Fig.2.1). These formula were applied to programs written for the University of St.Andrews

Figure 2.1

Integrated forms of the Michaelis-Menten equation.

Integrated forms of the Michaelis-Menten equations, as used for oxygen electrode progress curve analysis, are shown. These assume that product concentration plus substrate concentration (S) is equal to the initial substrate concentration (S_0). Data for oxygen electrode progress curves ($S=[O_2]$, t=time) were applied to the equations.

Integrated Eadie-Hofstee Equation. (y=mx+c) :-

$$\frac{S_0 - S}{t} = -K_m \left[\frac{1}{t} \ln\left(\frac{S_0}{S}\right) \right] + V_{max}$$

slope = $-K_m$

absicca intercept = V_{max}

Integrated Hanes Equation :-

$$\frac{t}{\ln\left(\frac{S_0}{S}\right)} = \frac{1}{V_{max}} \left[\frac{S_0 - S}{\ln\left(\frac{S_0}{S}\right)} \right] \frac{+K_m}{V_{max}}$$

$$\text{slope} = \frac{1}{V_{max}}$$

$$\text{absicca intercept} = \frac{K_m}{V_{max}}$$

Integrated Lineweaver-Burke Equation :-

$$\frac{t}{S_0 - S} = \frac{K_m}{V_{max}} \left[\frac{\ln\left(\frac{S_0}{S}\right)}{\left(S_0 - S\right)} \right] + \frac{1}{V_{max}}$$

$$\text{slope} = \frac{K_m}{V_{max}}$$

$$\text{absicca intercept} = \frac{1}{V_{max}}$$

VAX-11 computer network by R.A.Rothery. The integrated form of the equation applies its own "averaging" to collected data in the form of the integration constant, C. Previous analysis, using the differentiated equation, required prior averaging of data before smooth plots of Michaelis-Menten data could be obtained (see Rothery, 1989). The many limitations which must be applied to analysis of single progress curves (Wong, 1975; Cornish-Bowden, 1976) may make the application of either the differentiated or integrated forms of the Michaelis-Menten equations invalid in the presence of inhibitor. This point is further discussed in chapters 5 & 6. Previous assignment of nitrite inhibition for *E. coli* cytochrome-*bd* as competitive and carbon monoxide inhibition as mixed-type remain as these were determined from initial rates not complete progress curve analysis (Rothery, 1989).

2.5.3. Fumarate reductase activity.

Fumarate reductase activity of the amplified strain HB101/pFRD84 was determined using a modified method of Spencer and Guest (1973).

To 3ml of nitrogen purged 50mM TES pH7.5 (pH optimum for the membrane bound enzyme; Simpkin, 1985), in a stoppered 3ml cuvette, add benzyl viologen to 120μM and fumarate to 20mM. Add aliquots of a solution of dithionite until the absorbance at 550nm is approximately 0.9. The absorbance remains constant if the solution remains anoxic. When etp's are added (usually about 10μl of 5mg.ml^{-1}) a

decrease in absorbance is measured (benzyl viologen becomes oxidized). Two benzyl viologens are oxidized per fumarate reduced. The extinction coefficient for benzyl viologen is 7.78×10^3 $M^{-1}cm^{-1}$ at 550nm. This method gives rate values for etp's of 10-20mmoles fumarate.min^{-1}.mg $protein^{-1}$ in amplified strains (HB101/pFRD84) and 0.1-0.3mmoles fumarate.min^{-1}.mg $protein^{-1}$ for wild-type (EMG2).

The method is not suitable for whole cell analysis of activity because the dicarboxylic acid carriers for fumarate movement across the membrane appear to be rate limiting in the amplified strains (Simpkin and Ingledew, 1984). Benzyl viologen is freely permeable across the membrane when in the reduced form (Jones and Garland, 1977).

2.6. Spectrophotometry.

Optical difference spectra of *E. coli* were obtained using a room-temperature, liquid nitrogen temperature, split-beam spectrophotometer. This spectrometer was constructed by the workshop of the Biochemistry and Microbiology Department, University of St.Andrews.

Quinone, DNA and red/blue filter (chapter 5) spectra were recorded at room-temperature using an LKB Perkin-Elmer lambda 5 scanning spectrophotometer.

Routine assays, such as fumarate reductase activity and protein determination used a single wavelength CE272 (Cecil) spectrophotometer.

2.7. Electron paramagnetic resonance spectroscopy.

2.7.1. Spectrometer.

E.p.r. spectra were obtained using a Bruker ER200D electron paramagnetic resonance spectrometer (Bruker Analytische Messtechnik GmbH, Silberstreifen, D-7512 Rheinstetten 4, FRG) equipped with a variable temperature cryostat and liquid helium transfer line (ESR-9 Oxford Instruments, Osney Mead, Oxford, U.K.). Free radical spectra at room temperature were summated using a signal averager (Model 4202, EG & G, Princeton Applied Research, U.S.A.) in the summation averaging mode (signal to noise ratio improves as a square root function of the number of sweeps i.e. the signal of interest, as the synchronous component of the input, increases linearly with the number of sweeps, whereas the non-synchronous component, the noise, only increases as the square root of the number of sweeps).

2.7.2. Redox poised samples for freeze-quenching.

Potentiometric poising of freeze-quench samples were carried out as described by Dutton and Wilson (1974). A range of mediator dyes can be used at concentrations of 25-50μM: safranine (Em_7=-289mV); glutathione (Em_7=-222mV); anthroquinone 2,6-disulphonate (Em_7=-184mV); resorufin (Em_7=-50mV); duroquinone (Em_7=+7mV); ascorbate (Em_7=+55mV); 1,4-naphthoquinone (Em_7=+50mV); 1,4- naphthoquinone 2-sulphonate (Em_7=+115mV); 1,2-naphthoquinone (Em_7=+130mV); N,N-dimethyl-p-phenylene diamine (DMPD) (Em_7=+245mV);

N,N,N',N'-tetramethyl-p-phenylene diamine (TMPD) (Em_7=+260mV); tetrachlorohydroquinone (Em_7=+345mV); ferricyanide (Em_7=+420mV).

E_h was varied in the redox vessel with additions of strongly buffered dithionite solutions for reduction, and either ferricyanide or a fresh preparation of ammonium persulphate for oxidation. Nitrogen gas (>99.9%) was passed through a Nilox oxygen scrubbing apparatus before purging the redox vessel to maintain anoxic conditions. The redox electrode was a combination platinum/reference Ag/AgCl (Russell pH-Ltd, Auchtermuchty, U.K.).

2.7.3. Sample preparation for e.p.r. time course (chapter 6).

Time course samples were extracted from a temperature controlled water jacketted vessel into e.p.r. tubes under pressure of purging nitrogen gas. These samples were immediately frozen in an isopentane/methylcyclohexane mixture (4:1) which was pre-cooled to -150°C using a liquid nitrogen finger. Sample tubes were then stored at liquid nitrogen temperatures until reading in the spectrometer.

2.8. Purification of the pFRD84 plasmid from HB101.

The plasmid from the fumarate reductase overexpressing strain HB101/pFRD84 was purified for future transformation into other mutant strains (as discussed, chapter 4).

2.8.1. Plasmid purification.

Cells (HB101/pFRD84) were grown in 1l of luria broth, 100µg.ml^{-1} ampicillin at 37°C for 10hr. 0.15g of chloramphenicol was added and the cells were left to incubate (37°C) overnight. The harvested cell pellet was resuspend in 9ml Tris glucose buffer (50mM glucose, 25mM Tris/HCl, 10mM EDTA pH8.0), 4°C. Lysozyme (in 0.2M Tris/HCl pH8.0) was added to a final concentration of 2mg.ml^{-1} and the cells were left at 4°C for 10mins. At room temperature 20ml of NaOH/Sodium dodecyl sulphate (0.2M NaOH, 1% SDS, freshly prepared) was added and the solution shaken rapidly until clear and left on ice for 5mins. 10ml of chilled 5M acetate buffer (3M KOAc + 2M HAc) was added and left on ice for a further 10mins. The solution was centrifuged at 9000g for 15mins, 4°C, and the supernatant was poured through 4 thicknesses of cheesecloth onto an equal volume of isopropanol (in a centrifuge tube). The cheesecloth removes the larger chromosomal DNA and isopropanol precipitates DNA, RNA and proteins which pass through. The precipitate was left on ice or at -20°C for 30mins then centrifuged at 9000g for 15mins. The supernatant was removed and the pellet washed with 70% ethanol before re-centrifuging at 9000g for 15mins. The ethanol was poured off and the pellet air dried fully. The pellet was dissolved in 1ml TE (10mM Tris/HCl, 1mM EDTA, pH8.0) and placed in an Eppendorf tube (two tubes depending on the amount of precipitate). 1.2g of caesium chloride was added per ml TE and 0.4ml of a 0.5mg.ml^{-1}

ethidium bromide per ml of TE. Once the ethidium bromide (mutagen!) is added the sample tube was wrapped in aluminium foil to avoid exposure to light. This was left on ice for 20mins before spinning down fluoresence. The sample was pipetted into 1ml plastic tubes for caesium gradient centrifugation and centrifuged at 400000g overnight (or 650000g for 4hr) at 20°C. The plasmid band was extracted (lower band if there is chromosomal DNA contamination).

2.8.2. Butanol extraction to remove ethidium bromide.

The sample was pipetted into an eppendorf tube and 0.5-1.0ml butanol, saturated with caesium chloride, was added. The tube was shaken vigorously and microfuged for 20seconds (to sharpen the interface). The bottom layer was removed and placed in a fresh tube. This was repeated three times before checking the sample for lack of fluoresence under U.V.. The sample was then dialysed at 4°C against 500ml of TE changed several times over 6hr (removes caesium chloride). The DNA was precipitated by adding 2.5 volumes of ethanol and 1/15 volume of 5M sodium acetate (in TE), and left for 30mins at -20°C. The sample was microfuged and wash in 70% ethanol and pelleted.

The final pellet was resuspended in 100µl of ultrapure water and stored at -20°C.

2.8.3. DNA concentration.

The absorption spectra of the plasmid gave a DNA profile with a peak at 257.4nm (Fig.2.2). For 50µg.ml^{-1} DNA

Figure 2.2.

DNA optical absorbance spectra of purified plasmid pFRD84.

The optical absorbance spectra for the partially purified plasmid of *Escherichia coli* strain HB101/pFRD84, is shown. Concentration is 10μgml^{-1} in ultra-pure water. The peak is 257.4nm, 0.191 O.D..

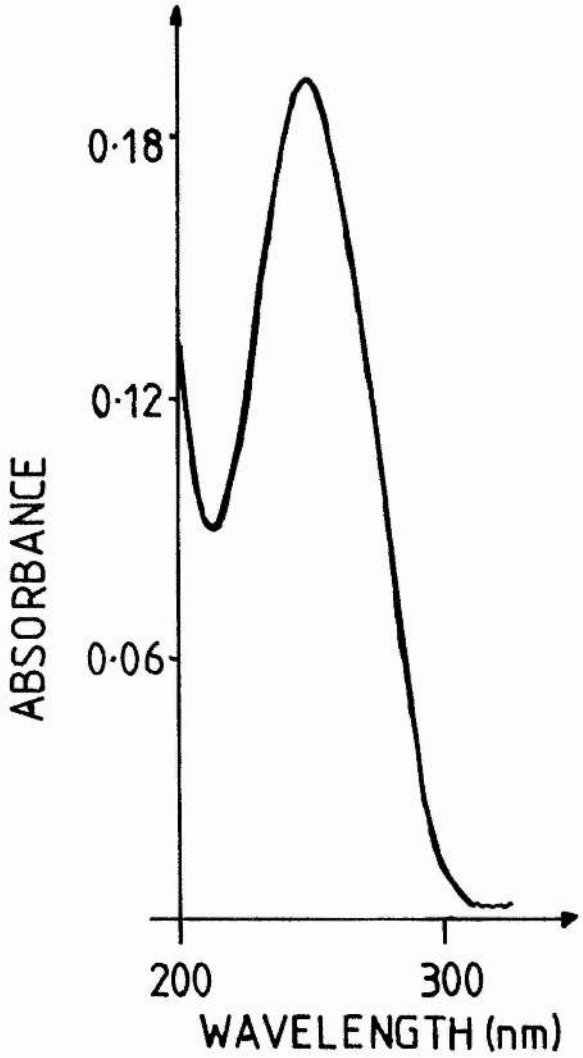
0·18
0·12
0·06
ABSORBANCE
200
300
WAVELENGTH (nm)

there is an expected 1.0 O.D. absorption change. From this the DNA concentration was calculated as 500ng.μl^{-1} in the stored sample.

To test for purification of the pFRD84 plasmid wild-type *E. coli* cells were transformed with the DNA and were found to have ampicillin resistance when plated.

2.9. Ubiquinone-2 synthesis (quinone derivative with a double isoprene unit).

FUN4/pNG2 levels of cytochrome-*bd* are amplified 10 fold by the multicopy plasmid compared to wild-type and the usual high ratio of ubiquinone-8 per oxidase complex (10:1) (Ingledew and Poole, 1984) will have reduced to nearer 1:1 in the amplified strains. This may reduce the maximal rates for dioxygen reduction in the amplified strains. Fumarate reductase of *Wolinella succinogenes* (Unden and Kroger, 1986) requires 10 times the level of quinone (vitamin K_1) compared to enzyme in reconstituted proteoliposomes if high rates of fumarate reduction are to be observed (in the steady state, c.f. chapter 4). A substitution for ubiquinone-8 must show a high degree of uptake into the membrane and so must be relatively lipophilic. From the data of Yu and Yu (1982) ubiquinone-2 (Q2) has the highest activity, at 100%, when substituted for Q10 of the mammalian bc_1-complex.

Q2 was synthesised to supplement membrane preparations. This included a collaboration with J.C.Salerno for freeze-quench work involving succinate-cytochrome c

reductase and quinone-cytochrome c reductase. The aforesaid work remains in its early stages and is not reported herein.

Synthesis of Q2 followed previous quinone derivative methods (R.B. Gennis, unpublished data; Yu and Yu, 1982; Shunk *et al.*, 1958).

2.9.1. Synthesis procedure.

All glassware was acid washed and the synthesis was performed within a fumehood.

1g of Q0 (2,3-dimethoxy-5-methyl-1,4-benzoquinone) was dissolved in 15ml 95% ethanol and 3ml 0.1M potassium phosphate pH7.5 was added. The mixture was reduced with dithionite until colourless then extract with 3x50ml ether. The ether extracts were combined and dried under a flow of nitrogen gas. The light yellow residue was dissolved in 15ml 1,4-Dioxane under a flow of nitrogen. To this 3g of powdered potassium bisulphate was added and the system was continually purged with nitrogen.

5ml of geraniol (3,7-dimethyl-2,6-octadien-1-ol) in 5ml of dioxane (useful solvent for both polar and nonpolar liquids) was add dropwise over several hours to the quinone under nitrogen and at 80°C. The mixture was cooled to room temperature and filtered (a fast paper filter). The solvents were removed from the filtrate by purging with N_2. The residue (which now contains 2,3-dimethoxy-5-methyl-6-(3',7'-methyl-2,6-octadienyl)-hydroquinone) was dissolved in 100ml ether. 5g silver(II) oxide and 2g of anhydrous $MgSO_4$ were added to this solution (silver(II) oxide acts as an

oxidizing agent forming the benzoquinone derivative or Q2 from the hydroquinone). The mixture was stirred overnight then filtered. The filtrate was concentrated in a rotary evaporator and the residue was dissolved in 100ml ether before extracting with 3x100ml water. The ether solution was dried over anhydrous ammonium sulphate then filtered and concentrated in a rotary evaporator. The 0.5g (approx.) of red oil was dissolved in a small volume of hexane.

The sample was then separated from contaminants by Florisil chromatography (an activated magnesium silicate column). The column (2cmx12cm) was packed with 60-100 mesh florisil. The sample was applied to the column and washed with 200ml hexane. Q2 was separated from brown contaminant by eluting the column with 2% ethanol in hexane and collecting the yellow elutant. This was dried to an oil under nitrogen and dissolved in 95% ethanol.

Q2 synthesis is shown for the absorption spectra of Fig.2.3. Reduced (borohydride) and oxidized (peroxide) spectra of both Q0 and Q2 are shown. A 10nm shift to 276nm gives the characteristic absorption peak for benzoquinones with isoprene units. The concentration of the sample was calculated from an extinction coefficient of $29.7 mM^{-1}cm^{-1}$ for quinone-hydroquinone in ethanol at 275nm (Brodie, 1963).

2.10. Chemicals.

Chemicals were purchased from Sigma Chemical Company

Figure 2.3.

Optical spectra of quinone-0 and quinone-2.

The upper spectra show peroxide oxidized (solid line) and borohydride reduced (dotted line) Q0 (2,3-dimethoxy-5-methyl-1,4-benzoquinone) used as a precursor for Q2 (2,3-dimethoxy-5-methyl-6-[3',7'-methyl-2,6-octadienyl]-benzoquinone) synthesis. The samples were dissolved in acidified (5mM HCl) ethanol; reduced peak, 288.2nm; oxidized peak, 287.4nm. The lower spectra show reduced Q2 (solid line), peak 278.4nm; oxidized sample (dotted line), peak 276nm.

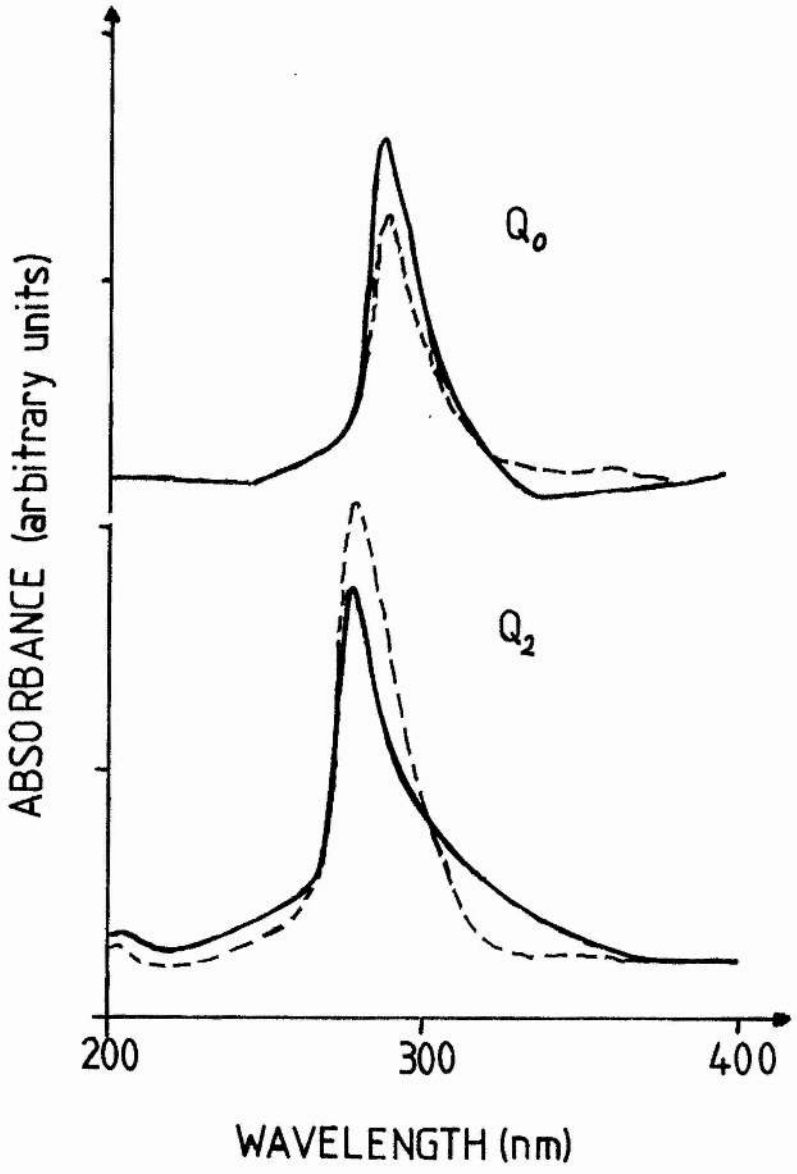
ABSORBANCE (arbitrary units)
Q_o
Q_2
200
300
400
WAVELENGTH (nm)

Ltd., Poole, Dorset,U.K.; Aldrich Chemical Company Ltd., Gillingham, Dorset, U.K.; BDH Ltd., Poole, Dorset, U.K.; Fluka Chemicals Ltd., Glossop, Derbyshire, U.K.; LabM, Bury, Lancashire, U.K.; Eastman Kodak Company, Liverpool, Merseyside, U.K.. Growth media for *E. coli* used general purpose graded chemicals, iso-pentane (BDH Ltd.) was general purpose grade, all other chemicals were of analytical grade.

Compressed gases were obtained through BOC Ltd., Guildford, Surrey, U.K..

2.11. Protocols of Chapters 3 & 5.

Chapter 3 presents methods which are a corporate part of the rapid-freeze quench technique.

Chapter 5 presents a protocol for analyses of oxygen electrode traces in conjunction with photodissociable affects for haem centres.

Chapter 3

THE DESIGN AND DEVELOPMENT OF A RAPID-FREEZE QUENCH APPARATUS TO BE USED IN CONJUNCTION WITH ELECTRON PARAMAGNETIC RESONANCE SPECTROSCOPY

Chapter 3

3.1. Introduction.

Rapid-freeze quenching is a technique which gives transient "frozen" redox and ligand bound states of an enzyme for application to discontinuous pre-steady state spectral analysis (see chapter 1). This apparatus was developed for application to freeze-quenching at -140°C. A test reaction for mixing-chamber efficiency applied room temperature chemical quench (section 3.5).

Only a handful of research groups have developed the freeze-quench technique because the protocol requires a specialized apparatus and the use of a readily available e.p.r. spectrometer.

In this study a basic ram system, similar to that of Gutteridge *et al.* (1978), is developed with the use of stainless steel HPLC parts to withstand the high pressures involved during the reaction event. The use of stainless steel tubing maintains the solutions under anaerobic conditions (when necessary) without the need for nitrogen gas jacketing of plastic tubing. The lack of flexibility of stainless steel tubing compared to plastic tubing was not found to be a handicap during experimental protocols. Also stainless steel tubes will not bulge under pressure, giving added uniformity to reaction times (although many of the newer plastics available claim to have this property). The syringe system is waterbathed for variable temperature work although all experiments in this project were carried out at room-temperature (22°C). The use of ice to slow reactions

would seem the most convenient method of temperature control in the system developed. Control of the ram system for the syringes was via computer interface to a BBC Microcomputer (Acorn Computers) as described.

The cryostat, to maintain iso-pentane at a constant -140°C, was developed to a more convenient and safer design than previously published temperature control devices (Bray, 1961; Ballou and Palmer, 1974; Hansen *et al.*, 1967). A fluted e.p.r. tube is maintained at -140°C enabling the reaction mixture to be fired into the iso-pentane while the tube remained held within the cryostat. The frozen sample is then packed down into the narrow bore e.p.r. tube, as described, and stored at 77K before analysis. The time between obtaining the sample and reading was kept to a minimum should there be electron transfer in the frozen state. Any such internal transfers are expected to be extremely slow when frozen (Palmer and Beinert, 1964) but samples were analyzed either immediately or within 24hr of preparation.

A continuous-flow system capable of observing transient e.p.r. signals at room-temperature was also developed although this was found to be unsuitable for either the flavin or menaquinone free radicals associated with fumarate reductase because of their fast e.p.r. relaxation rates. There is however the possibility of using this system in conjunction with other enzymes, e.g. *E. coli* nitrate reductase contains a *b*-type cytochrome and a molybdenum centre, with Mo being detectable at temperatures

as high as 300K (Palmer, 1985). As mentioned in chapter 1 molybdenum has been studied in xanthine oxidase by flow cells in the stopped-flow mode (Bray and George, 1985). Stopped-flow of slow reactions would theoretically appear to be possible with the continuous-flow cell presented herein.

3.2. The ram system.

The ram system was used both for rapid-freeze quenching into iso-pentane at -140°C, and for continuous-flow at room-temperature. As mentioned above the ram system (Fig.3.1a,b) is based on the system of Gutteridge *et al.* (1978) using a stepping motor and rotating threaded-worm to move the driving block. The syringe/mixing chamber assembly was developed for high pressure usage without leakage. The ram system housing was constructed by Mr. A. Shepherd (Workshop, Department of Biochemistry and Microbiology, University of St.Andrews). Computer programmed interfacing controls direction, speed and duration of each motor event.

A "Slo-Syn" stepping motor (A) (refer to Fig.3.1a,b) (Modulynx, Superior Electric, U.K.), capable of 400 steps per revolution and 1.12kg.m^{-1} torque, drives the threaded worm assembly (B). The stepping motor is connected in parallel to a bipolar 1054 stepping motor drive unit (PKS-Digiplan Ltd., Poole, Dorset, U.K.) via a four wire input. The drive unit is fitted with a 165 buffered clock card (Digiplan) which gives a sequence of clock (digital)

Figure 3.1

Ram system which actuates the syringes for rapid-freeze quenching and continuous-flow.

A schematic diagram of the ram system for the freeze-quench apparatus is shown. The principles involved are based on those of Gutteridge *et al.*, 1978.

a) The ram system is shown in side elevation.
   - A - stepping motor.
   - B - mounted threaded-worm assembly.
   - C - brass pushing block.
   - D - upper guiding rods.
   - E - microswitches.
   - F - rectilinear potentiometer.
   - G - perspex waterbath (used in this study as a housing for the mixing chamber assembly rather than temperature control).
   - H - syringe barrel holder.
   - I - brass support block for syringes.
   - J - hole in the base of "G" through which the reaction tube passes for firing into the freeze-quench tube.

b) The ram system is shown in plan view and is labelled as in Fig.3.1a. The insert shows an exploded view of the syringe holder, "H", as explained in the text.

a)

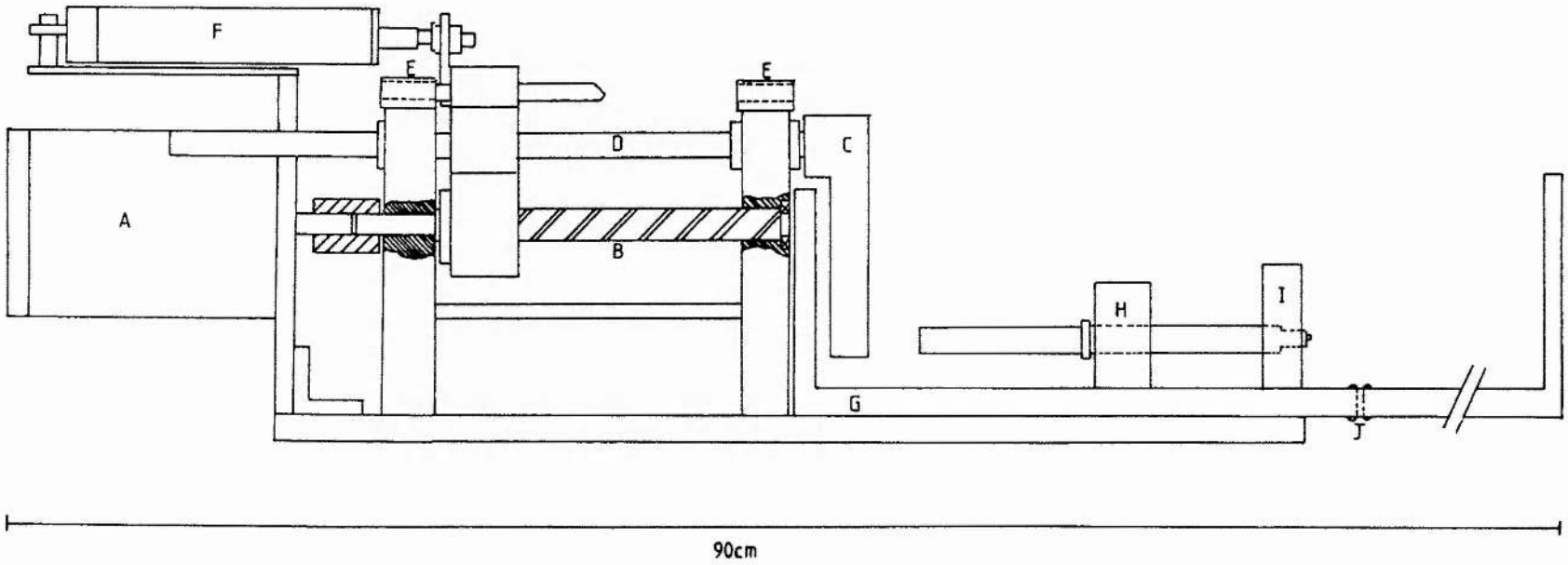

b)

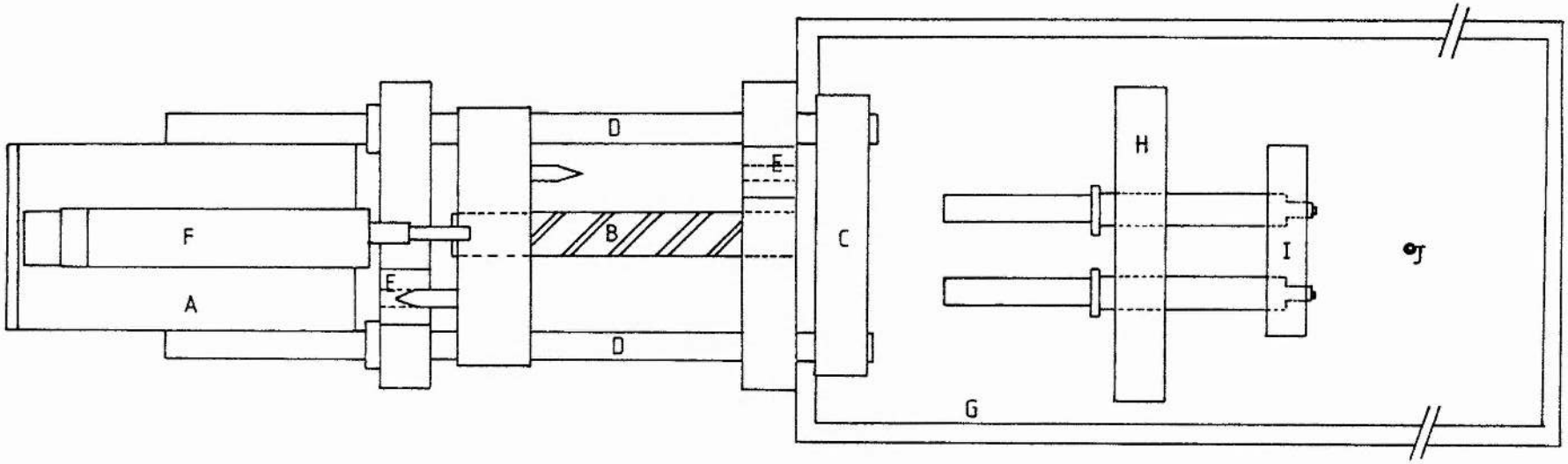

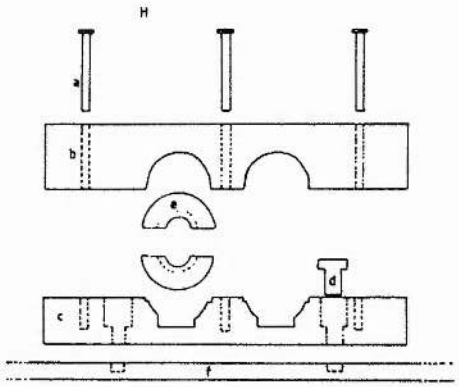

pulses delivered at a rate corresponding to the required motor speed (this prevents loss of synchronism in steps when varying speed). The controller is set for slow rates only (to prevent overload and/or damage to the ram system assembly). Electrical connections give control to rate and direction but not duration. For 'user-friendly' control the drive unit was interfaced to a BBC microcomputer via the 8-bit user port (the interface was constructed by Mr. A. Burnley, Department of Psychology, University of St.Andrews). Only 7 of the 8 bits are used to vary motor speed, giving 256 byte control in small increments, these bits also control direction and motor on/off. The 8th bit is used as a switch to activate the signal averager (when used in continuous-flow) simultaneously with the motor. The BBC Basic program written for control of motor speed, direction, and the duration of the event is given in appendix I.

The threaded screw assembly (B) is attached to the pushing block (C) via the upper guiding rods (D). The pushing block is prevented from overrunning by microswitches (E) which short circuit the digital input for the positive and negative motion limits of the drive unit. The motor performance was monitored by the rectilinear potentiometer (F) mounted on top of the ram system (see section 3.4). The perspex waterbath/syringe support area (G) is towards the front of Fig.3.1a,b and houses the syringe and mixing chamber assembly. The syringes are held at position "H", and pushed against the brass support block "I". The perspex syringe support "H" is shown in an exploded front view in

Fig.3.1b; the bottom plate "c" is fixed to the waterbath "f" ("G" in upper diagram) by two nylon screws, "d". The nylon half sections, "e" surround the syringe barrels and are changeable for the 2ml and 10ml syringe sizes. The cover "b" is gently screwed onto "c" with three brass screws, "a", securing the syringes in position.

The reaction tubing is passed through the hole, "J", for firing into the freeze-tube.

The mixing chamber assembly (Fig.3.2a) uses glass syringe barrels with luer-lock fittings (K); 2ml syringes for rapid-freeze quench studies, 10ml syringes for continuous-flow. The syringe plungers were constructed from stainless steel and fitted with two viton o-rings (L) to give a gas-tight fit. Pressures inherent in the system were calculated by Ballou (1971) to be >100psi, variable depending on tube length, diameter and the density of solution. The reaction mixture is drawn into the syringes via a 3-way teflon valve (M) (Omnifit, Cambridge, U.K.) connected to a glass filling chamber (N). The valves have zero internal dead space, are chemically inert and can withstand pressures of upto 500psi. The filling chamber includes addition and gas purging ports; a further vessel (not shown) was developed which could house a redox electrode and stirrer for potentiometric poising of samples prior to rapid mixing. All specialized glassware was constructed by Mr.C. Smith (Glassblower, Department of Chemistry, University of St.Andrews) unless otherwise stated. The mixing and flow devices were constructed from

Figure 3.2

a) Mixing chamber assembly.

The mixing chamber assembly, as positioned to the front of support block "I" of Fig.3.1, is shown. The upper diagram gives the side elevation, with the plan view below.

K - glass syringe barrels.

L - viton o-ring seals on stainless steel plungers.

M - 3-way teflon valve.

N - glass sample reservoir.

O - stainless steel T-mixer.

P - HPLC two-way valve.

Q - Stainless steel reaction tubes.

The individual components are described in the text.

b) Quartz glass continuous-flow cell for room-temperature e.p.r. studies.

The continuous-flow cell, as used directly in the e.p.r. cavity at room-temperature, is shown (see also Borg, 1964). The mixing chamber (R) is an integral part of the first section of the flat observation chamber. The offset entry tubes give an efficient mixing process. Internal dimensions for the cell portion are 40mm x 8mm x 0.25mm.

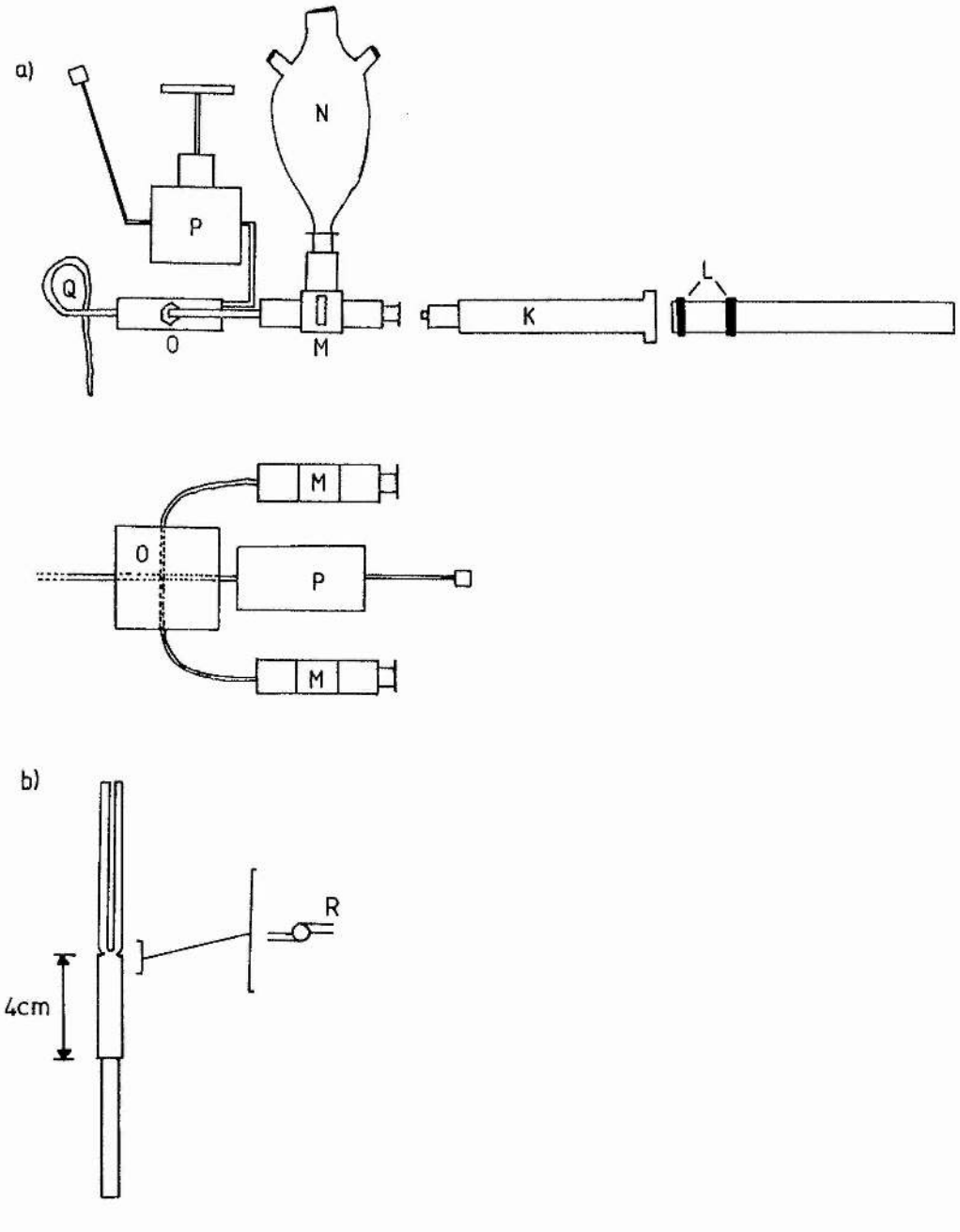
a)
N
P
Q
O
M
K
L
M
O
P
M
b)
R
4cm

stainless steel HPLC parts purchased from Anachem Ltd., Anachem House, Luton, Bedfordshire, U.K.. The mixing chamber (O) is a simple T-mixer where reactants mix in a zero dead volume chamber at a high velocity (calculated for a flow rate of $0.5ml.s^{-1}$ as $10m.s^{-1}$) and exit at 90^{0} to the entry at a higher velocity (two entry ports of same diameter as single exit port so $20m.s^{-1}$). This type of mixing chamber has been found to be highly efficient despite its simple design (Ballou, 1971). The chamber is a zero dead volume, four-way coupling cross (Cat. No. SG7455, Anachem Ltd.) with one exit closed off during mixing. The closed off exit is controlled by a two-way valve (P) (Cat. No. SG7001, Anachem Ltd.) and is used to purge the mixing chamber and reaction tube (Q) with nitrogen gas between each experimental run. Stainless steel HPLC tubing of internal diameters 0.0254-0.0762cm (Cat. Nos. U-105, U-106 and U-107, Anachem Ltd.) were used with a 0.0254cm diameter exit nozzle (half of capillary union junction Cat. No. U-412, Anachem Ltd.) to obtain a uniform fine spray for efficiency of quenching. A flow rate of $1ml.s^{-1}$ is routinely used with a time course obtained by varying tube length. Although the double-push method for obtaining longer reaction times (seconds) was not applied to the reactions studied in this project (short half-times) it could easily be incorporated into the computer program.

For chemical-quench, used here only as a test reaction (section 3.4), the reactants were quenched by direct firing into acid. For freeze-quench the reactants

were fired into iso-pentane at -140°C. In the latter, frozen crystal particles were of a size suitable for packing but were judged not to be so large as to hamper freezing efficiency (for photographs of sample crystalization see Bray and George, 1985). Two syringes delivering equal volumes of, for example, enzyme and substrate, to the mixing chamber were used in this apparatus. Variable volume delivery could be accommodated by slight modification of the syringe holder assembly although a more complex mixer than the simple "T" may be required.

3.3. The freeze-quench cryostat.

The cryostat was designed to maintain a freeze-quench vessel, which contains iso-pentane, at -140°C. The freeze-quench vessel comprises a short quartz e.p.r. tube (i.d. 3mm, ex.d. 4mm, length 7cm) connected to a fluted quartz glass tube by silicone tubing. The freeze-quench vessel was constructed in these two parts because breakage of the lower part of the vessel is a relatively common occurence. The junction was liquid tight and the silicone solidified upon cooling. Glycerol is smeared on the joint before assembly allowing ease of removal after packing (Ballou, 1971). The e.p.r. tubes are then stored in a conveniently narrower form when the funnel is removed. Extension of the small e.p.r. tubes for spectrometer reading was necessary for the Oxford Instruments cavity/cryostat. The extension piece involved a 3mm i.d. 4mm ex.d silicone

tubing bridge connecting the short tube and a quartz glass extension tube and an internal bridge of teflon tubing to align the two pieces as one. This assembly holds at liquid helium to room-temperature. A rubber stopper seals the top of the tube when it is under vacuum in the cavity.

To obtain a quenched sample the ram system was placed above the cryostat enabling the reaction mixture to be fired into the iso-pentane while the tube remained in the cryostat (see insert Fig.3.3). The reaction nozzle was placed approximately 1cm above the surface of the cooled iso-pentane. After freeze-quenching the ice particles are packed into the e.p.r. tube using a 3mm diameter steel plunger device based on the design of Bray and Petterson (1961), the plunger was precooled in liquid nitrogen. The e.p.r. tube, with sample, is stored under liquid nitrogen until used for spectrometer reading (within 24hr).

The cryostat was designed with the help of Mr. R.H.Mitchell, Department of Physics and Astronomy, University of St.Andrews (Mitchell *et al.*, 1973) and was constructed by A.S.Scientific Products Ltd., Abingdon, Oxon, U.K.. The principle of cooldown uses the flow of cold nitrogen gas to cool the small volume (50-60ml) of iso-pentane in the quench-tube. The apparatus (Fig.3.3) is constructed from stainless steel and is vacuum insulated at pump seal/port (type NW20), "A". The assembly is mounted directly onto a standard 35 litre narrow necked liquid nitrogen storage dewar using a hand nut and o-ring (BS No. 0445-30-perbunan) seal at "B". This assures minimum loss of

Figure 3.3

The freeze-quench cryostat.

A schematic diagram of the freeze-quench cryostat is shown. The cryostat maintains a quench-tube, filled with iso-pentane, at -140°C. The structure is made from stainless steel. The working structure is mounted at "B" into the neck of a liquid nitrogen storage dewar. The arrows show the direction of nitrogen gas flow from the lower heater, "E", to the upper blanketing ring, "L". The outline of a quench-tube is shown within the cage-assembly to the right of the main cryostat and an insert of the ram system/cryostat arrangement, as used during experimental protocols, is shown.

A - pump seal/port for applying an insulating vacuum to the system.

B - hand-nut and o-ring seal for a narrow necked liquid nitrogen storage dewar.

C - high pressure release valve.

D - outlet ball-valve.

E - lower heater and platinum temperature sensor.

F - heat exchanger.

G - upper heater and platinum temperature sensor.

H - open housing into which the support cage (shown to the right) is locked.

I - platinum temperature sensor.

J - multi-pin wiring socket for "G" and "I".

K - multi-pin wiring socket for "E".

L - blanketing ring for nitrogen gas.

M - ball-valve controlling gas input to "L".

N - teflon o-ring seal holding the quartz quench-tube in position.

O - adjustable metal plate for setting the height at which the quench-tube rests within the cryostat.

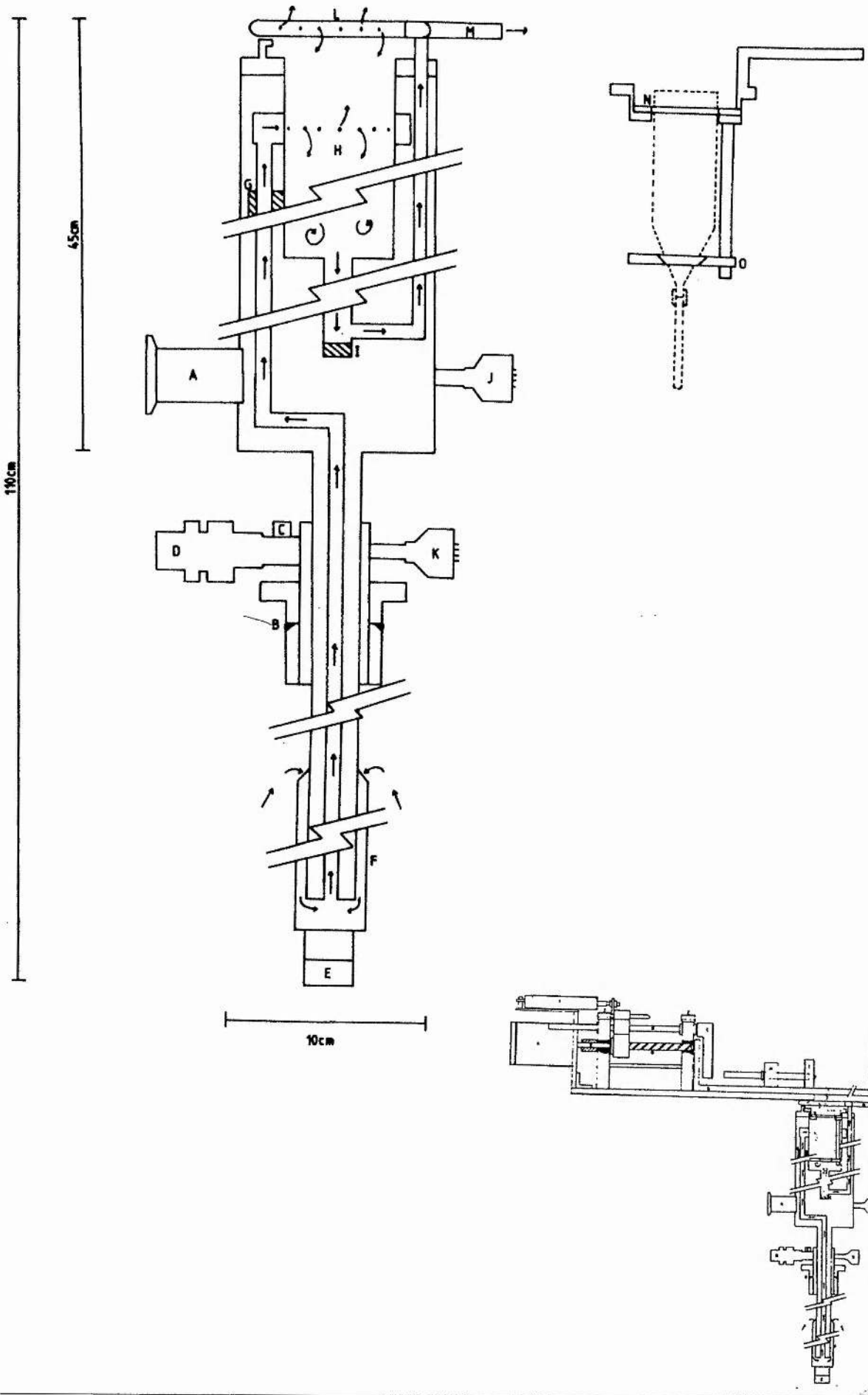
110cm
45cm
A
B
C
D
E
F
G
H
I
J
K
L
M
N
O
10cm

nitrogen with short distances travelled for efficiency of heat exchange within the system (c.f. Hansen *et al.*, 1967). The compact nature of the cryostat leads to ease of handling during the freeze-quench experimental protocols. A safety release valve (Circle Seal No. A532B-2M-4GN6), "C", is incorporated to prevent excessive pressure build-up in the dewar in the event of the upper outlet becoming blocked with frozen water vapour. There is also a 1/2 inch ball-valve outlet for $N_2(g)$ at "D" to prevent restriction in flow when the cryostat is first placed in the dewar. This outlet is closed before the lower heater (100W, 120V), "E", is operated. Heater "E" boils-off $N_2(l)$ in the dewar, this is monitored by a platinum temperature sensor (100ohm) connected via a relay switch to give digital readout (as resistance) and boil-off control. A safety cut-out is incorporated in the circuitry should the dewar empty, this is usually set to 0°C. The boil-off gas builds-up a slight pressure within the dewar and flows into the heat exchanger, "F", where it is recooled to almost liquid nitrogen temperature. The power of the heater is variable and determines the rate of cooldown. Arrows shown on the diagram give an indication of the nitrogen gas pathway through the cryostat. The second heater (100W, 120V) and platinum sensor (100ohm) located at "G" is for accurate temperature control of gas before it enters the open housing, "H", of the quench-tube support assembly. The main body of the quench-tube is cooled on all sides when cold gas flows into the top of the main chamber from a ring of small outlets.

When the cage-assembly, shown to the right of the main cryostat in Fig.3.3, is in position and contains the quench-tube, gas flows down around the narrow bore e.p.r. tube before rising back up and out of the cryostat. This allows for a more efficient cooling of the larger volume of iso-pentane in the flute without freezing the liquid in the base of the tube. A third temperature sensor (100ohm), "I", monitors the temperature at the lower extreme of the cooling area.

For one 35 litre liquid nitrogen storage dewar, filled with approximately 25 litres (initially) to prevent liquid nitrogen spitting into the upper housing, temperature control is +/- 1°C at -140°C over 20hrs. The temperature at "G" can be changed from -150°C to -100°C in 2.5mins then recooled to -150°C in a further 10mins, initial cooldown from room-temperature to -140°C takes 25mins. Flow rates at 60W consumed approximately 14litres N_2(g)/min given 1watt will boil-off approximately 0.35cc N_2(l)/min. Heaters "E" and "G" are rated at 100W, 120V although these can be changed if different rates of cooldown are required. The heaters are slowly brought to operating voltage using two variable resistors. Two multi-pin wiring sockets for heater and temperature sensor inputs/outputs are shown at "J" and "K".

The air gap between the reaction nozzle and the quench fluid is a potential oxygen contaminating region for anoxic freeze-quench experiments. To help maintain anoxic conditions at the quenching fluid the N_2(g), on exit from

the cryostat, can form a blanketing ring, "L", above the iso-pentane quench-tube. The restriction of gas at this exit point is controlled by a 3/8 inch ball-valve, "M". The iso-pentane can be bubbled with $N_2(g)$ from a cylinder during cooldown to purge oxygen. The temperature of the iso-pentane is further monitored with a type-K handheld thermocouple (RS Components Ltd., Corby, Northants, U.K., Cat. No. 151-186) and is cooled from room-temperature to -140°C in 10-15mins. The cage-assembly, shown to the right in Fig.3.3, holds the quench-tube in the main cooling area, "H", using a bayonet flange and silicone o-ring (BS No. 0616-24-silicon) seal. This seal is 4cm above the gas outlets for the open housing preventing the cage freezing in position. The cage is detachable for transport of the quench-tube in and out of the cryostat. The quartz quench-tube is sealed into the cage with a teflon o-ring, "N", and rests on an adjustable metal plate, "O". The handles of the cage were kept low above the blanketing ring allowing the mixing chamber assembly of the ram system to be placed directly above the cryostat. The outline of a quench-tube is shown within the cage-assembly of Fig.3.3. The insert of Fig.3.3 shows the arrangement of the ram system and cryostat together as used during freeze-quench experiments.

3.4. Ram system stepping motor efficiency.

The efficiency of the stepping motor was determined to set the limits of motor performance under operational

conditions. Acceleration and deceleration times are not instantaneous and were determined under free movement and full-load, pushing glycerol solutions. The wirewound rectilinear potentiometer mounted above the stepping motor is connected to the pushing block and gives variable voltage upon extension and contraction. The linear voltage produced upon movement of the pushing block can be monitored with a storage oscilloscope. These traces however only give a displacement profile (Fig.3.4a) for the motor, these were found to be linear for distance versus voltage under all loads, showing constant speed. To determine the acceleration and deceleration of the motor a velocity profile must be obtained by differentiating the input to the oscilloscope. The differentiation circuit (Fig.3.4) consists of a resistor and capacitor connected in parallel so that the timing of the circuit is in the low millisecond range. The time for the capacitor to charge or discharge must be small compared to the time to be resolved to prevent a delay in response. The timing circuit used had an RC (resistance multiplied by capacitance) of 6msecs which for $U=U_{\infty}(1-e^{-t/RC})^2$ gives a time for the capacitor to be fully charged of approximately 14msecs (Halliday and Resnick, 1978). The output from this circuit was amplified ten fold before it was monitored by the oscilloscope (see Fig.3.4b). Actual traces obtained gave acceleration and deceleration times of 50msecs. This was found to be a function of the motor and was the same under all loads. In freeze-quench experiments the syringes were always pushed for more than 1second which made the

Figure 3.4

Differentiation circuit for testing stepping motor efficiency.

The RC differentiation circuit, used in conjunction with the rectilinear potentiometer (c) (see Fig.3.1) and a storage oscilloscope (V), gave velocity and acceleration/deceleration profiles for the ram system stepping motor.

a) with the switch at "a" velocity profiles for the stepping motor are obtained as shown. This is a direct measurement of the voltage across the potentiometer. Linearity demonstrates constant speed.

b) with the switch at "b" the voltage across the resistor (30000ohm) is measured. When the motor starts there is a finite time between the zero voltage plateau and the new plateau for constant speed, this is the acceleration time. Equally, when the motor stops, there is a deceleration time. When the time to charge the capacitor (0.2μF) is not rate limiting the storage oscilloscope can record the acceleration/deceleration times. These were 50msecs under all load conditions, see text.

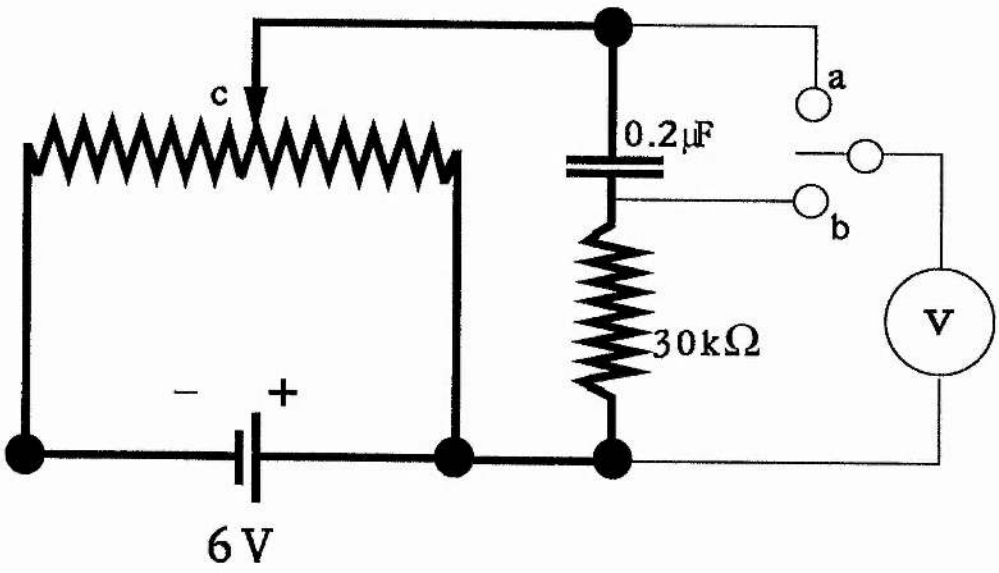
c
a
0.2μF
b
30kΩ
V
–
+
6V

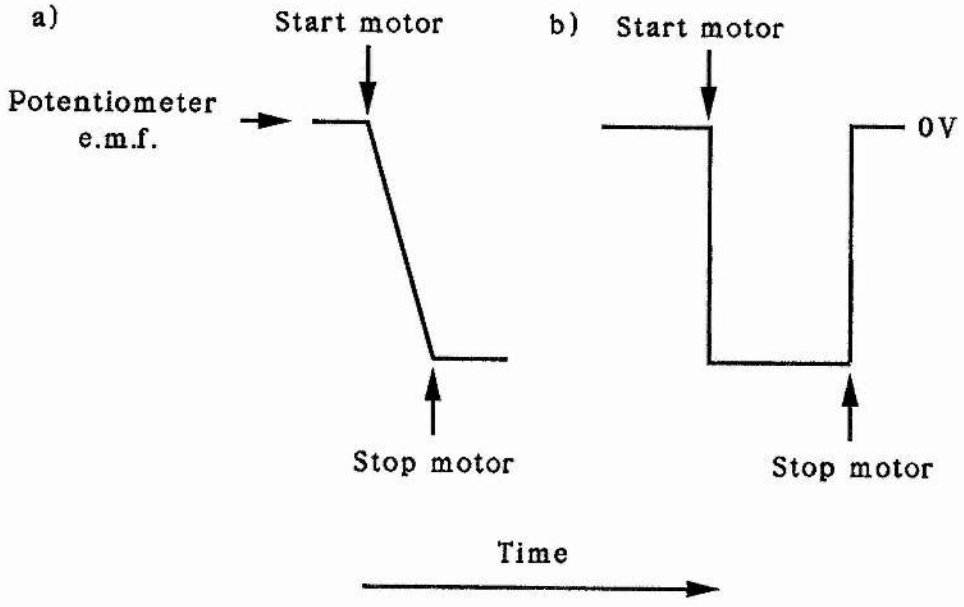
a)
Start motor
Potentiometer
e.m.f.
Stop motor
b)
Start motor
0V
Stop motor
Time

acceleration and deceleration times less than 10% of the total run time. For consistency of mixing and quenching tubing length was varied for different reaction times rather than varying flow rate. The flow rates used were $1ml.s^{-1}$ for timings between 20msecs and 235msecs, and $0.74ml.s^{-1}$ for the narrow bore tubing used for 10msecs. Higher flow rates of $8ml.s^{-1}$ were used in the continuous-flow cell. The equation to calculate the reaction times of the stainless steel tubing was :-

$$T_R = V_D \times (T_I / V_C)$$

where T_R is the reaction time to be calculated; V_D is the dead volume of the apparatus which is calculated from the dimensions (reaction chamber plus tube); T_I is the time interval used to discharge the syringes (always greater than 1second); and V_C is the volume of reactants collected.

3.5. Dinitrophenol acetate hydrolysis as a test reaction for the T-mixer efficiency.

The alkaline hydrolysis of 2,4-dinitrophenol (DNP) acetate under pseudo-first order conditions was a suitable chemical reaction for testing the efficiency of mixing (Barman and Gutfreund, 1964). The absorbance of dinitrophenolate liberated was monitored at 360nm with concentration determined from an extinction coefficient of $0.88\ M^{-1}cm^{-1}$, pH4.0. DNPacetate, 1.25mM in 5mM HCl (from a stock solution of 12.5mM DNPacetate in isopropanol) gave a pseudo-first order reaction when mixing 1:1 with sodium

hydroxide of around 0.5M. The second order rate constant for this reaction has been published as 50-60 $M^{-1}s^{-1}$ (Barman and Gutfruend, 1964; Kroger and Klingenberg, 1973); for a pseudo-first order reaction this gives half-times of around 20msecs when $t_{1/2}=\ln 2/k_{app}$ and $k_{app}/k_2=[NaOH]$ (k_{app} is the psuedo-first order rate constant and k_2 is the second order rate constant). Reaction times used in this determination vary from 10msecs to 91msecs. The reaction is quenched by firing into 1.5M HCl; the quenched solution is brought to pH4.0 (for analysis at 360nm) by the addition of 5M potassium acetate buffer, pH5.0. The reaction profile is plotted as a decay by plotting O.D. at reaction completion (reacted for several minutes) minus the O.D. at the set time intervals as the ordinate and time as abscissa (Fig. 3.5). The O.D. was measured against a blank of the reaction mixture to which 5M potassium hydroxide had been added not acetate buffer. The best-fit first order lines for the points gave second order rate constants of 78 $M^{-1}s^{-1}$, 76 $M^{-1}s^{-1}$ and 74 $M^{-1}s^{-1}$ for NaOH concentrations of 0.474M, 0.63M and 0.8M respectively (before mixing). The concentration of hydroxide was determined accurately by titration. The points were fitted using a pattern search program written by R.J.Benyon; this program was adapted for first order decay by implementing:-

$$A_t = A_0 \times \exp(-k_{app}t)$$

where A_t is the ordinate value for time t, A_0 is the ordinate value at zero time and k_{app} is the apparent first order rate constant. These best-fits gave dead times for

Figure 3.5

Chemical-quench reaction to test mixing chamber efficiency: dinitrophenol-acetate alkaline hydrolysis under pseudo-first order conditions.

The O.D. at reaction completion minus the optical O.D. at set quenching time intervals is plotted versus time. Best-fit lines are for first order decay. Three sets of data are given with OD_{max} at 1.3 showing the dead-time to the best-fit lines. Experimental conditions were; 1.25mM DNPacetate in 5mM HCL mixing with, (●) 0.474M NaOH, (○) 0.63M NaOH, (□) 0.8M NaOH in 1:1 ratios. Quenching in 1.5M HCl before adjusting to pH4.0 with 5M acetate buffer pH5.0. Absorbance was determined at 360nm.

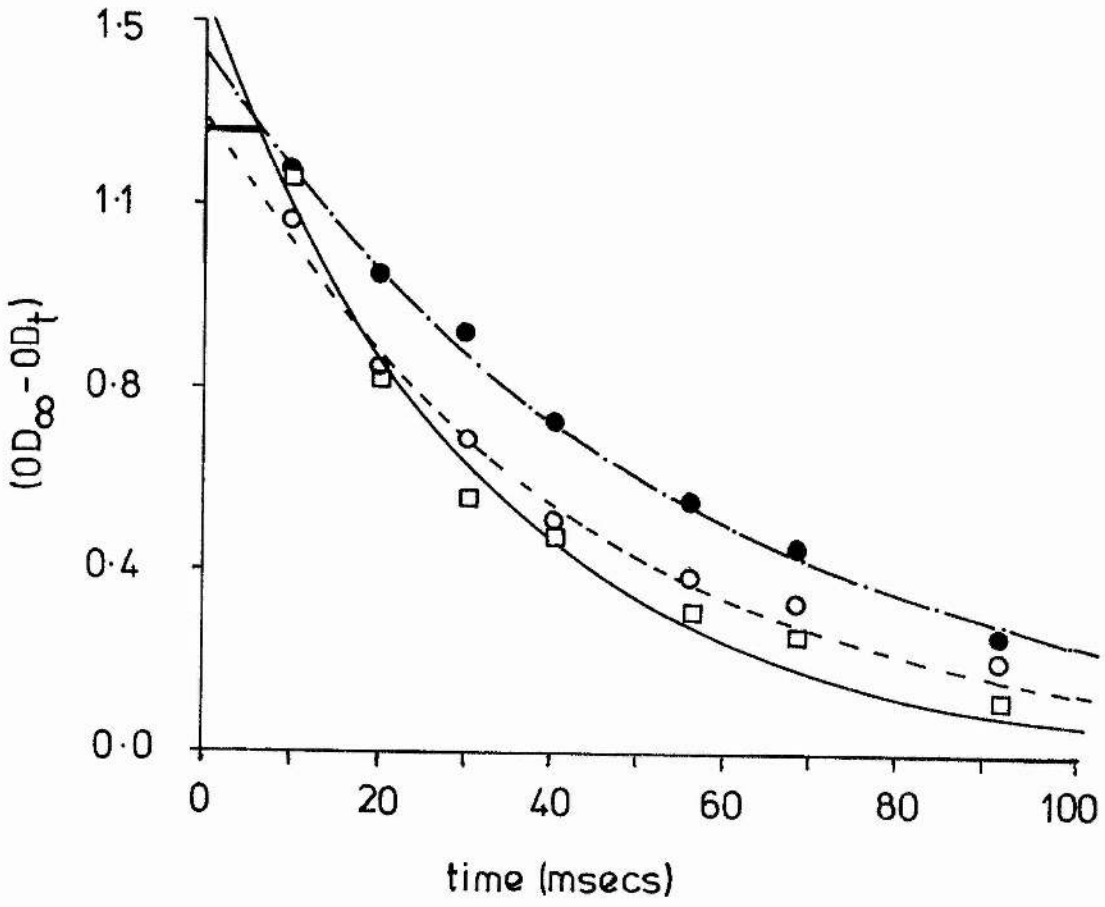
1·5
1·1
0·8
0·4
0·0
$(OD_\infty - OD_t)$
0
20
40
60
80
100
time (msecs)

mixing and quenching of between 1 and 5msecs for the maximum O.D. obtained for the reaction, 1.3. Acid quenching is often reversible in enzyme solutions and so should be used with care if analysis involves a change of pH towards neutrality.

Enzyme solutions are more viscous than the above test reaction so may decrease the efficiency of mixing in quenching studies. Ballou (1971) found this not to be the case when using glycerol solutions. Ballou also found the simple T-mixer to be highly efficient and comparable in mixing efficiency to more complex multi-jet mixers.

3.6. Freezing efficiency in iso-pentane following azide binding to oxidized ferrimyoglobin.

The freeze-quench apparatus was tested for the freezing efficiency of the pre-cooled iso-pentane by following the binding of azide to oxidized myoglobin (Ballou and Palmer, 1974). The high and low-spin signals attributable to azide binding were followed by e.p.r. spectroscopy. The reaction has a reported second order rate constant of 2.5×10^3 $M^{-1}s^{-1}$ at pH7.5, 25°C (Ballou and Palmer, 1974). For a pseudo-first order $t_{1/2}$ of 20-30msecs a sodium azide concentration of 11mM is required in the reaction mixture. Syringe 1 contained 20μM ferrimyoglobin in 0.1M potassium nitrate, 20mM Tricine, pH7.8. This is mixed 1:1 with syringe 2 which contained 22mM sodium azide in 0.1M potassium nitrate, 20mM Tricine, pH7.8. Potassium nitrate maintains myoglobin in the high-spin ferric form before

mixing with azide. The loss of the high-spin g=5.96 resonance was followed during the time course. The product is the low-spin azide complex with signals at g_x, g_y and g_z of g=1.82, 2.21 and 2.81, respectively; these are similar to previously published values (not shown, Knowles *et al.*, 1976). E.p.r. conditions were, for the high-spin g=5.96 resonance: temperature, 10K; microwave frequency, 9.47GHz; microwave power, 22.8mW; modulation amplitude, 2mTesla; modulation frequency 100kHz, and for the low-spin spectra the above settings were used at a temperature of 15K. Fig.3.6 shows data for the high-spin peak height plotted as ordinate against time (the average of two determinations is shown). The points show a good fit to the equation for first order decay described in section 3.5. From k_{app}/k_2 = [azide], when k_2 is the second order rate constant, $k_2 = 2.70 \times 10^3\ M^{-1}s^{-1}$ at pH7.8, reaction temperature 22°C. The dead-time of mixing and freezing was taken as the intersect of the signal height for zero time mixing (no azide) with the fitted line. This gave a value of 6+/-3msecs for mixing in the T-mixer plus freezing in iso-pentane. The error limit is a calculated maximum for the air gap distance between the reaction nozzle and the iso-pentane.

Figure 3.6

Rapid-freeze quench test reaction for mixing chamber plus iso-pentane freezing efficiency: sodium azide ligand binding to ferrimyoglobin.

The freeze-quench cryostat and the mixing chamber were tested to determine the dead-time for mixing plus freezing. 22μM ferrimyoglobin was mixed 1:1 with 22mM sodium azide (both in 0.1M potassium nitrate, 20mM Tricine pH7.8). The points show high-spin signal height (g=5.96 peak to low field baseline) variation with time. The line through the points is a best-fit first order decay. Dead-time for mixing plus freezing is shown as the intersect of the zero time signal height with the best fit line, giving approximately 6msecs. The points are an average of two determinations. The reaction was at 22°C. E.p.r. conditions are given in the text.

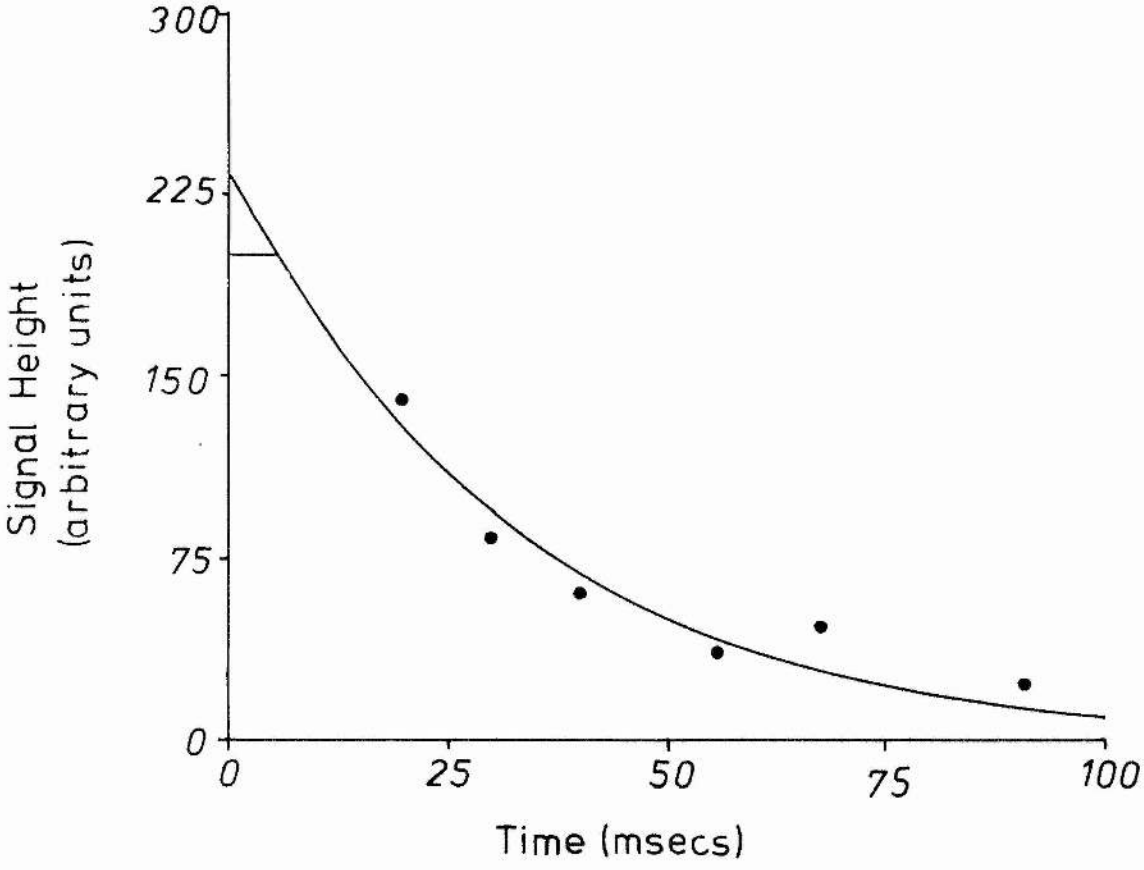
300
225
150
75
0
Signal Height
(arbitrary units)
0
25
50
75
100
Time (msecs)

3.7. Continuous-flow cell efficiency: ascorbic acid free radical formation and diminution.

The flow cell (Fig.3.2b) designed for use within the e.p.r. spectrometer cavity was similar to the design of Borg (1964). The mixing chamber (R) is an integral part of the flat cell portion giving a short dead time for observation 3msecs after reaction initiation. Dielectric absorption due to lossy samples (aqueous) has been kept to a minimum by improving the design of the flow cell. A liquid thickness of only 0.25mm is presented to the microwave cavity. Flow rates of 0.5-->8.0ml.s^{-1} are used to give timing intervals of 40-->3msecs 1cm from the mixing chamber. The flow cell is 4cm long enabling longer time intervals after mixing to be obtained. The cell is connected to the ram system syringes via teflon lined stainless steel tubing.

The flow-cell was tested in the e.p.r. spectrometer following the disproportionation of ascorbic acid free radical. Syringe 1 contained 0.03M ascorbic acid which was mixed 1:1 at room-temperature with syringe 2, 0.03M cerium sulphate in 0.1M sulphuric acid. Upon mixing, ascorbic acid is oxidized and a free radical signal is produced. This radical is only transient and decays in a second order manner at pH1-2 (Klimes *et al.*, 1980). The radical gave e.p.r. spectral peaks at g=2.0032 and g=2.0020 although these will have been distorted by the rapid sweep time necessary for observation. The e.p.r. spectra for the time course are shown in Fig.3.7. The signal was collected by

Figure 3.7

Continuous-flow e.p.r. spectra showing ascorbic acid free radical decay.

An e.p.r. time course for ascorbic acid free radical decay is shown. The continuous-flow cell (Fig. 3.2b) mixed 0.03M ascorbic acid with 0.03M cerium sulphate in 0.1M sulphuric acid. Time in milliseconds is shown to the right of the spectra with the g-values for the radical split-peak given below. The g-values will have been distorted by the fast sweep time. E.p.r. conditions were: microwave frequency, 9.77GHz; modulation frequency, 100KHz; modulation amplitude 0.2mT; microwave power, 7.4mW. The spectra were recorded by a signal averager as described in the text. Temperature, 22°C.

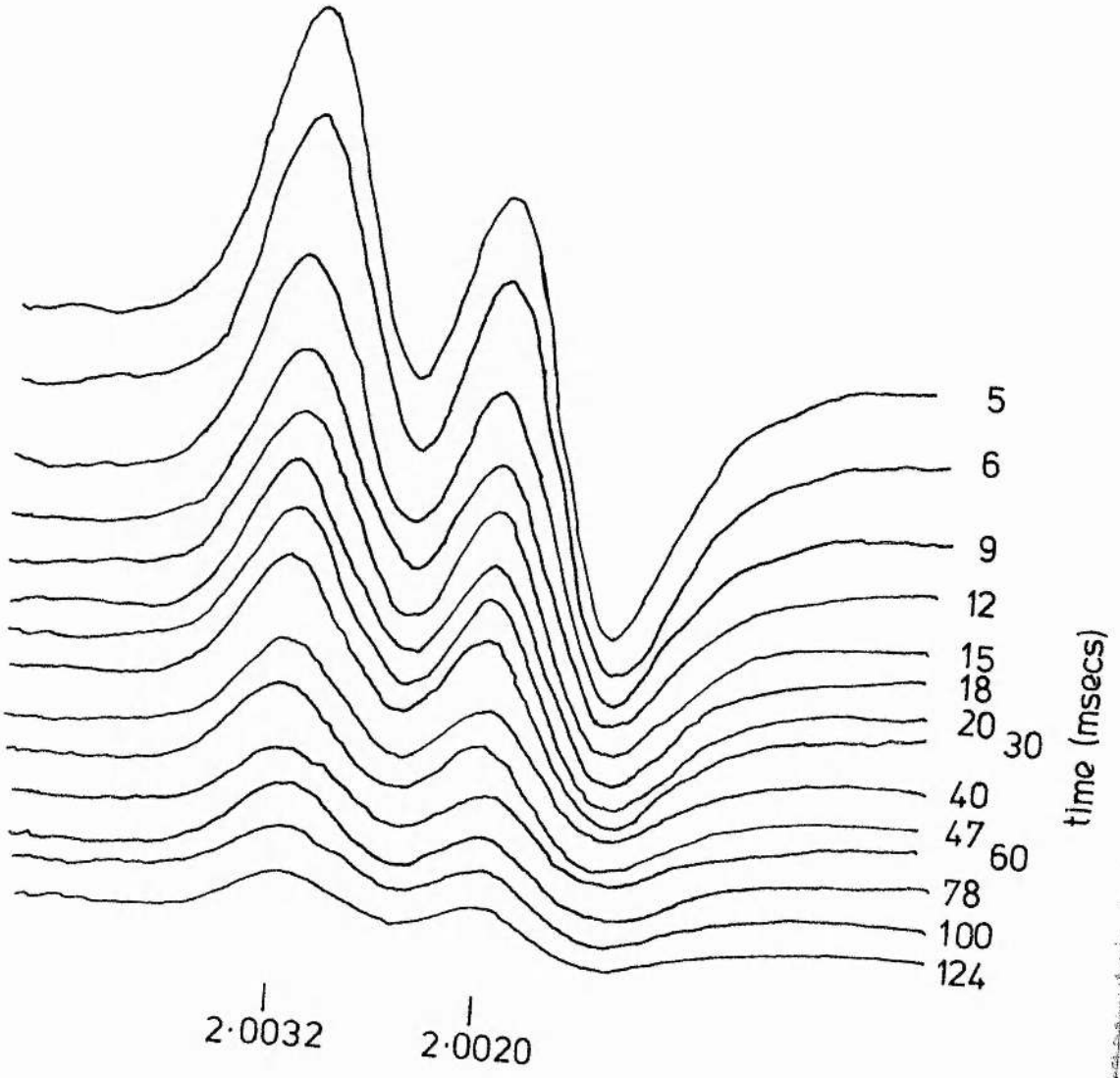
5
6
9
12
15
18
20
30
40
47
60
78
100
124
time (msecs)
2·0032
2·0020

summation averaging in a signal averager collecting one hundred 2mTesla sweeps each of 20msecs, total duration of event was three seconds (using a spectrometer time constant of 0.1msec).The signal height versus time is shown in Fig.3.8. The points are fitted to a second order best-fit line for a single component decomposition (a special case for second order where only one reacting species is initially involved). This equation takes the form of:-

$$A_t = A_0 / (1 + ktA_0)$$

where A_0 is the starting value on the ordinate at time=0 and A_t is the ordinate value at time=t, k is the second order rate constant; this equation was applied to the pattern search program of section 3.5. A concentration standard of benzyl viologen reduced with saturated dithionite solution was used to determine the concentration of the ascorbic acid free radical at t=0msecs. This gave a starting free radical concentration of 1.45mM with a second order rate constant of 6.9×10^4 $M^{-1}s^{-1}$. The first half-life is found from $t_{1/2}=1/(k_2 \times$ concentration of radical) and is calculated as 10msecs this is the same value as found by Klimes *et al.* (1980). The flow cell mixer has almost zero dead volume being part of the flat observation chamber, inefficiency in mixing at the slower flow rates (>20msecs) are assumed to be small because of the good fit to the second order curve. Visual mixing tests using 40mM HCl saturated bromophenol blue mixing with 0.1M NaOH showed slight streaming down one side of the flow-cell at lower flow rates, this was a small percentage of the area presented in the e.p.r. cavity.

Figure 3.8

The data of Fig.3.7 plotted and fitted to a second order decay.

Signal height (◯) of the g=2.0032 peak/trough versus time is plotted for the decay of ascorbic acid free radical as shown in Fig.3.7. The points are fitted to a second order decay process for a single species.

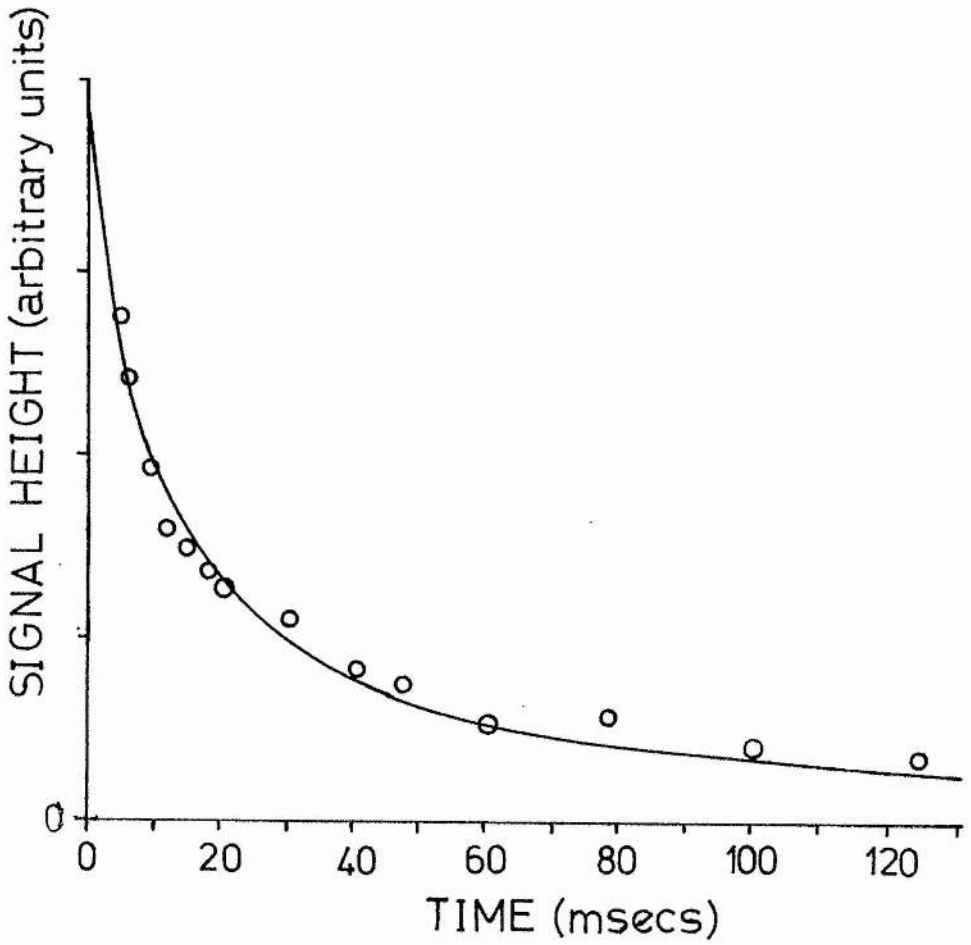
SIGNAL HEIGHT (arbitrary units)
0
0
20
40
60
80
100
120
TIME (msecs)

The flow-cell designed would be suitable for stopped-flow mode although reactions studied must be relatively slow as the ram system takes 50msecs to stop (section 3.4). Bray and George (1985) have exploited the use of "slow" substrates of xanthine oxidase in their e.p.r. stopped-flow studies.

3.8. Conclusions.

A rapid-freeze quench apparatus has been designed and constructed for discontinuous pre-steady state spectral analysis. The apparatus has been fully tested and shown to be suitable for kinetic analysis. The limitations of the apparatus and the inherent errors associated with this specialized technique are outlined. A simple T-mixer was found to be an efficient mixer giving a dead-time for mixing plus freezing of around 6msecs, the limit for error in timing values for all samples was calculated as +/-3msecs. A continuous-flow cell for room-temperature e.p.r. studies was presented. The cryostat designed is safer and more convenient to use than its predecessors than previously published temperature control devices for rapid-freeze quench studies (Bray, 1961; Hansen *et al.*, 1967; Ballou and Palmer, 1974). The design shown maintains an iso-pentane filled quench-tube at -140°C +/- 1°C. The cryostat requires no experimenter attention to sustain set temperatures over several hours. Freeze-quench protocols can be easily modified for use with other spectroscopic techniques and a

freeze-quench cell (not shown) has been developed for EXAFS (extended X-ray absorption fine structure) analysis in a present collaboration with the Science and Engineering Research Council EXAFS Station, Daresbury, U.K..

The expenditure for the complete apparatus has been <£5000 (1990 prices).

Chapter 4

ESCHERICHIA COLI MENAQUINOL-FUMARATE OXIDO-REDUCTASE: E.P.R. STUDIES

Chapter 4

4.1. Introduction.

Chapter 1 (section 1.2) outlined the experimental data presently available for *E. coli* menaquinol-fumarate oxido-reductase. The introduction also presented the model systems which have been proposed for this enzyme. The aim herein was to test these models experimentally.

The transfer of electrons from bound menaquinol to FR3, FR1 and FAD, then reducing fumarate to succinate, is proposed as the transfer sequence, this is in accordance with available e.p.r. data for spin-spin interactions (see chapter 1).

A *b*-type cytochrome was not detected and the role of FR2 remains ambiguous.

4.2. A b-type cytochrome associated with Escherichia coli fumarate reductase?

A *b*-type cytochrome has not been identified in *E. coli* fumarate reductase and yet is necessary for the high potential/low potential pathways proposed by Cammack and co-workers (see chapter 1).

The non-identification of cytochrome content may be a function of the fumarate reductase amplified strains if haem synthesis is not maintained at the high levels necessary for amplification or the haem is not constituted into the holoenzyme (or anchor subunits).

Haemin is coordinated as a cytochrome in the fumarate

reductase of *Bacteriodes fragilis* when grown on a haemin supplemented media (Macy *et al.*, 1975). Unfortunately the cytoplasmic membrane of *E. coli* is impermeable to haemin (Sasarman, *et al.*, 1968; McConville and Charles, 1979a,b), and as such haemin cannot be taken into the cell to act as a haem substitute.

The reconstitution of functional *b*-type cytochromes in membranes of a 5-aminolaevulinic acid-requiring mutant of *E. coli* has been detected spectrophotometrically (Haddock and Schairer, 1973; Reid *et al.*, 1981). This approach was applied to the amplified fumarate reductase membranes.

Membrane particles of HB101/pFRD84 (50mg.ml^{-1}, 0.1M BES, pH7.0) were incubated with 100µM haemin, 2mM ATP, 2mM $MgSO_4$ for 10mins to 1hr at 37°C. E.p.r. spectra of air oxidized samples in the low-spin g=3.0 region showed no increase in the low-spin signal intensity associated with six coordinate b-type haems (15K, 16.3-5.3mW, not shown). Spectrophotometric analysis of the reduced and oxidized absolute spectra were obscured in the 560nm region by the ubiquinol oxidase cytochrome-*bd* (haem-b558) but there was no apparent increase in intensity for any of the signals observed (not shown).

It was concluded that fumarate reductase membranes did not reconstitute haemin as a cytochrome and no cytochrome has yet been identified for *E. coli* fumarate reductase. The theoretical advantages of cytochrome association have been discussed (chapter 1). An electron transfer arm from a periplasmic quinol binding site to the

cytoplasmic FR3 (transmembrane electron transfer) would be advantageous for proton-electrochemical gradient formation (vectorial transfer). A low potential pathway for electron transfer is not consistent with the midpoint potential of the *b*-type cytochrome associated with *E. coli* succinate dehydrogenase. This cytochrome is associated with the anchor subunits, has a reported E_{m7} value of +36mV, and is fully reduced in the presence of succinate (Kita *et al.*, 1989).

Cytochrome content of *E. coli* fumarate reductase remains undefined. The cytochrome affiliation is thought to exist because of comparisons with other fumarate-succinate oxido-reductases.

To identify this elusive cytochrome future experimentation may need to concentrate on molecular biology applications. Transforming plasmid pFRD84 (fumarate reductase) into *E. coli* strain FUN4, which lacks both of the ubiquinol oxidases cytochrome *-bd* and *-bo* may facilitate spectroscopic cytochrome identification. The selective use of available *E. coli* mutant strains is now recognised as a necessity, rather than an advantage, if rapid advances in biophysical studies are to be made.

4.3. Fumarate reductase: rapid-freeze quench studies.

4.3.1. Succinate-oxidase activity.

The fully reduced and fully oxidized e.p.r. spectra for the iron-sulphur centres of fumarate reductase are shown

in Fig.1.2. Membrane bound fumarate reductase was applied to rapid-freeze quench studies to determine the pre-steady state internal electron transfers for the prosthetic groups.

The reduction/oxidation rates for centres was found to be towards the kinetic limit of resolution for flow techniques (low millisecond range). This was also predicted from the extrapolated steady-state data which suggests a maximal turnover for fumarate reduction by benzyl viologen of $30s^{-1}$ (Simpkin, 1985). From oxygen electrode studies membrane particles of the fumarate reductase amplified strain (HB101/pFRD84) have high levels of succinate dehydrogenase activity, fumarate reductase operating as the dehydrogenase. The main oxidase predominating in anaerobically grown cells was cytochrome-*bd*. The reductase could therefore be studied in the succinate dehydrogenase mode as a direct comparison to the mitochondrial succinate dehydrogenase freeze-quench data of Beinert *et al.* (1975).

A reduction/oxidation time course for FR1 and FR3 was obtained by mixing HB101/pFRD84 membrane particles (approximately $25mg.ml^{-1}$, 50mM BES, 5mM EDTA, pH7.0) with 60mM sodium succinate (in the same buffer).

This first time course highlighted areas of the technique which required improvement but was successful in showing variable oxidation/reduction states for fumarate reductase.

Samples were obtained from 0msecs (mixing with buffer only, no succinate) to 229msecs. Syringe 1 contained etp plus 30uM 1,4-naphthoquinone 2-sulphonate (as mediator), the

vessel contents were first poised at -300mV (aliquots of a strongly buffered dithionite solution) to inactivate oxaloacetate inhibition of the enzyme. The sample reservoir for syringe 1 was then poised 'oxidized' with ferricyanide at +140mV (redox electrode reading), the vessel was continually purged with nitrogen gas (through a Nilox oxygen scrubber) to maintain 'anoxic' conditions. From the zero time sample (not shown), mixing syringe 1 with buffer (no succinate) the centres were not oxidized but at least partially reduced. The redox electrode meter reading of +140mV was incorrect, most probably due to a lack of mediation when only one redox dye was present. Also, from comparison to later samples, the contents of syringe 2 (60mM sodium succinate in 50mM BES, 5mMEDTA, pH7.0) were not anoxic but oxygen contaminated, the 'zerotime' sample could not therefore be plotted as part of the time course.

Fig.4.1a & c show e.p.r. spectra for the 14msec sample FR3 and FR1 signals at 10K, 16.3mW and 30K, 5.2mW, respectively. Comparing these spectra to Fig.4.1b & d, the 146msec sample, both FR3 and FR1 are oxidized during the time course (from the zero time sample the initial states for FR3 and FR1 were at least partially reduced which was confirmed by comparison to the freeze-quench data of section 4.3.3). Fig.4.1e shows the e.p.r. spectra (30K, 5.2mW) for a freeze-quench sample of dithionite reduced syringe 1 mixing with buffer (excess dithionite). Dithionite reduced FR2 does not contribute significantly to the FR1 spectral lineshape under non-saturating conditions (30K, 5.2mW, Fig.4.1e)

Figure 4.1

Fumarate reductase rapid-freeze quenching: e.p.r. spectra for succinate-oxidase activity.

E.p.r. spectra are presented for the freeze-quench succinate-oxidase function of HB101/pFRD84 membranes with amplified levels of fumarate reductase (section 4.3.1).

a) e.p.r. spectra in the g=2.00 region for the 14msecs sample. E.p.r. conditions were: microwave frequency, 9.45GHz; modulation frequency, 100kHz; modulation amplitude, 1.0mTesla; microwave power, 16.3mW; temperature, 10K.

b) 146msecs sample for succinate-oxidase activity. E.p.r. conditions as in a).

c) 14msecs sample a) at temperature, 30K; microwave power, 5.2mW.

d) 146msecs sample b) at temperature, 30K; microwave power, 5.2mW.

e) Fully reduced freeze-quench sample mixing dithionite reduced membranes with buffer only. E.p.r. conditions as in d).

Peak g-values are shown above, and the relative gain increases are shown to the right of, each spectra. The low field peak is due to contaminating copper (Cu) and/or the cavity signal. Iso-pentane packing ratio 50%. Protein concentration for all samples approximately 6mg.ml^{-1}.

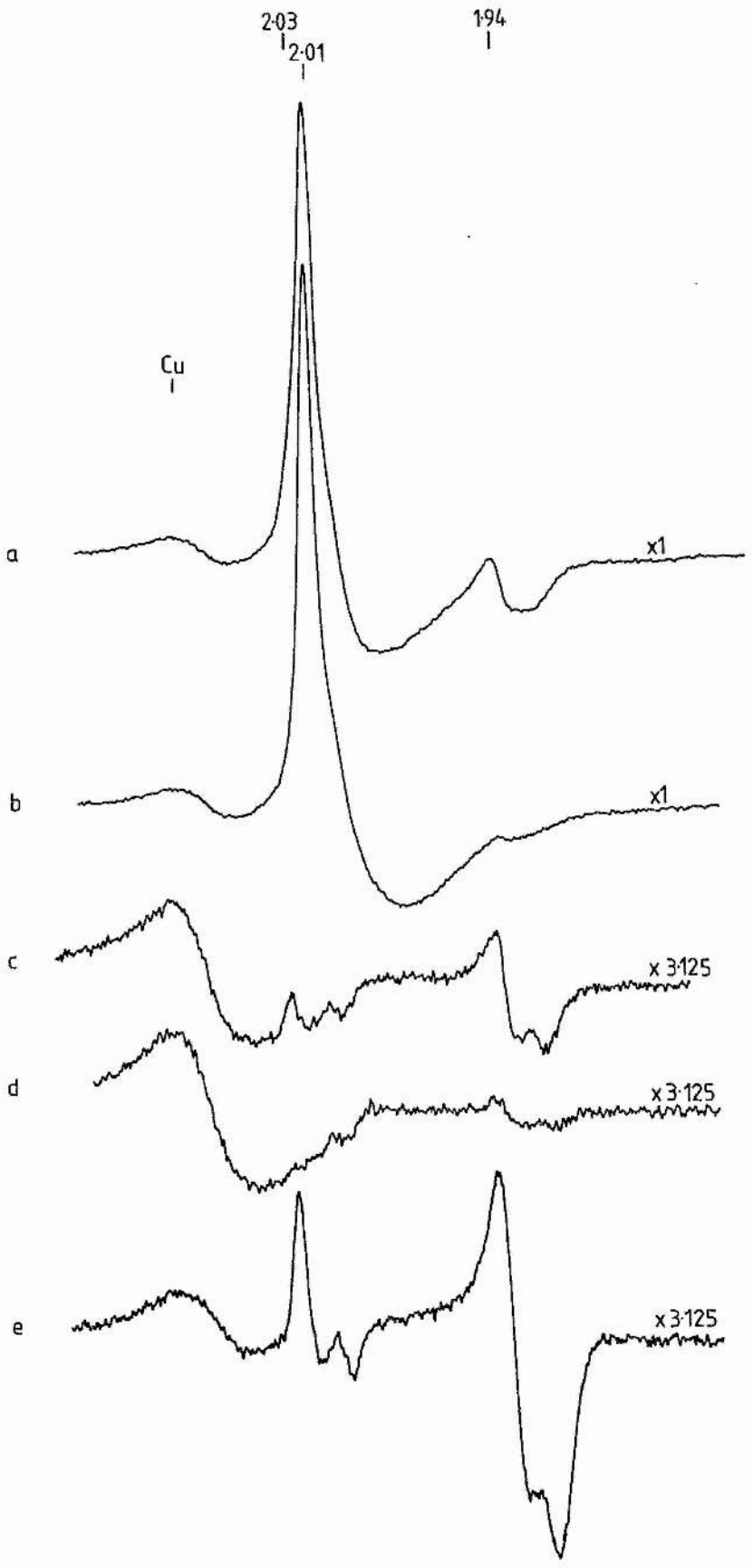
2·03
2·01
1·94
Cu
a
x1
b
x1
c
x 3·125
d
x 3·125
e
x 3·125

resulting in this spectra showing fully reduced FR1 only. No FR3 signal was observed for the dithionite sample at lower temperature (10K, 16.3mW, not shown), FR2 contributions to the spectra were observed as an increase in signal height for saturating FR1 e.p.r. conditions. The low field peak of Fig.4.1 is due to the cavity signal and/or contaminating copper. Although the etp sample was originally, at least, partially reduced, not fully oxidized, a time course of oxidation/reduction states of centres FR1 and FR3 was obtained (Fig.4.2) and this is described herein.

The FR1 g_{xy} signal height decreased upon mixing with succinate. The g=1.94 peak-trough was measured at 30K, 5.2mW (FR1 not saturated, see Fig.4.1). The FR3 signal height increased upon mixing with succinate and was measured from the g=2.01 peak height to the high field trough, 10K, 16.3mW. The decrease in FR1 and increase in FR3 both show oxidation of centres, not the expected reduction by succinate. However, as explained above, this was due to the succinate solution being contaminated with oxygen. The centres are then oxidized by the ubiquinol oxidase cytochrome-*bd*. These data agree with dehydrogenase limited oxygen reduction with, in this case, fumarate reductase acting as the dehydrogenase (succinate-oxidase activity being rate limited at fumarate reductase even in amplified membranes); because dehydrogenases are rate-limiting for respiratory chain reduction of oxygen, steady-state oxygen electrode data can be extrapolated to obtain dehydrogenase turnover values. The freeze-quench data of Fig.4.2 show the

Figure 4.2

Rapid-freeze quench time course for FR1 and FR3: succinate-oxidase activity.

Time course data of Fig.4.1 are plotted for the FR3 and FR1 signal heights versus time. Oxidation/reduction events are in the low millisecond range. FR1 g_{xy} (◆) was measured as the g=1.94 peak-trough; e.p.r. conditions as in Fig.4.1c. FR3 (●) was measured from the g=2.01 peak to the high field trough; e.p.r. conditions as in Fig.4.1a. The 'zero time' sample was taken as the fully reduced sample of Fig.4.1e as explained in the text. Sample times are calculated from the reaction tube dimensions plus the calculated deadtime for mixing and freezing (chapter 3). The FR3 signal height for 85msecs is not plotted as the e.p.r. tube cracked in the spectrometer cavity.

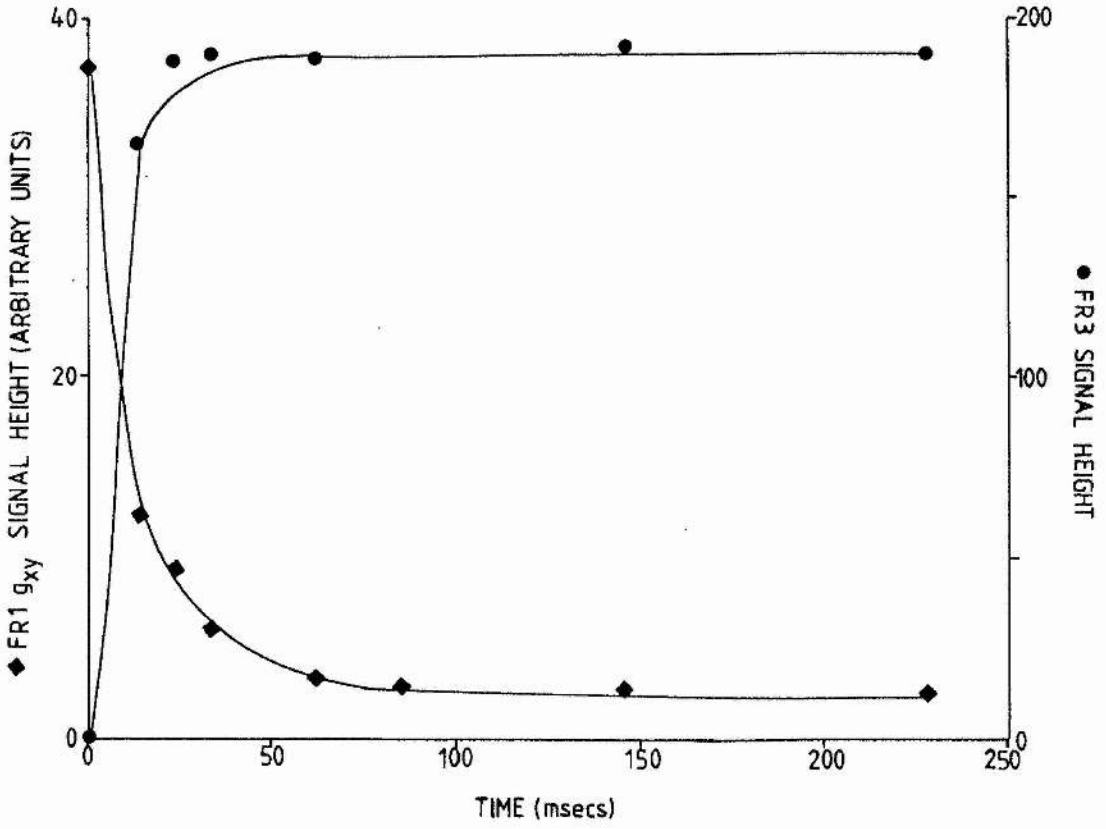
40
20
0
200
100
0
0
50
100
150
200
250
TIME (msecs)
◆ FR1 g_{xy} SIGNAL HEIGHT (ARBITRARY UNITS)
● FR3 SIGNAL HEIGHT

steady-state redox states for FR1 and FR3 during succinate-oxidase activity, both centres being largely oxidized (the rate limiting step at the 'reductase'). For this time course the zero time sample was plotted as the fully reduced dithionite sample of Fig.4.1e; this allowed an estimate of the half-time for full oxidation to be made. The time course (Fig.4.2) shows an apparent FR3 oxidation concomitant with FR1. The points for FR1 oxidation can be fitted to a second order decay process for a single component but FR3 oxidation cannot be fitted to a simple function (first or second order). The lines of Fig.4.2 are drawn "by-eye" to fit the points. The data were not computer fitted to model systems for electron transfer reduction/oxidation as the data presented here are only preliminary studies. FR3 oxidation reaches a plateau at around 30-40msecs and FR1 becomes a minimum at around 70msecs. The apparent half-time values for both FR1 and FR3 oxidations are equivalent at around 8msecs.

The timing values for Fig.4.2 and Fig.4.4 are calculated from the reaction tube dimensions plus the calculated deadtime for mixing and freezing (see chapter 3), the error for each timing is +/- 3msecs.

Oxidation of FR3 and FR1, by comparison to the spatial data of chapter 1, suggests electrons are transferred to quinone in a linear sequence. FR3 interacts with quinone and becomes oxidized and FR1 is oxidized simultaneously. Although FR1 transfers electrons through FR3 to quinone, FR3 is oxidized faster than it is reduced to

remain oxidized in the steady-state. Thermodynamically FR1 and FR3 have similar midpoint potentials, FR1 -50mV, FR3 -50mV (Simpkin and Ingledew, 1985) and so these data fit with a thermodynamic equilibration of electrons in the pre-steady state. Thermodynamically both centres give equivalent oxidation/reduction ratio in the pre-steady state when centres are oxidized and reduced at the same rate. For the midpoint potential values of Cammack *et al.*, 1986; FR1 -20mV, FR3, -70mV, FR3 may be expected to appear oxidized slightly before FR1 if internal equilibration is very fast.

No FR2 type e.p.r. signal was observed during the time course (samples oxidized) and although free radical signals were observed it was not possible to positively assign these to either semiflavin or semiquinone because of their low concentration (sample concentration $<10mg.ml^{-1}$).

This initial study has shown FR1 and FR3 to be oxidized at a rate which is compatible with the maximal turnover for benzyl viologen reduction of fumarate ($30s^{-1}$, Simpkin, 1985). FR1 and FR3 are not resolved in the low millisecond range. The oxidation/reduction events are at the limit of resolution for flow techniques.

4.3.2. Inhibition of succinate-oxidase activity?

To observe succinate reduction of the iron-sulphur centres, the oxidized reductase must be inhibited at the quinol binding site (from the data of section 4.3.1. and as found for mitochondrial complex II by Beinert *et al.*, 1975).

The classic mitochondrial respiratory chain inhibitors antimycin A, thenoyltrifluoroacetone (TTFA), and 2-n-Heptyl-4-hydroxyquinoline N-oxide (HOQNO) were tested for inhibition of succinate-oxidase activity in the fumarate reductase amplified strain (fumarate reductase acting as the dehydrogenase). TTFA was dissolved in dimethyl sulphoxide (DMSO) and antimycin A and HOQNO were dissolved in ethanol. For oxygen electrode studies inhibitor was incubated with etp (50mM BES, pH7.0) for 5 minutes before the reaction was initiated by addition of 10mM sodium succinate. TTFA inhibits mitochondrial respiration in micromolar concentrations acting at the quinone binding site of complex II (Ingledew and Ohnishi, 1977). At high micromolar concentrations of TTFA, no inhibition of *E. coli* fumarate reductase was observed (not shown), at millimolar concentrations the observed reduction in rate was due to affects of DMSO on the membrane (as observed for a DMSO control). The succinate dehydrogenase of *E. coli* is reportedly inhibited by TTFA but at millimolar concentrations (K_I=1.5mM, Kita *et al.*, 1989). These differing TTFA inhibitions are probably a function of the double quinone binding site of mitochondrial succinate dehydrogenase and association with complex III (bc_1-complex) and the predominating quinone species in the membrane (ubiquinone-10, menaquinone-8, ubiquinone-8). If inhibition concentrations are not in the micromolar range the efficiency of inhibition must be questioned. Antimycin A and HOQNO (low micromolar concentrations) gave approximately 50%

reduction in rate for *E. coli* succinate-oxidase activity. The low percentage inhibition in *E. coli*, compared to mitochondria, is probably related to the lack of a quinone cycle (Q-cycle), and the *b*-type cytochromes so associated.

The lack of a suitable inhibitor for the respiratory chain of *E. coli* ruled out their use in freeze-quench experiments. A useful mutant to observe succinate reduction of fumarate reductase would be to transform the fumarate reductase plasmid, pFRD84, into a menaquinone/ubiquinone deficient strain (Guest, 1977).

The anoxic conditions for syringes 1 & 2 reservoir contents were improved to prevent oxygen contamination. Future work should also use small amounts of glucose oxidase in syringe reservoirs to maintain anoxic conditions.

4.3.3. Oxidation by fumarate.

A second rapid-freeze quench time course mixed the reduced enzyme with fumarate, oxidizing the enzyme in the reverse direction to section 4.3.1. A time course was obtained for iron-sulphur centres FR1 and FR3 (measured as in section 4.3.1). Syringe 1 contained anoxic (N_2g) etp, approximately 30mg.ml^{-1}, plus 50mM sodium formate in 0.1M BES, pH7.0 and syringe 2 contained anoxic (N_2g) 200mM sodium fumarate in 0.1M BES, pH7.0. The contents of syringe 1 were incubated at room temperature for 3hrs to ensure full physiological reduction of all centres. From oxygen electrode studies the formate dehydrogenase activity of etp

was low, formate dehydrogenase being relatively unstable for stored membrane preparations. The high membrane concentration of syringe 1 will ensure full reduction within the 3hr incubation period. Fig.4.3a shows the zero time sample (10K, 17.3mW), mixing syringe 1 with anoxic buffer (no fumarate), FR3 is almost wholly reduced. Fig.4.3c gives the reduced FR1 signal for the same sample (30K, 5.5mW). A low field contaminating copper/cavity signal was present in all spectra. The radical signal present in all samples was characterized as semiflavin from the winged features observed to the high and low field areas of the radical peak-trough (Fig.4.4), the radical could not be observed at sufficient intensity, under non-saturating e.p.r. conditions, to determine a time course for radical formation.

From Fig.4.3a & c FR1 and FR3 were reduced at zero time and no FR2 signal was apparent. Upon mixing with fumarate both centres became oxidized. Fig.4.3b & d show the 146msecs sample with oxidized FR3 and FR1, respectively, as a comparison to the zero time samples, the packing ratio for both samples, 50% isopentane.

In the time course of Fig.4.5 both FR1 and FR3 are oxidized upon mixing with fumarate, the steady-state for these centres being oxidized as in Fig.4.2. FR1 is fully oxidized during the time course and therefore FR3 is also expected to be fully oxidized.

The dehydrogenase reaction (formate dehydrogenase, low activity) is rate-limiting and electrons are transferred

Figure 4.3

Fumarate reductase rapid-freeze quenching: e.p.r. spectra for fumarate oxidation of reduced enzyme.

E.p.r. spectra are presented for fumarate oxidation of formate reduced HB101/pFRD84 membranes. Experimental conditions were as explained in the text (section 4.3.3).

a) E.p.r. spectra in the g=2.00 region for the zero time sample, mixing formate reduced membranes with anoxic buffer (no fumarate). E.p.r. conditions were: microwave frequency, 9.46GHz; modulation frequency, 100kHz; modulation amplitude, 1.0mTesla; microwave power, 17.3mW; temperature, 10K.

b) 146msecs sample. E.p.r. conditions as in Fig.4.3a.

c) zero time sample of a). E.p.r. conditions as in Fig.4.3a except, microwave power, 5.5mW; temperature, 30K. The free radical signal is indicated.

d) 146msecs sample of Fig.4.3b. E.p.r. conditions as in Fig.4.3c.

Peak g-values are shown above, and the relative gain increases are shown to the right of, the spectra. The high field peak is due to contaminating copper (Cu) and/or the cavity signal. Iso-pentane packing ratio 50%. Protein concentration for all samples approximately 8mg.ml^{-1}.

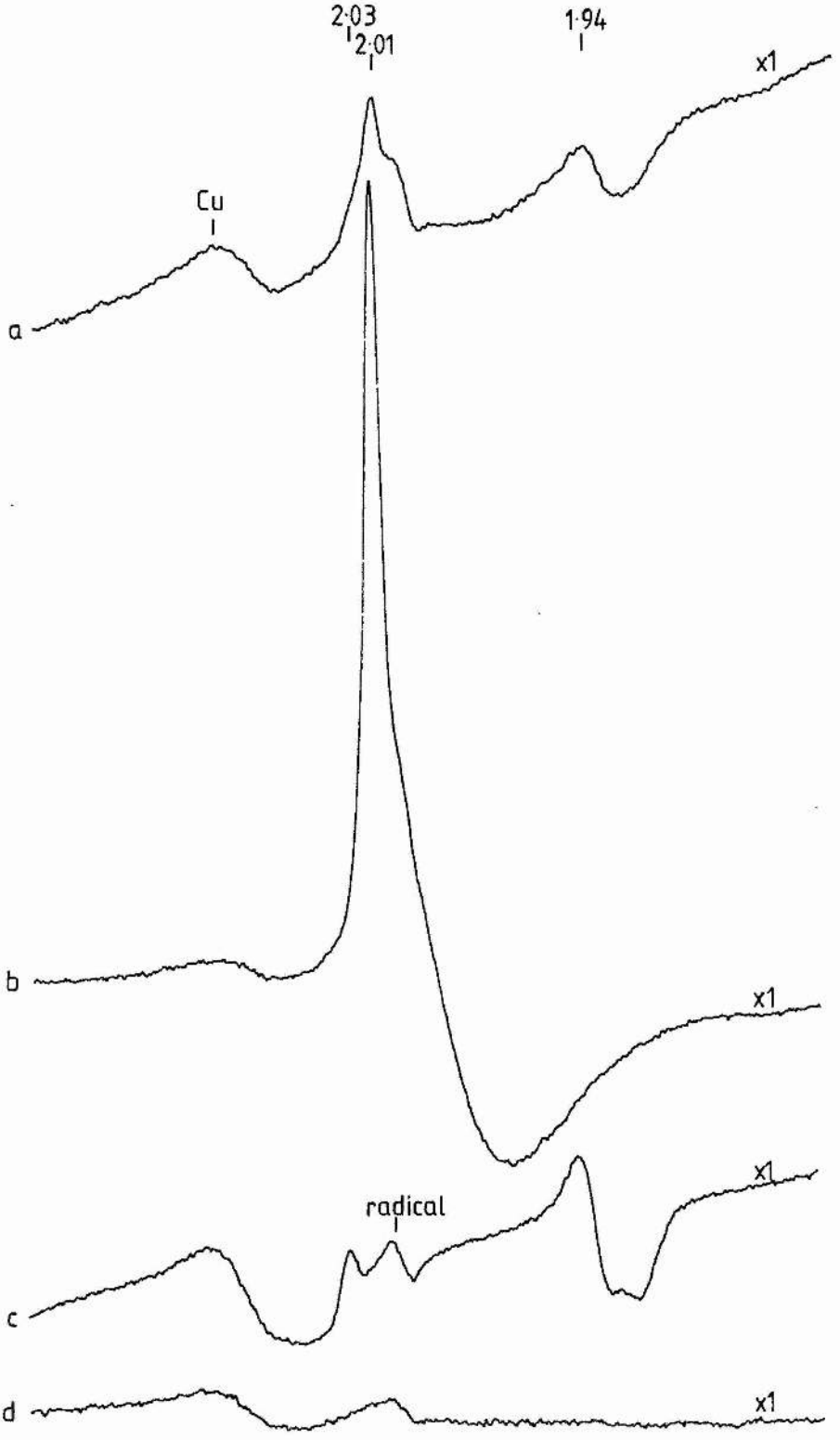
2·03
2·01
1·94
x1
Cu
a
b
x1
x1
radical
c
d
x1

Figure 4.4

The rapid-freeze quench flavin free radical signal observed for fumarate oxidation of reduced fumarate reductase.

The radical signal observed for the time course of Fig.4.3 and Fig.4.5 at 14msecs is shown. E.p.r. conditions are saturating but show the high and low field winged features characteristic of flavin free radical. E.p.r. conditions were: microwave frequency, 9.46GHz; modulation frequency, 100kHz; modulation amplitude, 0.8mTesla; microwave power, 172μW; temperature, 62K. Approximate protein concentration 8mg.ml^{-1}; spectrometer gain, 6.3 x 10^5. The peak-trough g-value is shown above the spectra and the 'winged' features are indicated.

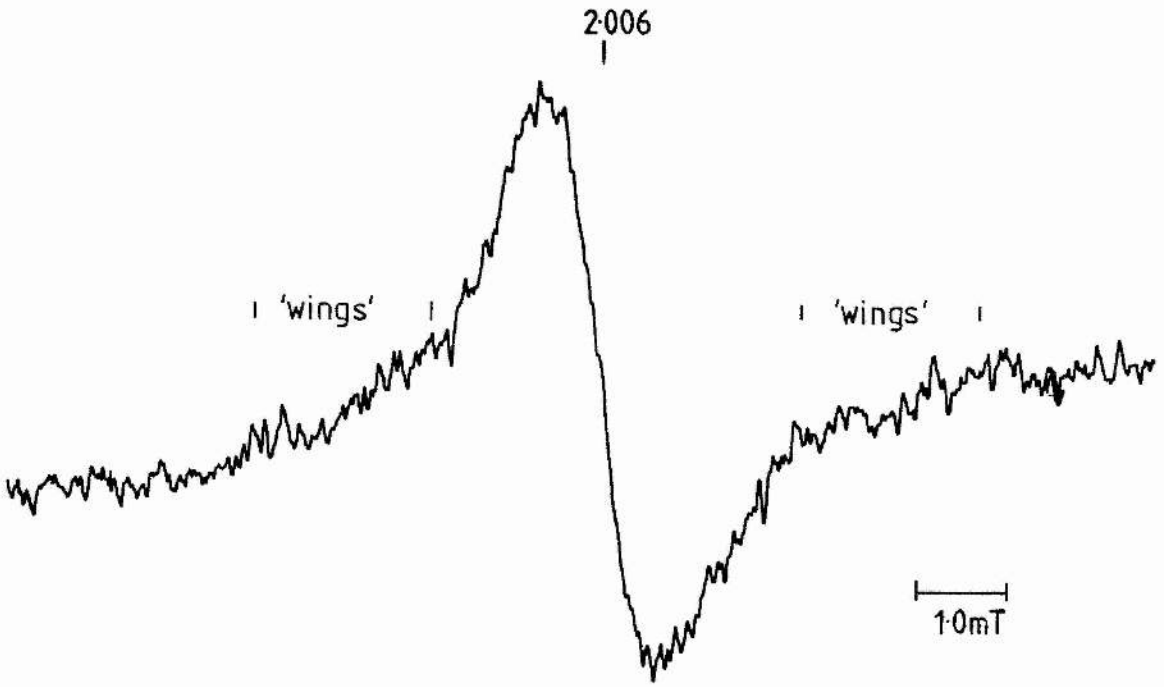
2·006
'wings'
'wings'
1·0mT

through the reductase at a faster rate than they can be transferred from the dehydrogenase i.e. the centres are oxidized faster than they are reduced.

The centres may appear reduced in the steady-state if a very slow substrate (not fumarate) decreased the turnover of the reductase appreciably, no such "slow" substrates are known for fumarate reductase. Potential "slow" substrates are unsaturated hydrocarbons such as acrylate (CH_2CHCO_2H) and crotonate ($CH_3CHCHCO_2H$) (acrylate/propionate; crotonate/butyrate; Kroger, 1978). When 15mM acrylate and crotonate were applied to a fumarate reductase assay (reduced benzyl viologen as reductant, see Materials and Methods) no oxidation of benzyl viologen was observed (not shown). The inability to act as a substrate was not due to a thermodynamic limitation for reduction/oxidation (E_{m7} values being favourable) but would appear to be due to a highly specific active site.

From Fig.4.5 the pre-steady state oxidation of FR1 and FR3 are again at the limit of resolution for the freeze-quench technique. FR1 and FR3 oxidations have similar half-times of around 8msecs as in Fig.4.2. The arbitrary units for the FR1 and FR3 signal heights have been multiplied by the spectral gain factor to give an equivalence to Fig.4.2 for direct comparisons, protein concentrations were also similar (around 6-8mg.ml^{-1} in the e.p.r. tube). The oxidation of FR1 fits a theoretical second-order decay process for a single centre but FR3 oxidation cannot be fitted to a simple equation (first or

Figure 4.5

Rapid-freeze quench time course for FR1 and FR3: fumarate oxidation of reduced enzyme.

Time course data of Fig.4.3 are plotted for FR3 and FR1 signal heights versus time. Oxidation/reduction events are in the low millisecond range. FR1 g_{xy} (◆) was measured for the g=1.94 peak-trough; e.p.r. conditions as in Fig.4.3c. FR3 (●) was measured from the g=2.01 peak to high field trough; e.p.r. conditions as in Fig.4.3a. FR1 and FR3 arbitrary units for signal height have been multiplied by the spectrometer gain factor to be directly comparable with Fig.4.2. Sample times are calculated from the reaction tube dimensions plus the calculated deadtime for mixing and freezing (chapter 3). The FR3 signal height for 34msecs is not plotted as the e.p.r. tube cracked in the spectrometer cavity.

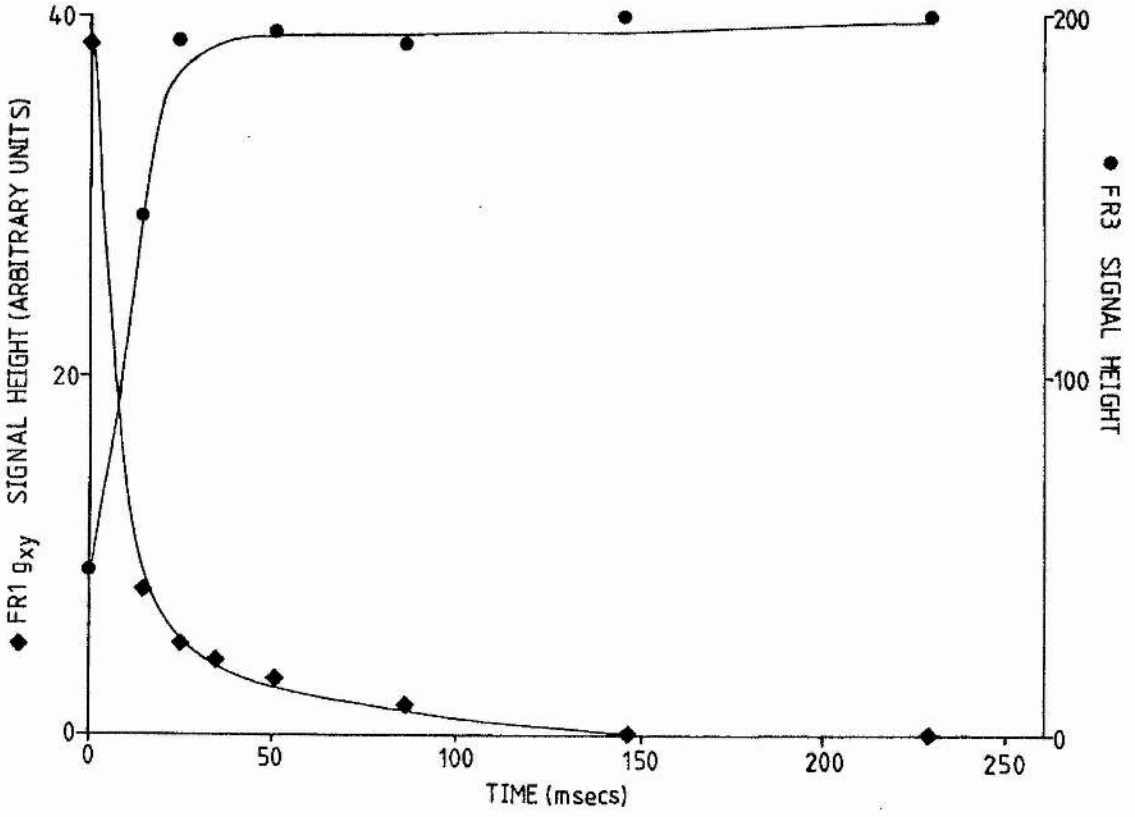
40
20
0
200
100
0
0
50
100
150
200
250
TIME (msecs)
◆ FR1 gxy SIGNAL HEIGHT (ARBITRARY UNITS)
● FR3 SIGNAL HEIGHT

second order). This may suggest differing kinetics for internal electron transfers between iron-sulphur centres which may then be related to a role for FR2. From thermodynamic parameters the midpoint potential values of Simpkin and Ingledew, 1985 (FR1, -50mV; FR3, -50mV) would suggest equivalence for oxidation/reduction events; the values of Cammack *et al.*, 1986 (FR1, -20mV; FR3, -70mV) would suggest FR3 oxidation slightly preceding FR1 if internal equilibration is fast.

Again, from Fig.4.5, FR1 and FR3 oxidation/reductions are kinetically competent for turnover but are not resolved. The lineshape of Fig.4.2 and Fig.4.5 are similar for oxidations from either flavin or menaquinone suggesting rapid internal equilibration for centres. If pre-steady state internal equilibration is more rapid than turnover it would appear that a faster substrate would be required to resolve the two centres and this would obviously be outwith the kinetic resolution of flow techniques.

4.4. Conclusions.

Preliminary freeze-quench studies have shown the oxidation/reduction states of fumarate reductase FR1 and FR3 to be observed in the pre-steady state millisecond range to give a time course of redox behaviour.

Centres FR1 and FR3 are kinetically competent for the turnover of the enzyme (approximately $30s^{-1}$ from extrapolated steady-state data; Simpkin, 1985) but were not

resolved in the millisecond time course.

In agreement with spatial data for FR1 and FR3 (see chapter 1) FR3 oxidation may precede FR1 oxidation in the presence of oxygen (Fig.4.6a) and FR1, being closer to the flavin, may be oxidized before FR3 in the presence of fumarate (Fig.4.6b), the rate determining steps (RDS) for Fig.4.6 are shown at the dehydrogenase level to be consistent with the data of sections 4.3.1 and 4.3.3.

The data of Beinert *et al.* (1975) for mitochondrial succinate dehydrogenase (complex II) suggest succinate reduction of FR1 slightly precedes FR3 reduction even though thermodynamically FR3 (E_{m7}=+60mV) would be reduced before FR1 (E_{m7}=0mV) if internal equilibration is fast. To observe the reduced state the enzyme was inhibited at the quinone binding site by TTFA which was not possible with *E. coli* fumarate reductase.

The role of FR2 is ambiguous and an e.p.r. signal assignable to FR2 was not observed in the above study. A fully reduced (chemically) FR2 species will probably be oxidized upon mixing with fumarate but a role for this low potential centre during catalytic turnover would remain undefined. It seems unlikely that FR2 is vestigial as it is present in all of the succinate-fumarate oxido-reductases, FR2 may maintain a steady-state redox balance for FR1 and FR3 during the n=1/n=2 conversions of menaquinol (E_{m7}=-74mV,) and flavin (E_{m7}=-12mV). FR1, FR2 and FR3 are so closely connected that their separation into independent thermodynamic components would be a misrepresentation.

Figure 4.6

Electron transfer sequences for Escherichia coli menaquinol-fumarate oxido-reductase: reductase and dehydrogenase activity.

The fumarate reductase electron transfer sequence for the freeze-quench experiments of Fig.4.2 and Fig.4.5 are shown.

a) Electron transfer sequence for fumarate reductase succinate-oxidase activity (section 4.3.1). FAD, flavin of subunit A; FR1, FR2, FR3, iron-sulphur centres of subunit B; MQH_2, menaquinol; b_{558}, b_{595}, d, cytochrome-*bd*. The role of FR2 is ambiguous and is not include in the linear sequence. Menaquinol is bound at fumarate reductase and cytochrome-*bd* to stabilize the free radical intermediate for n=1/n=2 conversions. The rate determining step, RDS, is indicated in accordance with the freeze-quench steady-state data of Fig.4.2.

b) Electron transfer sequence for fumarate reduction by formate. The electrons are transferred in the reverse direction to Fig.6a and the rate determining step, RDS, is indicated in accordance with the steady-state data of Fig.4.5.

a)

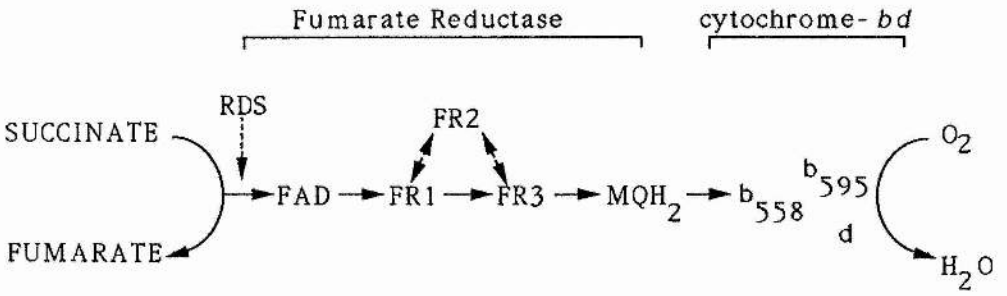
Fumarate Reductase
cytochrome- bd
RDS
FR2
SUCCINATE
FAD
FR1
FR3
MQH2
b558
b595
d
O2
FUMARATE
H2O

b)

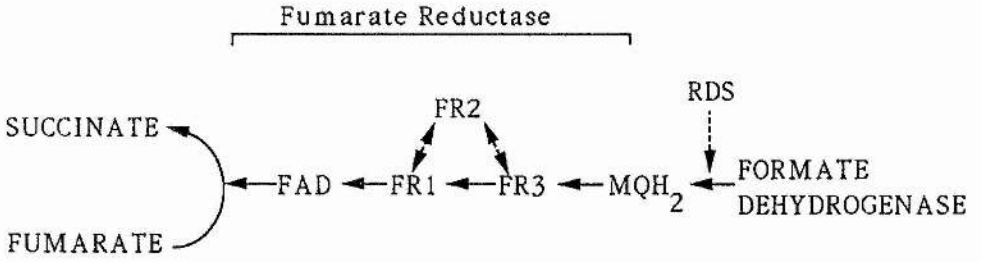
Fumarate Reductase
RDS
FR2
SUCCINATE
FAD
FR1
FR3
MQH2
FORMATE
DEHYDROGENASE
FUMARATE

An interesting approach to elucidating the role of FR2 lies in site-directed mutagenesis of iron-sulphur centres, a technique now being applied to *E. coli* dimethyl sulphoxide reductase (R.A.Rothery and J.H.Weiner, personal communications). Using this approach selective removal of FR1, FR2 and FR3 followed by subsequent kinetic experimentation will identify which centres are necessary for activity.

Sequential electron transfer in fumarate reductase is consistent with the available data with no apparent need, or supporting evidence for, a high potential/low potential pathway (Fig.1.3). No *b*-type cytochrome was identified for fumarate reductase and cytochrome-b556 of *E. coli* succinate dehydrogenase with a midpoint potential value of +36mV (E_{m7}) is not compatible with the low potential pathway, this cytochrome is also fully reducible by succinate (Kita *et al.*, 1989).

From the high stability constant for the flavin free radical (FADH·, $K=1.63\times10^{-2}$) a sequential transfer of electrons from a single electron carrying iron-sulphur cluster (FR1) to the flavin is postulated. The double pathway model would not require the flavin radical to be highly stabilized, stabilization being required for n=1/n=2 conversion (Simpkin,D., Moodie,A.D., Salerno,J.C. and Ingledew,W.J., 1990, submitted). As a comparison of radical stability the stability constant for the free ubiquinone/ubiquinol couple in a hydrophobic milieu has been estimated as 10^{-10} (Mitchell, 1976). A menaquinol binding

site is also envisaged, most probably at the anchor subunits involving a close interaction with FR3 (Simpkin,D., Moodie,A.D., Salerno,J.C. and Ingledew,W.J., 1990, submitted).

These rapid-freeze quench studies for *E. coli* fumarate reductase are preliminary. The freeze-quench apparatus of chapter 3 was shown to be functional and general problems associated with experimenter handling were eradicated. Analysis was maintained at a simple kinetic level within the limitations of the flow technique. Repeat and further experimentation is required before a kinetic model for all of the centres can be positively resolved. Succinate reduction of centres may be more easily resolved and, as mentioned in section 4.3.1, a menaquinone/ubiquinone deficient mutant of *E. coli* (Guest, 1977) containing the fumarate reductase plasmid, pFRD84, and grown fermentatively in the presence of fumarate, may facilitate iron-sulphur centre kinetic resolution. To prevent problems with transfer of electrons to the oxidases the pFRD84 plasmid may also be inserted into *E. coli* strain FUN4 which is deleted in both cytochrome-*bd* and cytochrome-*bo*. Fumarate reductase will not lend itself to a more indepth kinetic study if the limitations set out above are not taken into consideration.

The above data, along with the data presented for fumarate reductase in chapter 1, is presented in chapter 7 as a model for the internal electron transfers of *E. coli* fumarate reductase.

Chapter 5

ESCHERICHIA COLI UBIQUINOL-OXYGEN OXIDO-REDUCTASE CYTOCHROME-*bd*: PHOTODISSOCIATION OF LIGATED CARBON MONOXIDE

Chapter 5

5.1. Introduction.

The original photochemical action spectra of Castor and Chance (1955, 1959) were obtained with a simple apparatus. This has been slowly improved over the last 30 years to now include dye lasers as light sources with improved electronics for monitoring small changes in oxidase rate (Edwards *et al.*, 1981; Lloyd and Scott, 1983, 1987). The technique is based on carbon monoxide (CO) ligated haem having a higher sensitivity to photodissociation than oxygen ligated haem.

This chapter deals with a photodissociation apparatus developed to monitor oxygen reduction as the relative $CO:O_2$ ratio increased. A photochemical action spectra was not recorded with the apparatus because the light source (150W xenon arc lamp) was not of a high enough intensity to observe photodissociation at individual wavelengths (μW power levels). The apparatus illuminates 1.3ml of cell/buffer suspension and would require the intensity of a tunable dye laser for action spectra (mW power levels; Lloyd and Scott, 1987). The room-temperature action spectra of Castor and Chance (1955, 1959) applied a relatively low powered lamp source focussed on a small drop of respiring cells but had the following disadvantages: a) cells settled to the bottom of the drop; b) a steady baseline could not be obtained; and c) gas gradients existed within the drop. The intensity of white light from the arc lamp used herein was sufficient to observe photodissociable rate affects and, in

conjunction with blue/red and neutral density filters, data was obtained for the CO inhibited *E. coli* ubiquinol-oxygen oxido-reductase cytochrome-*bd*.

Reduced haem-d and haem-b595 both bind CO although haem-d has a higher CO affinity (Poole *et al.*, 1983; Rothery, 1989). The room-temperature reduced + CO minus reduced optical spectra of cytochrome-*bd* show a trough-peak at 626-642nm with a weak associated trough in the Soret region at 445nm both assigned to CO ligated haem-d; a larger trough at 429nm in the Soret region, associated with changes in the 560nm region, is assigned to CO ligated haem-b595 (Poole and Chance, 1981; Rothery, 1989).

At the high CO concentrations used herein both haem-d and haem-b595 are CO inhibited. The data obtained suggest a direct correlation between photodissociation of b595-CO and increased oxidase rate, this is related to inhibition and the catalytic mechanism of dioxygen reduction for the haem pocket.

5.2. Development of a photochemical apparatus.

The photodissociation of CO bound cytochrome-*bd* was monitored by a Clarke-type oxygen electrode. A standard oxygen electrode base (Rank Brothers, Cambridge, U.K.) was fitted with a specialized water-jacketed glass vessel (Mr. C. Smith, Glassblower, Department of Chemistry, University of St.Andrews). The vessel had a spherical inner chamber of volume 1.3mls and was silvered to give a higher Q-value

(pathlength) for light within the chamber (Fig.5.1a). The vessel was sealed with a ground glass stopper which had a capillary portal for microsyringe additions, gas diffusion at this portal was negligible during the time course of reactions. The vessel was internally illuminated by focussing light down a 4mm diameter silvered light tunnel. The contents were stirred with a glass magnetic flea and a stirring block held below the electrode base.

The 150W xenon arc lamp light source was filtered with a 03FCG165 glass filter (Melles Groit, Arnhem, Holland) which transmits light at 300-->900nm. From the data sheet for the arc lamp the power output is constant over the wavelength regions applied (Oriel Corp. Stratford, CT, USA). The light was also filtered by passage through a 1cm pathlength of 10mg.ml^{-1} bovine serum albumin to absorb extraneous wavelengths which may be damaging to proteins (around 300nm) and prevent heating of the electrode vessel contents (Fig.5.1b). The transmission profiles for the blue and red filters, with filter 03FCG165, as used during photodissociation, are shown in Fig.5.2. The blue and red filters have a cut-off at around 600nm.

The oxygen electrode was interfaced to a BBC microcomputer (Acorn Computers) for data collection as described by Rothery (1989). Progress curves were analysed by fitting polynomial series equations to the curve and differentiating the equation at a known oxygen concentration, this gives the oxidase rate for that concentration. The polynomial fitting program was written in

Figure 5.1

Schematic representation of apparatus used for photodissociation.

a) The glass photodissociation vessel is shown. (constructed by Mr.C. Smith, Glassblower, Department of Chemistry, University of St.Andrews). The sides of the internal chamber were curved and silvered to reflect light towards the centre of the chamber.

b) The lightpath from the 150W xenon arc lamp to the electrode vessel of Fig.5.1a is depicted. Filter 03FCG165 transmits light from 300-->900nm. The 1cm pathlength of 10mg.ml^{-1} bovine serum albumin (BSA) is a further filter. Convex lenses focussed light into the oxygen electrode vessel.

a)

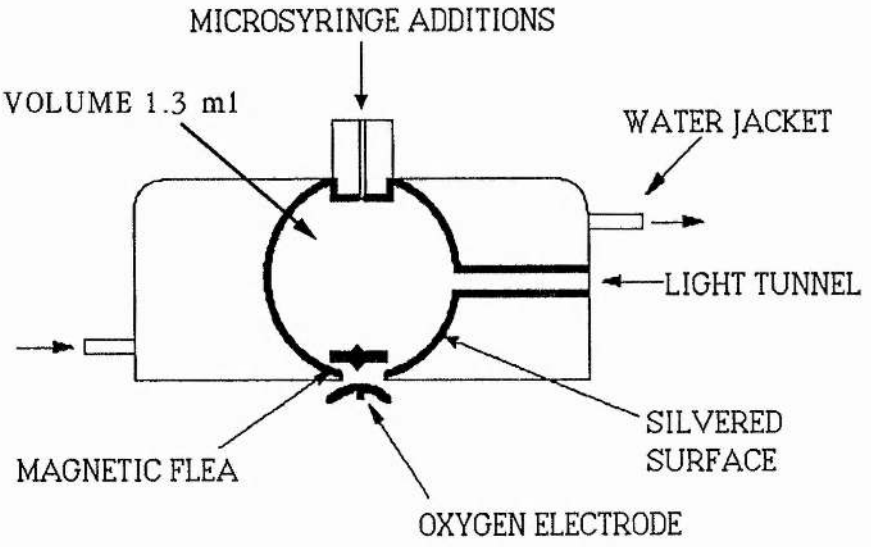
MICROSYRINGE ADDITIONS
VOLUME 1.3 ml
WATER JACKET
LIGHT TUNNEL
SILVERED SURFACE
MAGNETIC FLEA
OXYGEN ELECTRODE

b)

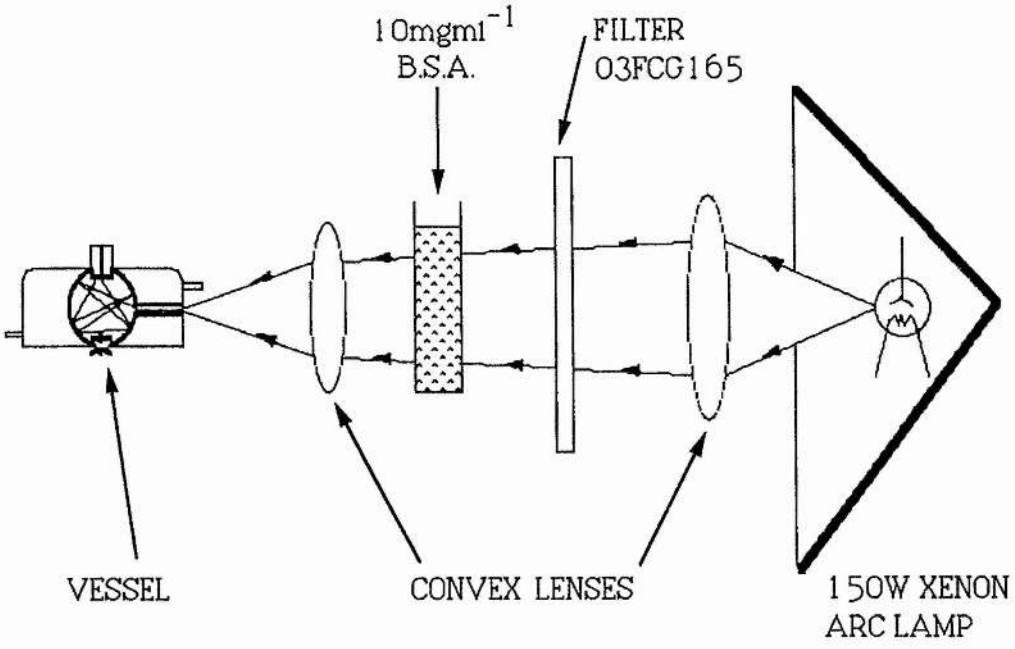
10mgml^{-1} B.S.A.
FILTER 03FCG165
VESSEL
CONVEX LENSES
150W XENON ARC LAMP

Figure 5.2

Transmission properties for red and blue photodissociation filters.

The transmission spectra for the red and blue filters with filter 03FCG165 are shown. The cut-off wavelength for both filters is around 600nm. The spectra were recorded with a LKB Perkin-Elmer Lambda 5 scanning spectrophotometer.

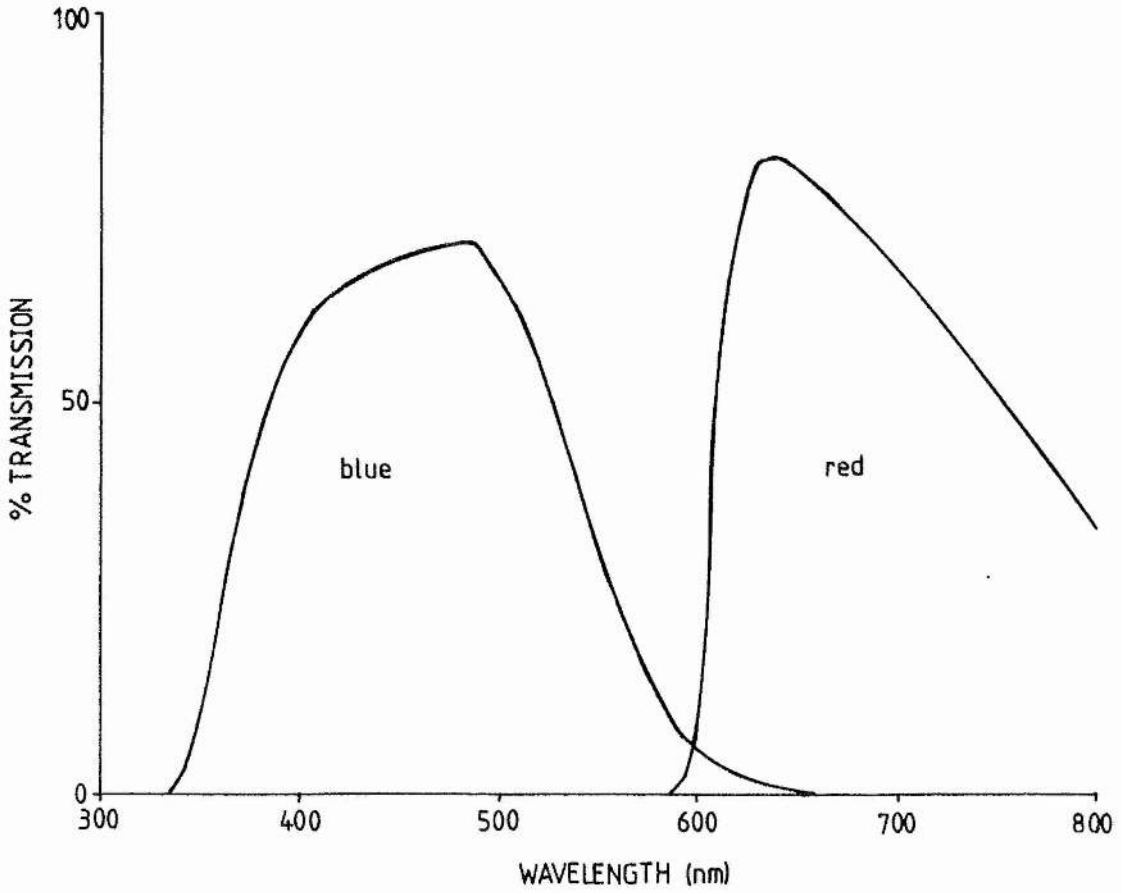
100
50
0
% TRANSMISSION
blue
red
300
400
500
600
700
800
WAVELENGTH (nm)

VAX-11 BASIC language for the University of St.Andrews computer network. The program fits values of x to predicted values of y using the correlation coefficient. Specified areas of the curve could be fitted with 1st order (y=mx+c) to 5th order polynomials; an example of the 5th order polynomial used for rate analysis is given in Fig.5.3. The original points collected from the oxygen electrode were fitted to the polynomial using a large scale matrix inversion as outlined by Spain (1982). The statistical parameters of correlation coefficient, F statistic and residual mean square are given for each fit. The correlation coefficient gives a better fit for each order of polynomial as it approaches the perfect fit value of 1.000 (more usually values of 0.999 were obtained, 0.000 would show no correlation), this statistical value has limitations for complex polynomials often giving the same high value when fitting 3rd or 4th or 5th degree equations. The F statistic, when used in conjunction with the correlation coefficient, gives a better fit when higher values are obtained, the F statistic can often get lower for higher polynomials. The residual mean square value should be minimal for best fit. These statistical parameters were presented only as a means of fitting the best-line "by-eye" and cannot be related to the variable parameters. The fitted data were applied to a filing system for the VAX-11 computer network enabling hard copy plots to be obtained. The fitting of points to polynomials smoothed the slight jumping found on progress curves at low oxygen tension and high electrical

Figure 5.3

5th order polynomial equation.

An example of the polynomial equation used to fit data points of oxygen electrode progress curves is given. The 5th order polynomial is shown with the differentiated form which was applied to obtain oxidase rates at specified oxygen concentrations.

5th Order Polynomial

$$y = a_0 + a_1x + a_2x^2 + a_3x^3 + a_4x^4 + a_5x^5$$

$a_0, a_1, a_2 \ldots\ldots\ldots\ldots a_n$ are real constants which are determined for each value of x and y.

Differential for $y = [0_2]$, x = time.

Rate of Oxygen reduction

$$= a_1 + 2a_2x + 3a_3x^2 + 4a_4x^3 + 5a_5x^4$$

amplification.

All experiments were at 30°C where the concentration of CO in saturated buffer is 0.859mM, and for air saturated buffer the oxygen concentration is 0.22mM (oxygen saturated buffer, 1.121mM). To calculate the CO and oxygen concentrations in the vessel the voltage output from the electrode was measured at the computer. For air saturated buffer (0.22mM oxygen) the zero input voltage (residual) was subtracted from the 0.22mM value, stirring buffer in the vessel. CO saturated buffer was then added to the empty vessel and the vessel was stoppered, the voltage difference was again measured. The new oxygen concentration in the CO buffer was calculated from the voltage differences (oxygen concentration in the CO buffer approached zero but never attained this value). The nitrogen contamination of CO buffer was considered to be constant; as only relative ratios were calculated, not actual CO concentration, this assumption is within the limitations of the analysis. The oxygen concentration was increased with microlitre additions of oxygen saturated buffer. The concentration of CO in the vessel was taken as the CO saturated value (0.859mM) minus the oxygen concentration. To measure the small oxygen concentrations (0.05mM starting concentration) the electrode output was amplified 300 fold by a simple amplification circuit, this output was then digitally converted before interfacing with the computer (components from RS Components Ltd., Corby, Northants, U.K.). All wiring used was heavily sheilded to prevent external electrical interference at high

gain. The xenon arc lamp assembly was housed within an earthed metal box to act as a Faraday cage arrangement. Photochemical data can be analysed by differentiating oxygen electrode outputs (Scott and Lloyd, 1987) but differentiated rates were found to be susceptible to electrical interference and therefore progress curves were analysed.

5.3. Photodissociation.

For all photodissociation data wild-type *E. coli* (EMG2), grown anaerobically for 24hr on glycerol-fumarate media, were used. Membrane particles (etp) are more easily inhibited by CO and show higher respiration rates than coupled cells. All progress curves were initiated by adding sodium lactate (30mM) to 0.32mg.ml^{-1} of membrane particles (etp) which had equilibrated with CO buffer for 5mins (50mM phosphate buffer, pH7.0).

CO inhibited the dioxygen binding site of cytochrome-*bd* to give the oxygen electrode progress curves of Fig.5.4a. This progress curve was recorded for a starting oxygen concentration of 0.058mM, 0.801mM CO (CO:O_2 around 14:1). The ratio of CO:O_2 increases to 20:1, 40:1, 60:1, 80:1, and so on with the rate at each ratio measured from the single progress curve. Using this form of analysis rates should not be determined at oxygen concentrations which approach the Km value (Hoffman *et al.*, 1980). The Km for oxygen of cytochrome-*bd* is very low (<1μM) and the ratios at which photodissociation rates were measured, mainly 60:1,

were within this limitation.

At higher $CO:O_2$ ratios the relative increase in rate due to photodissociation is more easily observed due to the slower non-dissociated rate. The progress curve (Fig.5.4a) was analysed by application to the integrated Michaelis-Menten equation (section 2.5.2). An Eadie-Hofstee plot of Fig.5.4a is shown in Fig.5.4b. This plot indicates apparent cooperative kinetics for dioxygen reduction (curved plot; c.f. Rothery *et al.*, 1987; Rothery, 1989). The 'cooperativity' is not necessarily a function of a multiple dioxygen binding site however (c.f. haemoglobin) and may be a function of the single progress curve and inhibition. This point will be discussed further in the conclusion section of this chapter and in Chapter 6 with added reference to nitrite inhibition.

To demonstrate a photodissociable affect CO must recombine with haem when the light source is removed i.e. photodissociation must be purely a function of the quanta of light incident on the haem and photodissociated CO must potentially be capable of rebinding. Fig.5.5. shows a progress curve for CO inhibited oxidase reduction of dioxygen, this overlays a second time course where the vessel was illuminated with white light at 200secs (ON) and the rate increased, the increase is due to photodissociation at the active site. At 390secs the light source was removed (OFF) and the rate decreased due to re-association of CO. The points in Fig.5.5 have been fitted by polynomials to smooth out the slight electrical interference of the trace;

Figure 5.4

Carbon monoxide inhibited progress curve for cytochrome-bd dioxygen reduction (and subsequent application to the integrated Eadie-Hofstee equation).

a) Oxygen electrode progress curve for CO inhibited cytochrome-*bd* activity. Points were collected with a BBC microcomputer and analysed as described in the text. 0.32mg.ml^{-1} EMG2 etp, 50mM phosphate buffer pH7.0, were incubated for 5mins at CO concentration, 0.801mM; oxygen concentration, 0.058mM; 30°C. The oxidase reaction was initiated by addition of 30mM sodium lactate.

b) The points collected for Fig.5.4a were applied to the integrated Eadie-Hofstee equation (see section 2.5.2). s_0, starting oxygen concentration (mM); s, oxygen concentration (mM); t, time in seconds.

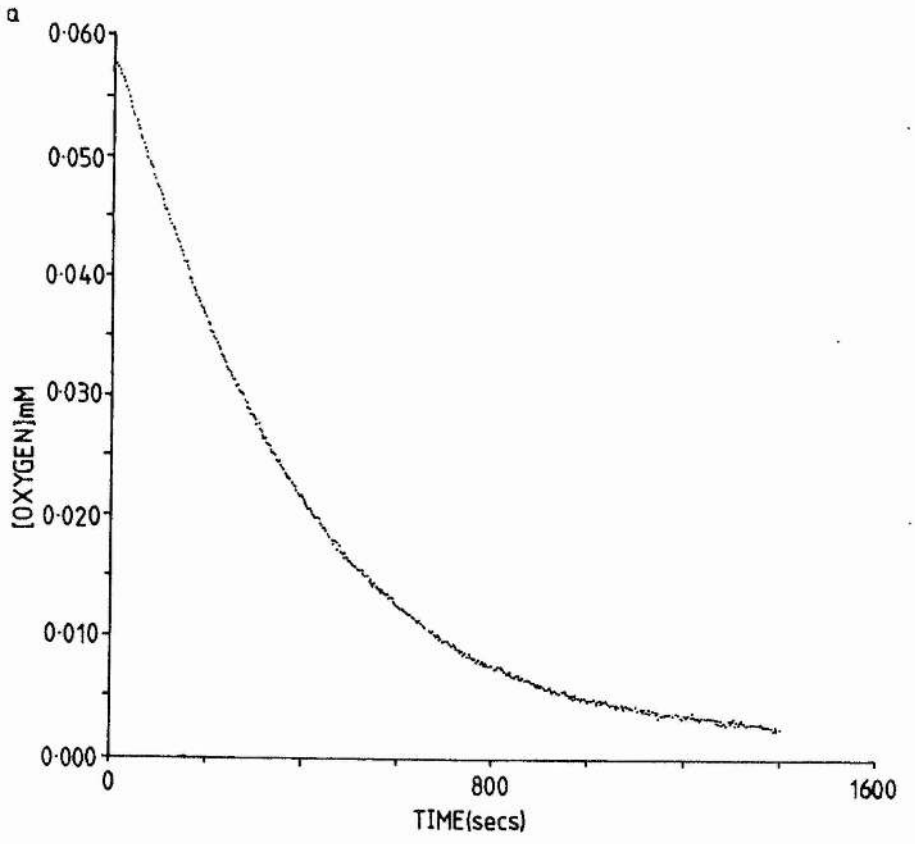
a
0·060
0·050
0·040
0·030
0·020
0·010
0·000
[OXYGEN]mM
0
800
1600
TIME(secs)

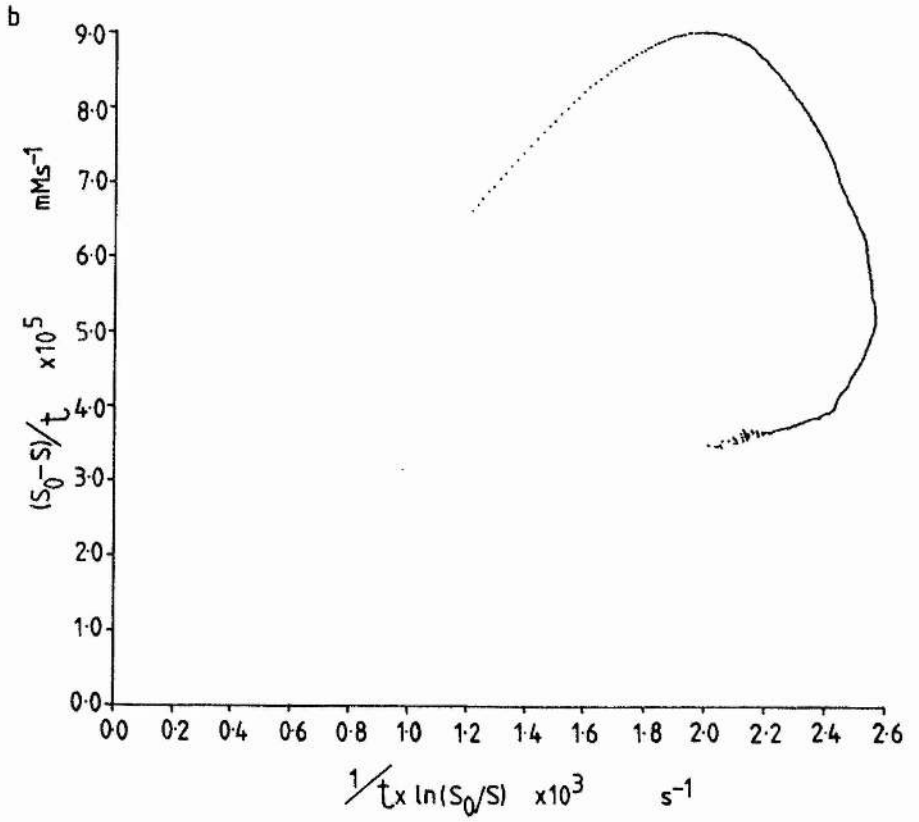
b
9·0
8·0
7·0
6·0
5·0
4·0
3·0
2·0
1·0
0·0
$(S_0-S)/t$ x10^5 mMs^{-1}
0·0 0·2 0·4 0·6 0·8 1·0 1·2 1·4 1·6 1·8 2·0 2·2 2·4 2·6
$1/t \times \ln(S_0/S)$ x10^3 s^{-1}

Figure 5.5

Photodissociation of CO ligated cytochrome-bd.

Photodissociation of CO inhibited cytochrome-*bd* dioxygen reduction is shown. Two progress curves are overlayed, the non-illuminated control (O) is fitted with a 5th order polynomial (c.f. Fig.5.4a). The second progress curve (●) was illuminated with white light after 200 seconds (ON) and the light source was removed at 390 seconds (OFF); the points are fitted by three 4th order polynomials. Experimental conditions were: CO concentration 0.805mM, 0.054mM oxygen; 0.32mg.ml^{-1} EMG2 etp, phosphate buffer pH7.0, temperature 30°C. The reaction was initiated by addition of 30mM sodium lactate. Oxidase rate increases in the presence of light. All points collected (around 500) were fitted but for improved resolution only a maximum of 100 points are displayed by the computer program.

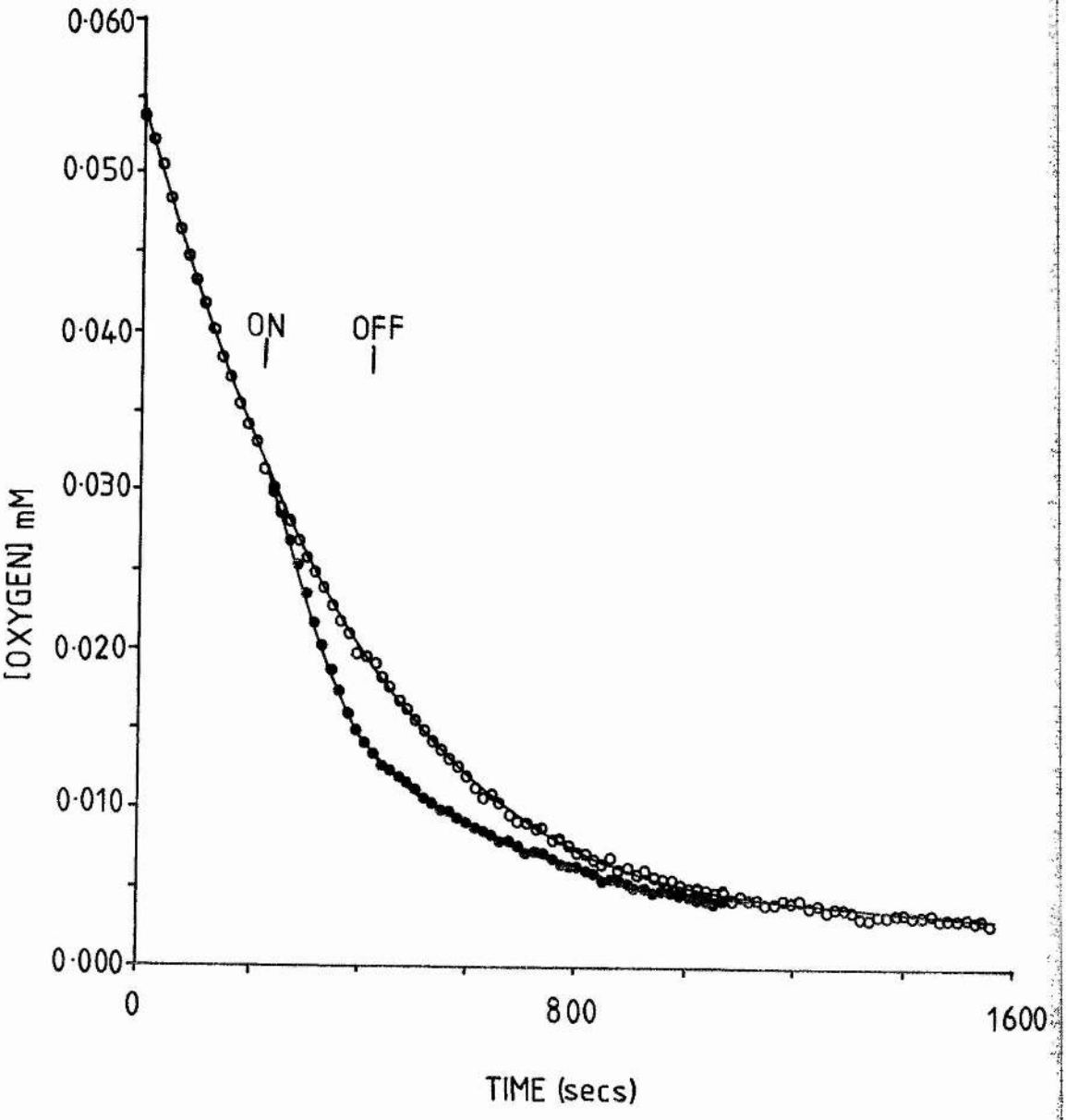
0·060
0·050
0·040
0·030
0·020
0·010
0·000
[OXYGEN] mM
ON
OFF
0
800
1600
TIME (secs)

the number of points originally collected (around 500) have been reduced by the fitting program to a maximum of 100 to give pictorial resolution of points on the computer screen.

To show that the increase in rate is due to photodissociation of haem, and not due to a light effect at the electrode surface the vessel was illuminated in the presence of buffer only (no etp) and no change in input voltage was observed. The buffer temperature in the vessel was monitored with a thermocouple junction and remained constant when illuminated. Temperature affects due to light must be considered when photodissociation is observed at very low temperatures, the lower temperatures (liquid helium and liquid nitrogen) increasing the sensitivity of the haem centre to photodissociation (triple trapping).

Fig.5.6. shows the increase in rate for white and blue light illumination of the CO inhibited oxidase. Red light stimulation was virtually undetectable (not shown). The points were computer analysed and the best-fit lines are 5th order polynomials. The non-dissociation of d-CO at wavelengths where haem-d absorbance is greatest (alpha region) suggested the increase in rate observed for white light and blue light can be attributed to photodissociation of b595-CO only. The slightly lower rates observed for blue light compared to white light being due to the decrease in intensity in the presence of the blue filter (see Fig.5.2). If d-CO is not photolysed by red light, yet haem-d binds dioxygen, the light source must be of a lower intensity than required to appreciably dissociate this haem (haem-d having

Figure 5.6

White and blue light photodissociation of CO inhibited cytochrome-bd.

Oxygen electrode progress curves are shown for CO inhibited cytochrome-*bd*. Individual curves for a dark control and white (WL) and blue (BL) light illumination are overlayed. The collected points have been fitted with 4th and 5th order polynomials. Experimental conditions were as in Fig.5.5 except CO concentration, 0.804mM; oxygen concentration, 0.05mM.

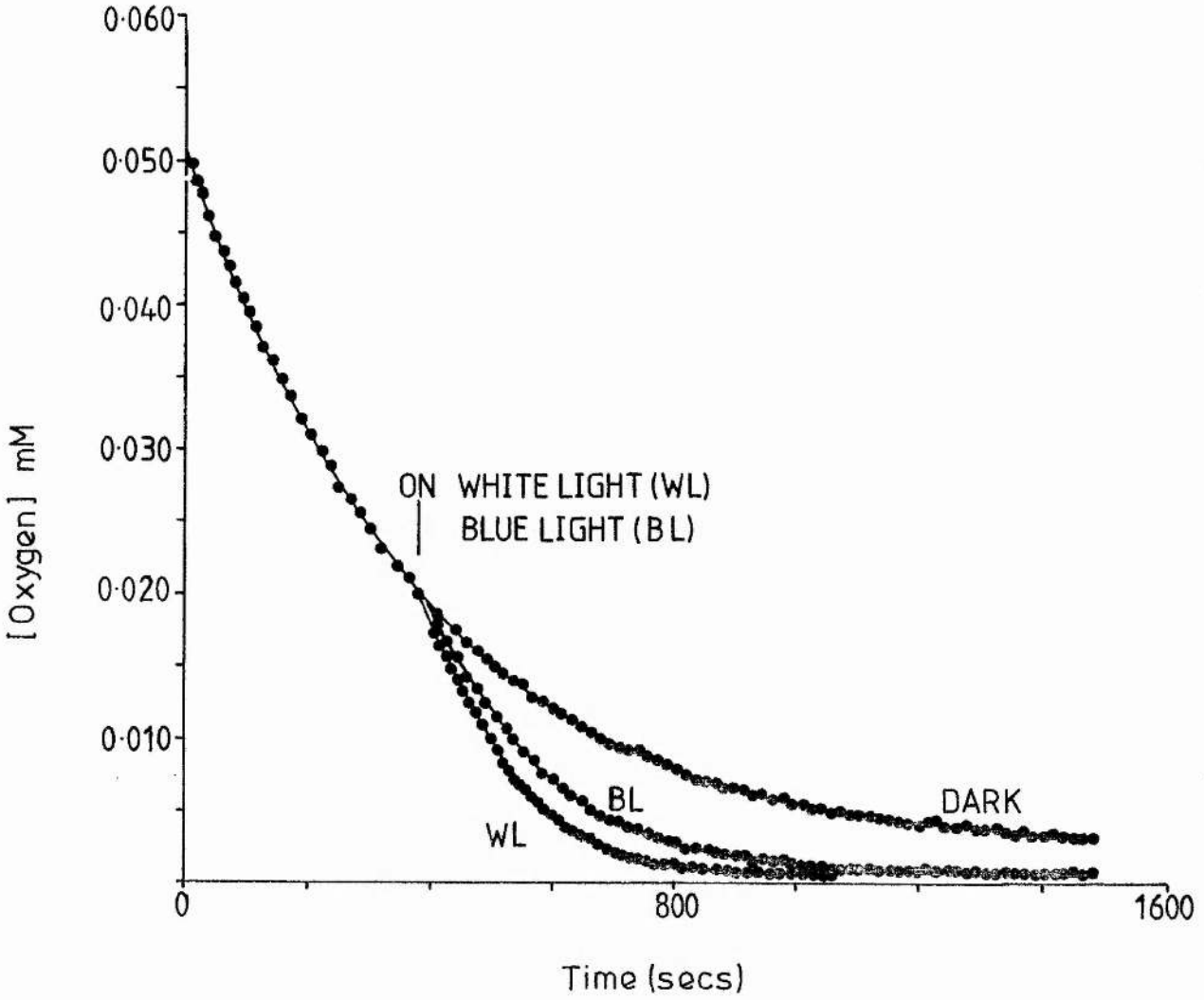
0·060
0·050
0·040
0·030
0·020
0·010
[Oxygen] mM
ON WHITE LIGHT (WL)
BLUE LIGHT (BL)
BL
WL
DARK
0
800
1600
Time (secs)

a very high affinity for CO, see Poole *et al.*, 1982a).

To calculate the relative increase in rate for photodissociation the rate at oxygen concentrations for the dark control were compared with the same concentrations in the presence of light. This gives the percentage stimulation as a function of the control rate (dark). Slight deviation between control rates are accounted for by comparing the initial non-illuminated area of each progress curve. The progress curves were illuminated at around 350 seconds (<40:1, $CO:O_2$) and the rate for 60:1 (around 450 seconds) was determined for percentage light stimulation. The ratios were calculated from the starting concentrations of CO and dioxygen.

To test for the limiting low intensity of the xenon arc lamp, and its resultant degree of photodissociation, an intensity (power) profile for blue and white light photodissociation was determined. Gelatin neutral density filters (Kodak) reduced, by known increments, the intensity (% transmission) of light and the relative increase in rate was calculated. The gelatin filters were protected by glass plates to prevent melting. Fig.5.7. gives the percentage of light relief for white and blue light intensities. The 100% transmission value is for light in the absence of neutral density filters and the 100% light relief value is the maximum value for relative rate increase, the points are an average of two determinations at 60:1, $CO:O_2$. The percentage light relief of the inhibited control (dark) rate was calculated by taking the rate at 60:1 $CO:O_2$ for photolysed

Figure 5.7

Percentage inhibition relief for variable white and blue light intensities.

The percentage transmission for white and blue light were reduced by neutral density filters. The increase in oxidase rate upon illumination was calculated as a percentage of the control (dark) rate and plotted as % light relief versus % transmission. 100% transmission is in the absence of neutral density filters and 100% light relief was the maximal value obtained for rate increase. The points are the average values for two determinations at $CO:O_2$, 60:1; (●), white light; (□), blue light. Experimental conditions were as described in Fig.5.5.

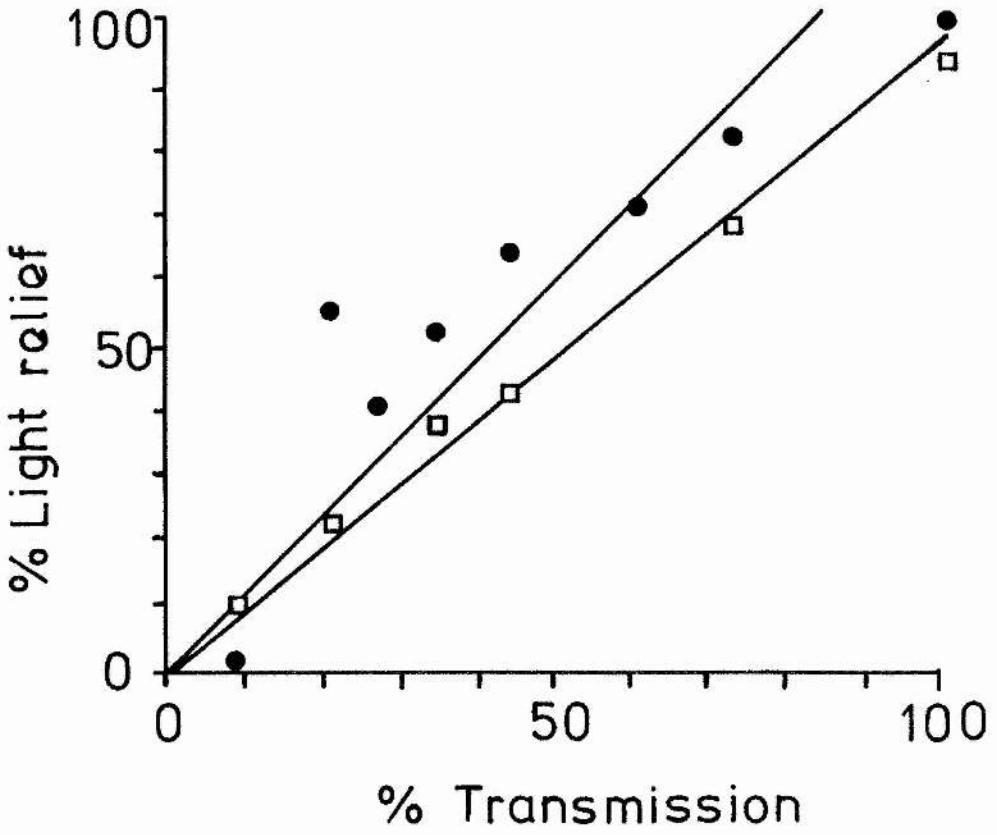
100
50
0
% Light relief
0
50
100
% Transmission

inhibition minus the control rate and dividing by the control rate. The lines through the points of Fig.5.7 indicate photodissociation for white light and blue light are roughly equivalent, the slight decrease for blue light being attributable to the lower intensity of light due to the blue filter. The saturation value for light relief of CO inhibited respiration was not attained. Future experimentation will therefore require laser light sources to obtain higher degrees of stimulation.

Oxidase rate, at low oxygen concentration, in the absence of CO is much higher than obtained for white light photodissociation (Fig.5.8). The non-inhibited rate was obtained with nitrogen saturated buffer (50mM phosphate buffer, pH7.0) not CO saturated buffer. Fig.5.8 compares the rate of dioxygen reduction for no inhibition with a white light photolysed (410secs) progress curve. The nitrogen control rate would be approached if the CO inhibited haem centres were fully photodissociated. The maximal rate for white light is only 10% of the nitrogen control rate. Photodissociation studies for *Azotobacter vinelandii* have shown maximal increases of rate for CO bound haems as 60-80% (laser light, Hoffman *et al.*, 1980). 100% increases would be unlikely because of the specific K_D for CO. Although using the xenon arc lamp maximal rates were not obtained increased rates were clearly observed (Fig.5.6).

Figure 5.8

Oxygen electrode progress curves for CO inhibited and uninhibited cytochrome-bd.

A CO inhibited oxygen electrode progress curve, illuminated by white light at 410seconds (ON), is compared to the uninhibited rate for a progress curve at low oxygen concentration. The uninhibited rate was obtained by substituting nitrogen saturated buffer for CO saturated buffer. Oxygen saturated buffer was added to bring the starting concentration to 0.045mM. Experimental conditions were as in Fig.5.5. The CO points are fitted to 5th order polynomials and the nitrogen control is fitted to a straight line (1st order polynomial).

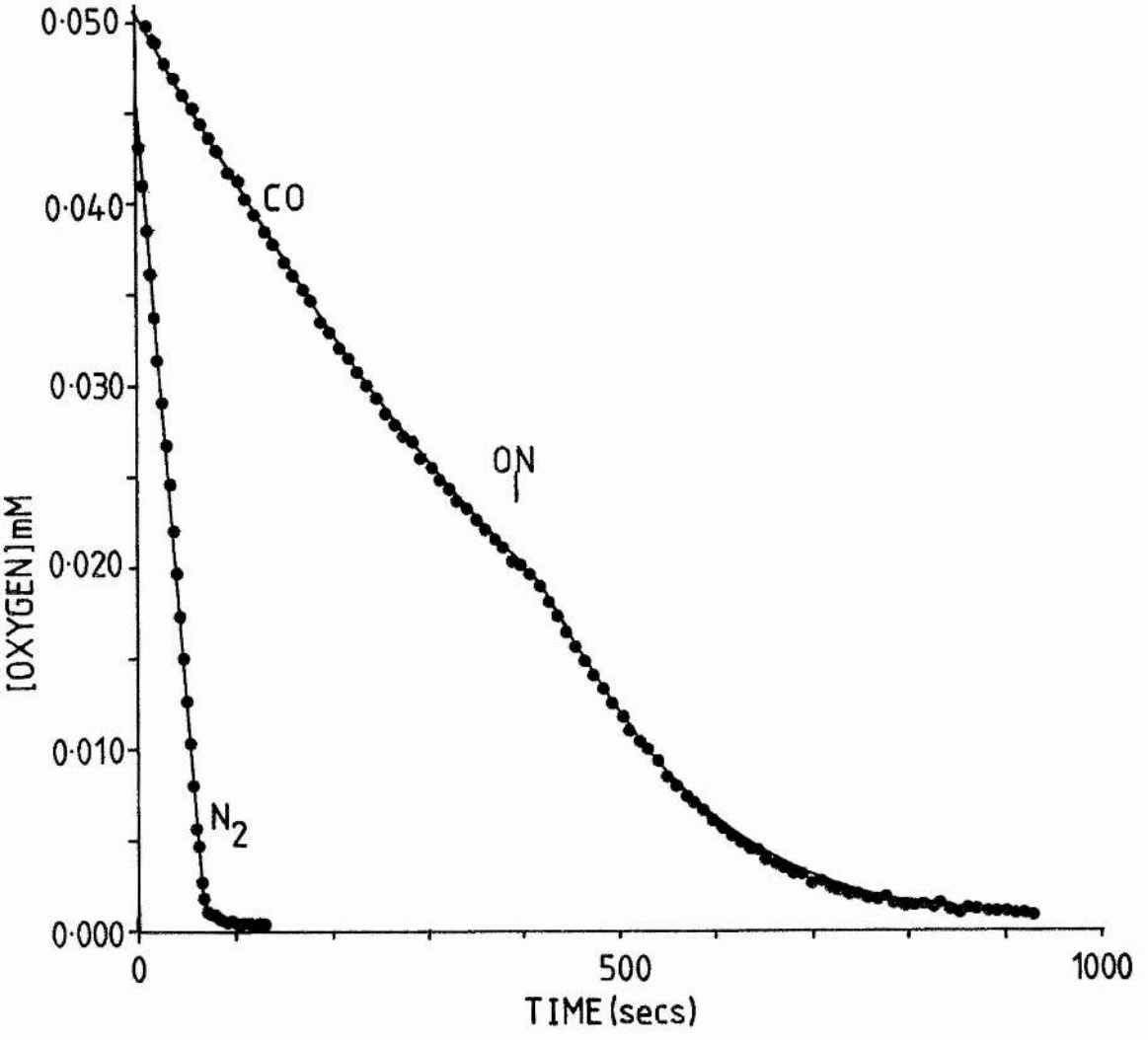
0·050
0·040
0·030
0·020
0·010
0·000
[OXYGEN]mM
CO
ON
N2
0
500
1000
TIME (secs)

5.4. Conclusions.

From these data the xenon arc lamp was not of a high enough intensity to appreciably photodissociate CO ligated haem-d of *E. coli* cytochrome-*bd*. Haem-d has a very high affinity for CO (Poole *et al.*, 1982a) and, as shown for other CO ligated d-type haems, is difficult to photolyse at room-temperature with low power (Lloyd and Scott, 1987). Photodissociable stimulation of respiratory rate is attributed to dissociation of b595-CO.

If b595-CO is photodissociated and causes an increase in rate this haem centre must be involved in active site dioxygen reduction. This does not however necessarily suggest haem-b595 binds and reduces dioxygen to be assigned an independent "oxidase" function. The advantages of a bimetallic site for dioxygen reduction (see chapter 7) suggest both haem-b595 and haem-d are involved in catalysis. For dioxygen reduction haem-d must be uninhibited for both haem-b595 and haem-d to ligate dioxygen between the two centres (bimetallic site).

Double dioxygen binding at the active site (with both haem-d and haem-b595 bound) followed by reduction to peroxide and disproportionation to form water leaving one dioxygen bound (Fig.5.9), would be unlikely as more than one dioxygen is required for reduction and this oxidase functions principally when little oxygen is available.

Presenting the above data as a double bound CO pocket which binds only a single dioxygen (bridged between haem-d

Figure 5.9

A double dioxygen binding site for Escherichia coli cytochrome-bd?

The double dioxygen reduction scheme for *Escherichia coli* cytochrome-*bd* is presented (Rothery *et al.*, 1987). The scheme requires both haem-d and haem-b595 to ligate dioxygen with subsequent four electron reduction to form bound peroxide with disproportionation to give water and leave one dioxygen bound.

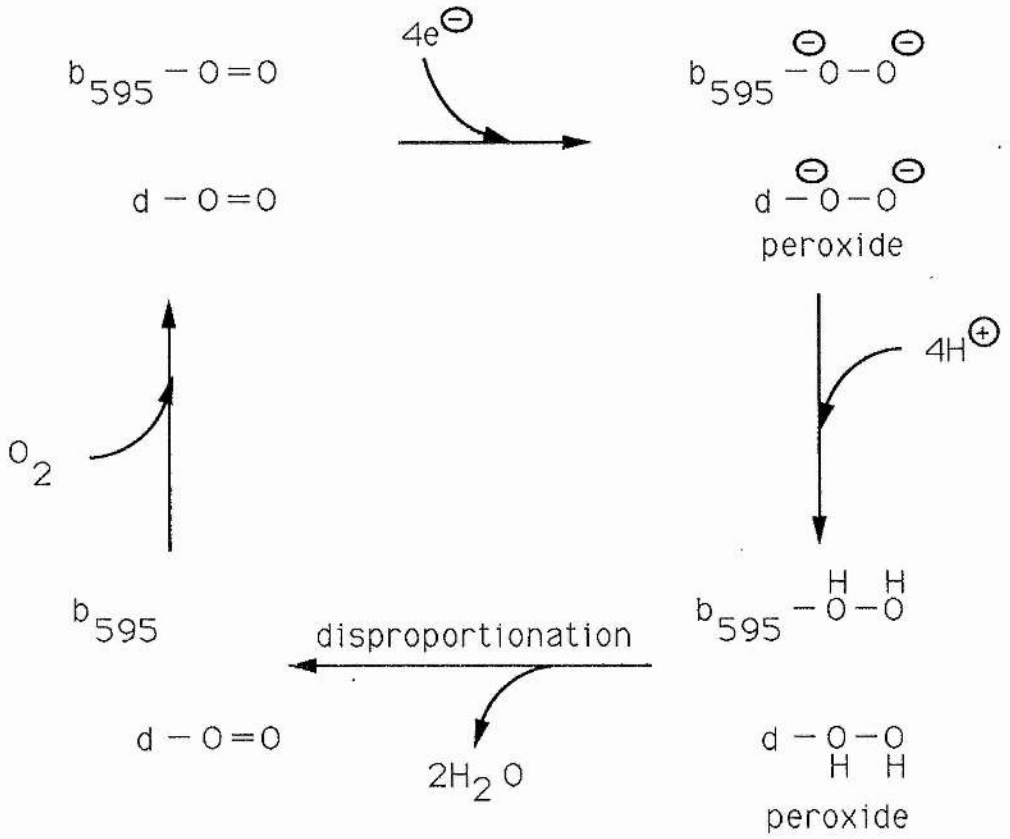

Double dioxygen binding and reduction?

and haem-b595) gives the cytochrome-*bd* enzyme/inhibitor/substrate equilibrium complex of Fig.5.10. In this representation CO is inhibitor, I; dioxygen is substrate, S; and cytochrome-*bd* is enzyme, E. The relative equilibrium constants are given as reference to each step. The photodissociable states in the complex are EI_bI_d, $E\_{b}I_d$, EI_{b}_{d}, EI_bS_d and ES_bI_d but only the I_b states were dissociated by the xenon arc lamp. The relative rates for each pathway in the steady-state are not known and so the major catalytic pathway in the presence of CO cannot be given. Taking the model at equilibrium Michaelis-Menten analysis suggests the slope factor and the intercept factor contain the inhibitor concentration as a variable (Fig.5.10). This will give mixed-type inhibition in the presence of CO, not pure competitive. Mixed-type inhibition was observed by Rothery (1989) for CO inhibition of cytochrome-*bd*, both Vmax and Km vary with inhibitor concentration. Fig.5.10 suggests an enzyme state exits, in the presence of CO, where haem-b595 is ligated by dioxygen and haem-d is ligated by CO (ES_bI_d). As a comparison the binding of dioxygen to Cu_B before bridging with haem-a_3 in cytochrome oxidase has been postulated (Alben *et al.*, 1981). Here, because haem-d has a higher affinity for ligands (dioxygen), substrate binding to haem-b595, in preference to haem-d, is a function of CO inhibition (the binding of dioxygen to haem-b595 may decrease the affinity of haem-d for CO, a cooperative affect?). Haem-b595 may bind dioxygen while haem-d is inhibited if haem-b595 is susceptible to

Figure 5.10

Enzyme/inhibitor/substrate complex for Escherichia coli cytochrome-bd: double CO binding, single dioxygen binding. The equilibrium complex for carbon monoxide inhibited cytochrome-*bd* is shown. A single dioxygen ligating bimetallic site is envisaged. The substrate binding (K_S) and inhibitor binding (K_I) equilibrium constants are shown for each step. For Michaelis-Menten analysis the equilibrium constants were multiplied by arbitrary values, a, b, c, d, etc. Cytochrome-*bd* enzyme complex, E; carbon monoxide inhibitor, I; and dioxygen substrate, S; with water product P, are shown.

The schematic representation of the active site is from unpublished e.p.r. studies (see section 1.4.2) and show haem-d perpendicular to the membrane plane with haem-b595 at 45°. From orbital chemistry carbon monoxide binds to haem with a linear conformation and dioxygen binds at an angle. The distance between haem-d and haem-b595 has not been determined. From the data of Rothery and Ingledew (1989) haem-d and haem-b595 show haem-haem interaction and a maximum distance apart of 12Å is envisaged (W.J.Ingledew, personal communications), the ideal distance for dioxygen ligation in a bimetallic site is around 5A. Michaelis-Menten analysis presents the inhibitor variable in both the slope and the intercept factors suggesting mixed-type inhibition.

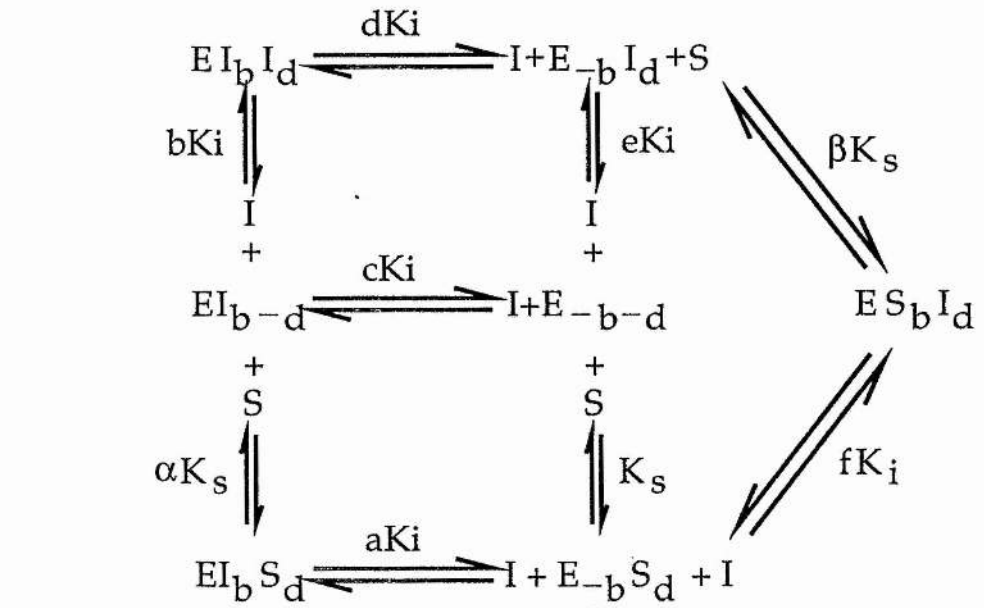

E = Enzyme
I = Inhibitor (carbon monoxide)
S = Substrate (dioxygen)

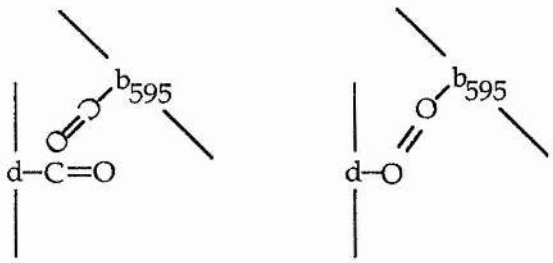

When

$$\frac{v}{[E]_t} = \frac{kp\,[E_{-b}S_d]}{[E_{-b-d}] + [E_{-b}S_d] + [EI_bS_d] + [EI_{b-d}] + [EI_bI_d] + [E_{-b}I_d] + [ES_bI_d]}$$

Then

$$\frac{v}{V_{max}} = \frac{[S]}{K_s\left[1 + \frac{[I]}{cKi} + \frac{[I]^2}{bcKi^2} + \frac{[I]}{eKi}\right] + [S]\left[1 + \frac{[I]}{aKi} + \frac{[I]}{fKi}\right]}$$

slope factor — intercept factor

oxygen as a ligand. This can be related to the chemistry for CO binding to haem centres: because CO binds in a straight configuration to haem-d (see chapter 7 for chemistry) there is enough "space" in the haem pocket for dioxygen to bind to haem-b595. In Fig.5.10 the plane of haem-d is perpendicular to the membrane plane and haem-b595 is at 45° to the membrane plane (see section 1.4.2). The distance between haem-d and haem-b595 is not known although they are both associated with subunit II of the enzyme and from haem-haem interactions the distance is less than 12Å (W.J.Ingledew, personal communications), the ideal distance for dioxygen ligation would be in the region of 5Å. There is no evidence for haem-b595 ligating dioxygen in preference to haem-d and if ES_bI_d was excluded from Fig.5.10 equilibrium analysis would still predict mixed-type inhibition.

A simple flipping of carbon monoxide between the haem centres (EI_{b_d}/E_bI_d) has not been demonstrated in cytochrome-*bd* although it is thought to occur for anoxic cytochrome oxidase photolysed at low temperature. When CO ligated haem-a_3 (a_3-CO) is photolysed under anoxic conditions the unbound copper centre binds the CO (Alben *et al.*, 1981). Interestingly, photolysed haem-d-CO, under anoxic conditions, recombines with CO so quickly that the reduced spectrum of haem-d is not observed (Poole *et al.*, 1982a). Recombination of CO to haem-d also occurs at much lower temperatures (helium) than observed for reduced haem-a_3 photolysed species and may be a function of the second centre in the bimetallic site. In cytochrome oxidase

the unligated copper can bind the photolysed CO from haem-a_3 but in cytochrome-*bd* haem-b595 may not be susceptible to the haem-d photolysed CO and the CO reassociates with haem-d. This again may be related to the chemistry of ligand binding and possibly the very low Km for dioxygen (see chapter 7). The flipping of CO between haem centres in the cytochrome-*bd* may be observed if very low concentrations of CO were present so that only haem-d was bound.

The photodissociation apparatus presented will lend itself to further study with higher powered light sources (tunable lasers) for observing kinetics when both d-CO and b595-CO are photolysed individually or simultaneously at specific wavelengths (two light tunnels into the vessel). The rate increases for individual haem dissociation and double dissociation will give information on the relative rate increases for the haem centres showing possible cooperative affects for oxygen binding in the presence of inhibitor (cooperativity for the bimetallic ligation of a single dioxygen). High powered light sources may also determine the actual action spectra of cytochrome-*bd*. *Escherichia coli*, strain FUN4/pNG2, which is deleted in cytochrome-*bo* and amplified in cytochrome-*bd* should be studied to improve resolution.

In conclusion two CO molecules can bind at the active site but for catalytic reduction of dioxygen only one dioxygen is ligated at the bimetallic site.

Chapter 6 deals with the interesting case of inhibition by nitric oxide and gives reasons for nitric

oxide inhibition being competitive (not mixed), this also being a function of the binding chemistry for that ligand.

The conclusions reached in this chapter are related to dioxygen catalysis in chapter 7.

Chapter 6

UBIQUINOL-OXYGEN OXIDO-REDUCTASE CYTOCHROME-bd: NITRIC OXIDE LIGAND BINDING.

Chapter 6

6.1. Introduction.

Section 1.4.2 outlined the binding properties of nitric oxide (NO) as a sixth coordinate ligand of haemoproteins. The aim herein is to verify and expand the work of Rothery (1989), identifying the NO binding properties of *E. coli* ubiquinol-oxygen oxido-reductase cytochrome-*bd* and relate these data to the catalytic mechanism of dioxygen binding and reduction. Rothery demonstrated the NO binding properties of anaerobically grown *E. coli* (wild-type strain, EMG2) and the work presented herein studied the cytochrome-*bd* amplified strain, FUN4/pNG2, which is deleted in cytochrome-*bo*.

Optical spectra of reduced + nitrite minus reduced cytochrome-*bd* revealed a previously undefined absorbance in the Soret region. The e.p.r. assignment of haem-NO spectra are in accordance with Rothery (1989) showing haem-d-NO and haem-b595-NO formation. A double binding pocket for NO does not necessarily suggest a double dioxygen binding pocket. A free radical species observed in e.p.r. spectra of NO bound cytochrome-*bd* is assigned to a ubiquinol binding site at the oxidase complex.

Models are presented for anoxic nitrite reduction and dioxygen reduction in the presence of nitrite.

6.2. Optical spectra: reduced + nitrite minus reduced.

Fig.6.1 shows a time course of reduced + nitrite

Figure 6.1

Reduced + nitrite minus reduced optical spectra of Escherichia coli FUN4/pNG2 membranes, pH7.0.

A time course of spectral changes in the 400-->700nm absorbance range are shown for nitrite addition to reduced membranes of the cytochrome-*bd* amplified strain, FUN4/pNG2. Spectra were recorded with a split-beam spectrophotometer at room-temperature. The baseline (bl) was obtained with the two stoppered cuvettes containing 7mg.ml^{-1} etp, 50mM BES pH7.0 reduced with 10mM sodium lactate. Spectra are shown for set time intervals after addition of 10mM sodium nitrite: a, 10 seconds; b, 10 mins; c, 21 mins; d, 31 mins; e, 41mins; f, 52 mins; g, 70 mins; h, 120mins; i, 240 mins. The major peak/trough wavelength values are shown above the spectra (nm).

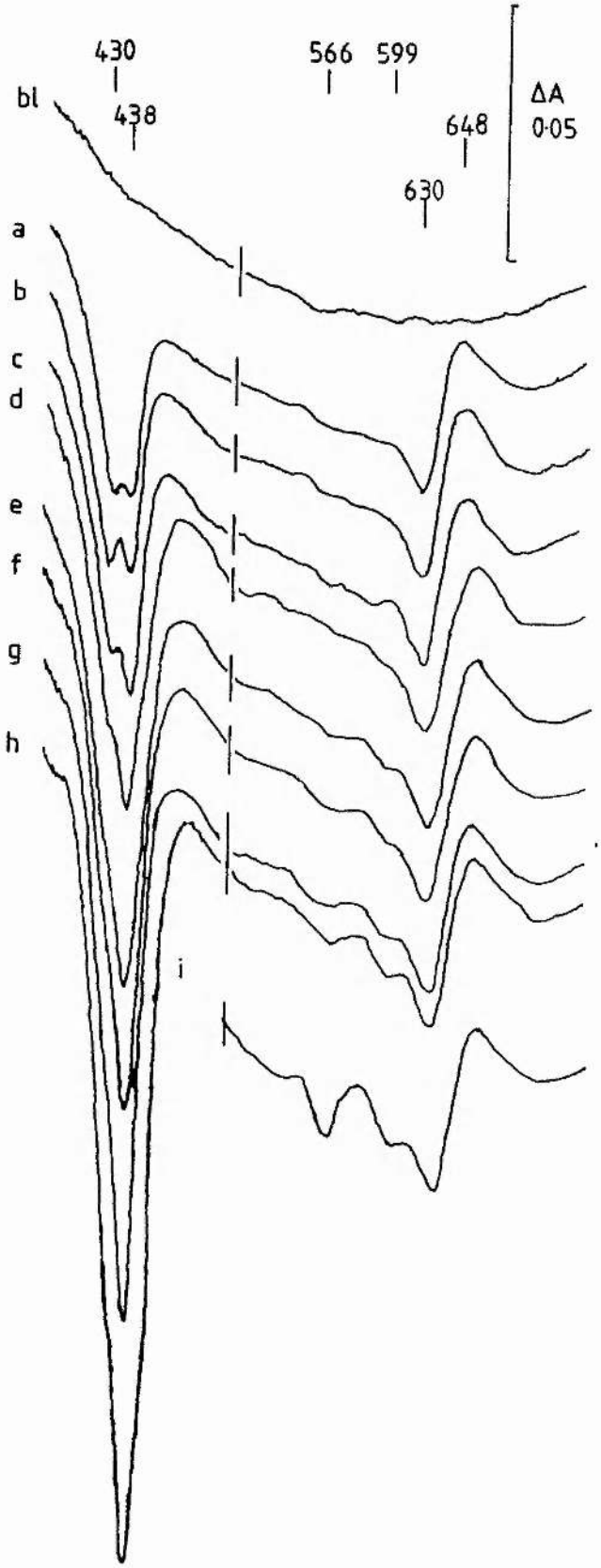
430
566
599
438
648
630
ΔA
0·05
bl
a
b
c
d
e
f
g
h
i

minus reduced room-temperature optical spectra adding 10mM sodium nitrite to reduced anoxic FUN4/pNG2 membranes (7mg.ml^{-1} etp, 50mM BES, pH7.0, 10mM sodium lactate). Cytochrome-*bd* reduces nitrite to leave nitric oxide ligated to the haem:

$$NO_2^- + 2H^+ + e^- \longrightarrow NO + H_2O \qquad E_{m7} = +350mV$$

The d-NO species is completely formed within the first scan time (Fig6.1a) and is assigned an alpha region trough-peak at 630-648nm in accordance with Rothery *et al.* (1987). Fig.6.1a also shows a W-shaped trough at 430nm and 438nm with the 438nm trough assigned to b595-NO (Rothery *et al.*, 1987). The 430nm trough was assigned to oxidized haem-b558, not haem-d, as this is the major Soret absorption region of this haem. Haem-b558 oxidation occurs for the single electron reduction of nitrite to nitric oxide, haem-d remaining reduced (higher potential) and ligand bound (c.f. stopped-flow data where, upon mixing with oxygen, both haem-d and haem-b558 are oxidized within 3msecs; Haddock *et al.*, 1976; D.S.Wariabharaj and W.J.Ingledew, unpublished data). As b595-NO slowly forms (Fig.6b-->h, 10mins-->2hr) the 438nm trough incorporates the 430nm trough and possible re-reduction of haem-b558 by the quinol pool could not be observed. Previous studies with wild-type *E. coli* have not resolved a 430nm trough. Fig.6.1a does not show obvious spectral changes in the alpha region at 558nm suggesting haem-b558 is only partially oxidized. Partial oxidation of haem-b558 is related to a free radical signal observed in e.p.r. haem-NO spectra (section 6.2). The apparent

non-identification of a d-NO absorbance in the Soret region is consistent with this haem showing minimal Soret absorption (see section 1.4.1).

Haem-b595 reduction of nitrite in amplified cytochrome-*bd* was slower than observed for the wild-type strain of Rothery *et al.* (1987). At high nitrite concentrations (30mM sodium nitrite) b595-NO formation is over several hours (not shown). Haem-b595-NO is fully formed in wild-type *E. coli* in approximately 60 minutes (anaerobic growth, Rothery *et al.*, 1987) and in Fig.6.1i in 4hrs. Slower binding in the amplified strain (aerobic growth) may be a function of the different growth conditions and the conformation of the enzyme. The measured midpoint potentials of the haem centres vary for anaerobic and aerobic growth (Reid and Ingledew, 1979; Lorence *et al.*, 1984; Koland *et al.*, 1984) and different quinone species predominate in the membrane (Ingledew and Poole, 1984).

The low nitrite (NO) affinity of haem-b595 should be noted, the slow formation of the b595-NO Soret trough is associated with concomitant changes in the alpha region at around 566nm. The 566nm trough of Fig.6.1i (4hrs) was assigned to the large β-band absorbance of haem-b595 and a trough at 599nm to the alpha absorbance.

Many *E. coli* cytochromes absorb in the 560nm region resulting in difficulties with analysis and deconvolution: for example, early triple trapping studies assigned a specific spectral feature to a new type of o-oxidase which may equally have been attributed to haem-b595 of

cytochrome-*bd* (Poole and Chance, 1981), this latter haem receiving little attention in previous analyses. Haem-b595 is now known to be an integral haem in cytochrome-*bd* and, due to multiple-phase oxidation kinetics, is kinetically competent for inclusion in all models presented herein (see, Ingledew, 1977; Haddock *et al.*, 1976; Poole and Williams, 1987; Wariabharaj and Ingledew, 1987). Section 6.4 presents active site conformational arrangements to explain low haem-b595 NO affinity (c.f. CO affinity, chapter 5 and Rothery, 1989).

These optical studies were compared to similar haem-NO formation time courses prepared for e.p.r. spectroscopy. The data confirmed and expanded the e.p.r. data of Rothery (1989) showing two high-spin haems reducing nitrite (or binding NO) with differing affinities.

6.3. *Electron paramagnetic resonance spectroscopy: cytochrome-bd haem-NO.*

6.3.1. E.p.r. spectral assignements of d-NO and b595-NO.

E.p.r. spectra of NO ligated amplified cytochrome-*bd* were similar to the wild-type *E. coli* spectra of Rothery (1989). Fig.6.2 shows the e.p.r. time course for cytochrome-*bd* haem-NO formation under similar experimental conditions to Fig.6.1. E.p.r. samples were prepared as described in section 2.7.3 adding 30mM sodium nitrite to

Figure 6.2

E.p.r. time course in the g=2.000 region for nitrite addition to reduced cytochrome-bd, pH7.0.

E.p.r. samples were prepared to show a time course of haem-NO formation for FUN4/pNG2 membranes at 30°C. The baseline (bl) was recorded for 25mg.ml^{-1} etp, 50mM BES 5mM EDTA, pH7.0, 10mM sodium lactate (reaction vessel under anoxic conditions purged with nitrogen gas, section 2.7.3). The baseline was not subtracted from subsequent spectra. After addition of 30mM sodium nitrite samples were extracted and frozen at set time intervals: a, 1 min; b, 3 mins; c, 7 mins; d, 12 mins; e, 25 mins; f, 60 mins. Spectral g-values are shown above the spectra. E.p.r. conditions were: microwave frequency, 9.47GHz; modulation frequency, 100kHz; modulation amplitude, 0.63mTesla; microwave power, 5.3mW; temperature, 30K. Spectrometer gain was equivalent for all spectra.

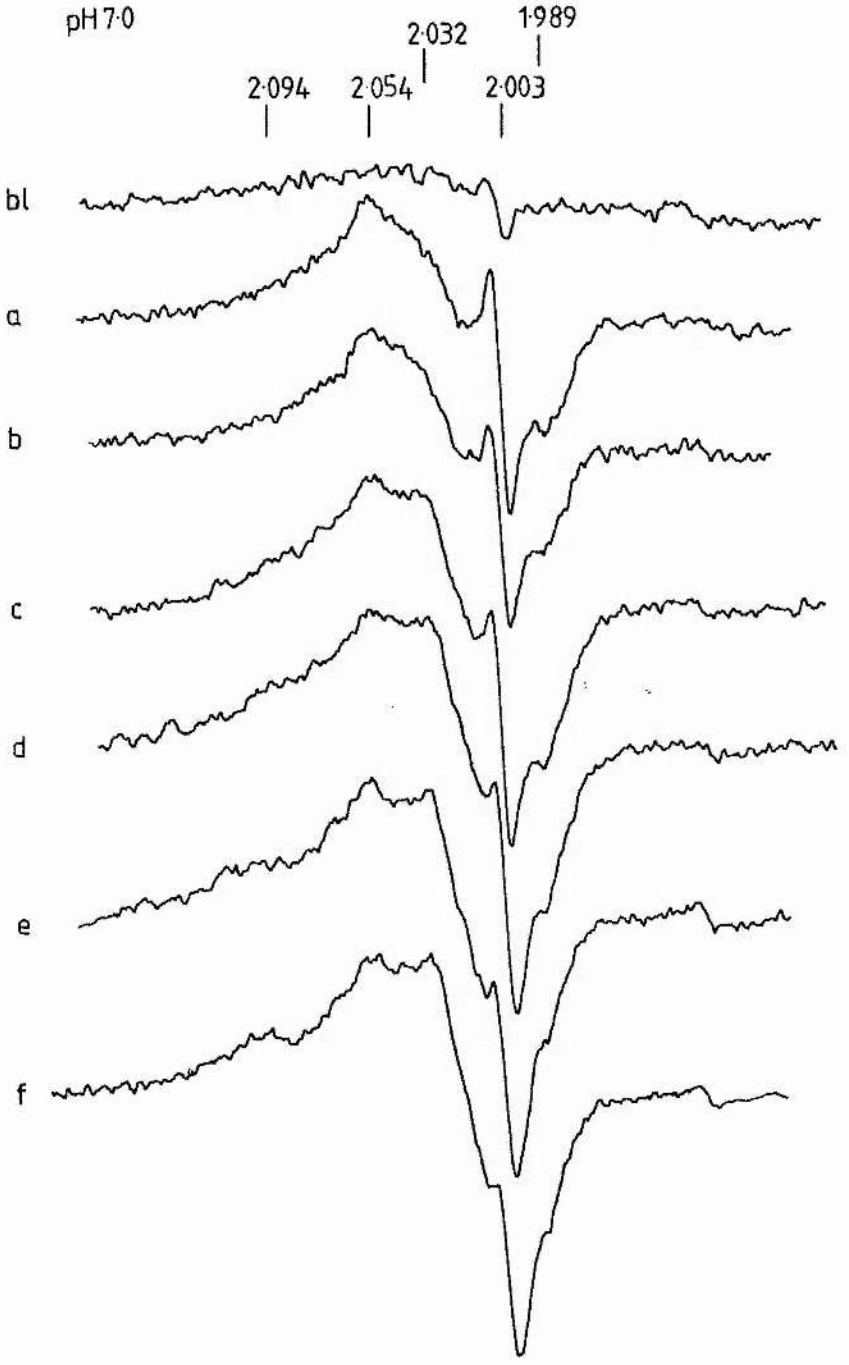
pH 7·0
2·094
2·054
2·032
1·989
2·003
bl
a
b
c
d
e
f

reduced anoxic membranes (25mg.ml^{-1} etp, 50mM BES 5mM EDTA pH7.0, 10mM sodium lactate, 30°C). The lactate reduced baseline has few spectral features and was not subtracted from subsequent spectra (Fig.6.2b1). 1 minute after nitrite addition the d-NO species forms along with a large free radical signal (Fig.6.2a). A peak at g=2.054 and a trough at g=1.989 is assigned to d-NO, the free radical signal obscures the peak-trough and is centred at around g=2.003. At 3-12mins (Fig.6.2b,c,d) the d-NO signal becomes more rhombic with spectral changes in the g=2.094 region followed by further changes at around g=2.032. From the saturation parameter, P1/2, the g=2.094 signal is also attributable to d-NO (Rothery, 1989). The spectral lineshape change suggests a d-NO type II to type I transition. Type I haem-NO species have the haem Fe displaced towards the proximal ligand and type II species have the haem Fe displaced towards the distal ligand (Morse and Chan, 1980). The g=2.032 peak is attributed to the slow formation of b595-NO in accordance with the data of Rothery (1989). The b595-NO species is not fully formed after 60 minutes (Fig.6.2f). This work assigns type I rhombic haem-d-NO $g_{x,z,y}$ values at pH7.0 of 2.094, 2.000 and 1.989, respectively, with a type II transition $g_{?}$=2.054 in accordance with assignment of other NO ligated haemoprotein species (see Morse and Chan, 1980).

The data of Rothery *et al.* (1987) suggested lower pH will increase the extent of b595-NO formation giving a more intense signal. Fig.6.3a shows the pH6.0 b595-NO g=2.032 peak with associated d-NO spectral features at temperature,

Figure 6.3

E.p.r. spectra of d-NO and b595-NO at 10K and 64K (pH6.0).

E.p.r spectra are shown for FUN4/pNG2 membranes, 25mg.ml^{-1} etp, 50mM MES, 5mM EDTA, pH6.0, reduced with 10mM sodium lactate as in Fig.6.2 and incubated with 30mM sodium nitrite for 8hrs, 30°C. Both d-NO and b595-NO are fully formed.

a) at 10K the rhombic d-NO spectral features are observed with b595-NO slightly saturated.

b) at 64K only the axial b595-NO spectral features are observed.

Spectral g-values are shown above the spectra. E.p.r. conditions were: microwave frequency, 9.47GHz; modulation frequency, 100kHz; modulation amplitude, 0.63mTesla; microwave power, 0.55mW. The spectrometer gain was equivalent for a) and b).

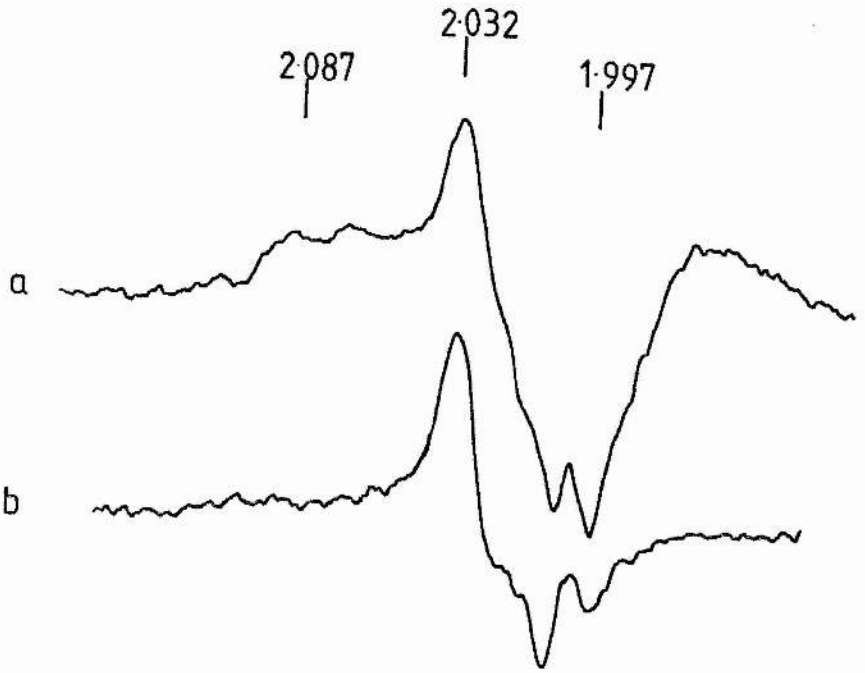
2·032
2·087
1·997
a
b

10K; microwave power, 0.55mW; b595-NO slightly saturated. The sample was prepared by incubating 25mg.ml^{-1} etp, 50mM MES, 5mM EDTA, 10mM lactate, pH6.0, for 8hrs with 30mM sodium nitrite to ensure complete formation of b595-NO. Fig.6.3b is the same sample at higher temperature (64K; microwave power, 0.55mW), showing the unsaturated b595-NO signal, the d-NO spectral features are not observed at higher temperature because of the high relaxation rate of d-NO (see also Rothery, 1989). The b595-NO signal is axial with a peak at g=2.032 and a trough at around g=1.997 (slightly obscured by free radical in Fig.6.3b). The low-field spectral g-value attributable to d-NO has moved slightly up-field from Fig.6.2 (pH7.0, 30K, g_x=2.094; pH6.0, 10K, g_x=2.087).

Fig.6.4a shows e.p.r. spectra 1 minute after addition of nitrite with d-NO g-values shown above the spectra (sample preparation as for Fig.6.3). The free radical is around g=2.000 and the g=2.054 feature of Fig.6.2 is indicated as the g_z of the typeII/typeI transition. Upon lowering the temperature of the the 1 minute sample from 30K to 12K the g=2.054 peak became more rhombic with the g=2.087 feature observed, suggesting a type II to type I transition on lowering the temperature (compare Fig.6.4, 12K with Fig.6.8a, pH6.0, 30K). Fig.6.4b shows a similar sample after 8hrs incubation with nitrite, Fig.6.4a overlaps Fig.6.4b (dashed line), the g-values for the b595-NO axial peak-trough are shown below the spectra. The g_y of d-NO (g=1.984) is obscured by the large b595-NO trough at 8hrs.

Figure 6.4

E.p.r. spectra for haem-NO formation 1 minute and 8 hrs after nitrite addition to reduced cytochrome-bd.

E.p.r spectra are shown for FUN4/pNG2 membranes, 25mg.ml^{-1} etp, 50mM MES, 5mM EDTA, pH6.0, reduced with 10mM sodium lactate as in Fig.6.2 and incubated with 30mM sodium nitrite for; a) 1 minute and, b) 8hrs, at 30°C. In b) the spectral lineshape of a) is shown as an overlayed dashed line. The d-NO spectral g-values are shown above the spectra and the b595-NO values are shown below. E.p.r. conditions were: microwave frequency, 9.47GHz; modulation frequency, 100kHz; modulation amplitude, 0.63mTesla; microwave power, 0.55mW; temperature, 12K. Spectrometer gain was equivalent for a) and b).

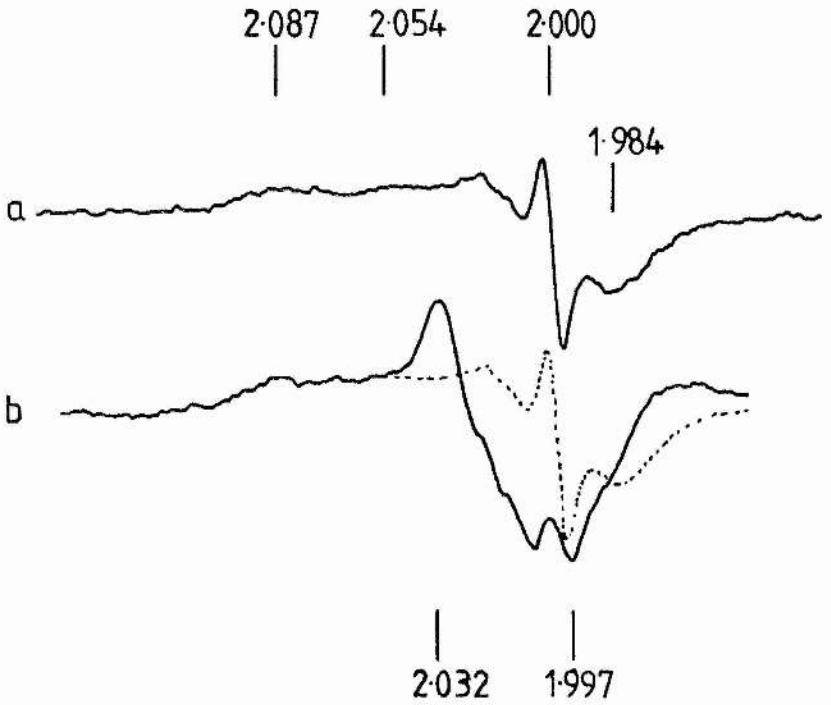
2·087
2·054
2·000
1·984
a
b
2·032
1·997

The g_z of d-NO (around g=2.000) is also obscured and appears to be incorporated into the b595-NO signal (b595-NO is slightly saturated). These spectral changes do not appear to be a simple overlap of two signals and suggest either a structural/conformational change to d-NO upon b595-NO formation or a spin-spin interaction (T_2, spin-spin relaxation time for linewidth variation) between the unpaired electrons of the two NO species, or both (close proximity?).

In conclusion, from Fig.6.2, 6.3 and 6.4 two e.p.r. detectable NO species are present and in accordance with Rothery (1989) these are assigned to nitrite reduction and NO ligation by both haem-d and haem-b595, haem-b595 showing a low affinity for nitrite reduction (NO binding). The d-NO g_z signal is not observed independently, the signal always being associated with either free radical or b595-NO. Meindhart *et al.* (1986) have suggested only haem-d reduces nitrite with no e.p.r. signal attributed to b595-NO, the incubation time for nitrite reduction was not however stated and no further work has been published.

6.3.2. Electronic interactions of NO ligated haem-d and haem-b595.

Fig.6.5 shows the microwave power profile for the low-field peak (g=2.087, d-NO, pH6.0) 1 minute after addition of nitrite when, from Fig.6.1, little b595-NO has formed, and also after 8hrs when a large b595-NO signal is

Figure 6.5

Microwave power profile for the d-NO g=2.087 spectral feature (pH6.0).

Microwave power saturation profiles of Fig.6.4 were recorded to obtain the P1/2 values for d-NO (g=2.087), when little b595-NO has formed (1 minute), and when b595-NO levels are maximal (8hrs). P1/2 = 69mW at 1 minute (◆) and 55mW at 8hrs (●). E.p.r conditions were as in Fig.6.4 with variable microwave power.

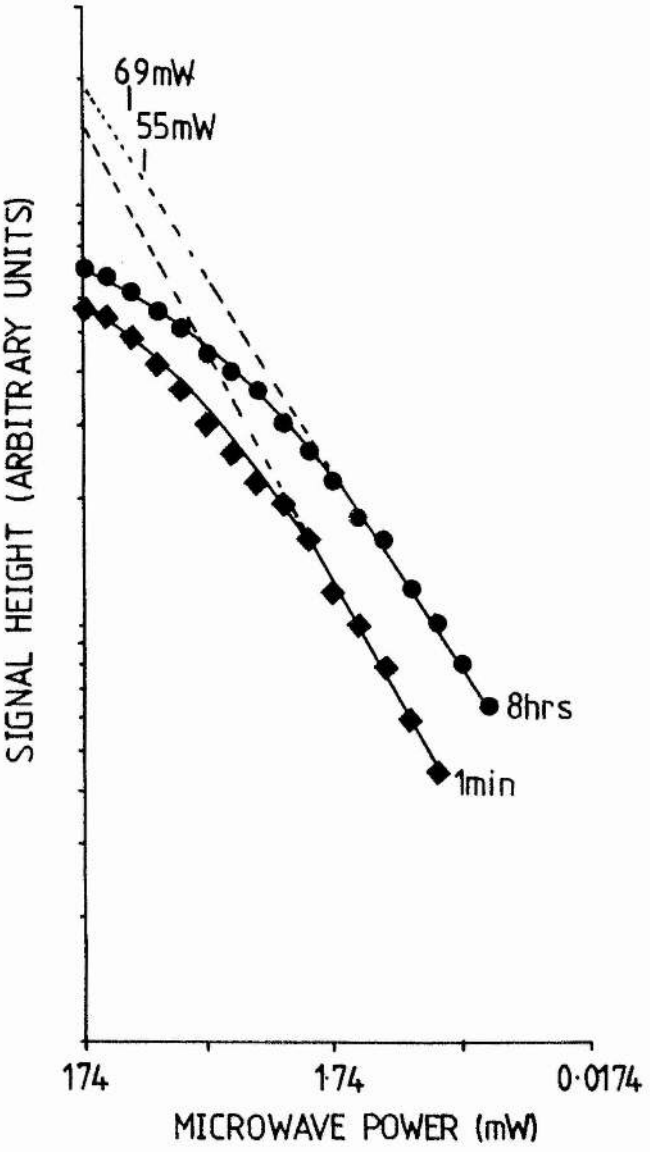
69mW
55mW
SIGNAL HEIGHT (ARBITRARY UNITS)
8hrs
1min
174
1·74
0·0174
MICROWAVE POWER (mW)

observed (Fig.6.3, 6.4b). The d-NO species has a fast relaxation and required low temperatures (12K) and high microwave powers to saturate the signal. The P1/2 value was determined from the extrapolated straight line portion of the saturation profile; P1/2 is the microwave power at which the signal height is half of the theoretical height which would be obtained in the absence of saturation. P1/2 = 69mW 1 minute after nitrite addition and 55mW 8hrs after nitrite addition. The P1/2 values for d-NO are virtually unchanged in the presence of b595-NO suggesting either little interaction between the unpaired electron of each ligated haem centre or, because the b595-NO e.p.r. signal has a slow relaxation rate, the b595-NO contribution to d-NO T_2 (spin-spin relaxation time) will be small.

The lack of haem-NO e.p.r signals in specific preparations of mitochondrial cytochrome oxidase (aa_3) has been interpreted as a strong spin-coupling between a_3-NO and Cu_B-NO resulting in an even spin system (Brudvig *et al.*, 1980); such spin-coupling does not occur in cytochrome-*bd* and there is little spin-spin interaction between the centres. The metal species at the active site (haem-haem or haem-Cu) may cause these differences. The haem planes of haem-d and haem-b595 may be held at an angle where spin overlap does not occur and the NO molecules may be held at specific angles within the haem pocket preventing spin-coupling. Analysis of two paramagnetic centres in close proximity has been theoretically analysed by Leigh (1970) and it was conclude that a "magic angle" can exist between

the g-tensors of two paramagnetic species giving negligible dipolar interaction. The electronic interaction differences between cytochrome oxidase and cytochrome-*bd* do not, therefore, necessarily suggest haem-d and haem-b595 are spatially further apart than haem-a_3 and Cu_B.

6.3.3 Nitric oxide g_z hyperfine.

A free radical signal slightly obscures the cytochrome-*bd* haem-NO e.p.r. spectra in the g_z area (around g=2.000) but, from observed spectra (Fig.6.4), there appears to be little evidence for the superhyperfine splitting (3 sets of 3 lines) associated with a nitrogenous 5th coordinate ligand (as found for haem-a_3 in cytochrome oxidase, Morse and Chan, 1980; Stevens and Chan, 1981). To detect spectral hyperfine the modulation amplitude was reduced and gain increased but only an apparent triplet was observed (not shown but discernable in Fig.6.4b between the g=2.032 peak and the g=1.997 trough). The predicted hyperfine splitting for ^{14}N (of nitric oxide) is a triplet when in general a nucleus with spin I splits the resonance line of an electron into 2I + 1 lines of equal intensity (^{14}N nuclear spin = 1, ^{16}O nuclear spin = 0). The triplet of hyperfine in Fig.6.4b gave a hyperfine splitting constant, A_z, of 1.5mT which is within the splitting range expected for nitrogen in NO (Knowles *et al.*, 1976), this splitting is most probably for b595-NO if the d-NO g_z is obscured at 8hrs.

Cytochrome-*bd* has 10 histidines in subunits I & II but, from site directed mutagenesis, 8 of the histidines do not appear to coordinate haem-b558, haem-b595 or haem-d (Fang *et al.* 1989). Histidine 186 in subunit I may be associated with haem-b558 but the 4 histidines in subunit II are not haem associated. Histidine 19 in subunit I may be associated with either haem-d or haem-b595 suggesting a bridging of the haem between the two subunits. Changes in haem binding upon modification of histidine may however only be conformational and not directly associated with the 5th coordinate ligand.

The lack of the superhyperfine multiplet in the e.p.r. spectra presented herein cannot positively rule out a nitrogenous proximal ligand (histidine) for either haem-d or haem-b595 (c.f. Lukat *et al.*, 1988), especially in the presence of spectral overlap for each signal.

6.3.4 Haem-NO species not attributable to cytochrome-bd?

Haem-NO e.p.r. spectra of FUN4/pNG2 have been assigned to haem-d and haem-b595 on the basis that: a) FUN4/pNG2 is deleted in the *cyo* locus and cannot synthesise the ubiquinol-oxygen oxido-reductase cytochrome-*bo*; b) the e.p.r. data is consistent with the time dependent optical formation of d-NO and b595-NO species; and c) other ligand binding centres such as catalase, peroxidase etc, are in lower relative concentration (especially in membrane

preparations). Nitrite reductase will not be expressed in the aerobically grown cells used in this study although this was a possibile candidate for NO binding in the wild-type cells of Rothery (1989). Nitric oxide can bind to purified succinate dehydrogenase (Salerno and Ohnishi, 1976), but it is unlikely that membrane bound fumarate reductase or succinate dehydrogenase would reduce nitrite and bind NO. The S-Fe-NO e.p.r. spectra are however very similar to the signal assigned to b595-NO with a peak at g=2.032. A membrane preparation of the fumarate reductase amplified strain, HB101/pFRD84 (30mg.ml^{-1}, 50mM BES, pH7.0), was incubated anoxically with dithionite followed by addition of sodium nitrite crystals. These samples showed no NO signal which could be attributed to the high levels of fumarate reductase (not shown). It was therefore assumed, from the time course comparison with the optical spectra, and the lack of a fumarate reductase NO signal, the axial peak at g=2.032 is attributable to b595-NO. The similarity between the axial S-Fe-NO (Salerno and Ohnishi, 1976; Reddy *et al.*, 1983) and the b595-NO spectra may be significant in assigning the 5th coordinate ligand (amino acid) of haem-b595. The ligand of haem-b595 may then be either cysteine or methionine, there being 1 cysteine and 5 methionines in subunit II (Fang *et al.*, 1989). This lends an interesting comparison with the cytochrome oxidase a_3-Cu_B bimetallic site where a bridging ligand between haem-a_3 and copper may involve either cysteine or methionine (although EXAFS analysis showing a sulphur centre is similar to the

chloride ion?). The bridging ligand is present in the relaxed state of the active site in cytochrome oxidase (absence of dioxygen, no turnover; George *et al.*, 1987). A useful approach to assigning the proximal ligands of haem-d and haem-b595 will involve site directed mutagenesis, perhaps concentrating on the sulphur amino acid.

6.3.5. Assignment of the cytochrome-bd haem-NO free radical species.

The free radical signal observed in the haem-NO e.p.r. spectra of cytochrome-*bd* has not been previously assigned. The haem-NO spectra of mitochondrial cytochrome oxidase show no obvious radical-like signals.

The linewidth of the radical peak-trough in spectra 1 minute after addition of nitrite remained constant at 1.0mT for pH6.0, pH7.0 and pH8.0, and was centred at 2.005 (Fig.6.6). In a comparison with free radical titrations of flavin and quinone (Ohnishi *et al.*, 1981, Salerno and Ohnishi, 1980; Simpkin,D., Moodie,A.D., Salerno,J.C. and Ingledew, W.J., 1990, submitted), both the neutral (pH6.0) and the anionic (pH8.0) species of quinone may predominate. The spectra of Fig.6.6 do not show the high and low field wings associated with flavin (c.f. Fig.4.4) and as such the radical signal can be assigned to semi-ubiquinone-8 (which predominates over menaquinone-8 in this preparation). The high degree of radical stability for haem-NO formation and the high concentration in the amplified cytochrome-*bd*

Figure 6.6

E.p.r. spectra of the free radical signal associated with cytochrome-bd haem-NO formation.

The free radical species associated with the haem-NO e.p.r. spectra of cytochrome-*bd* are shown. Samples were obtained as in Fig.6.2 1 minute after addition of 30mM sodium nitrite to 10mM sodium lactate reduced: 25mg.ml^{-1} etp, 50mM MES, 5mM EDTA, pH6.0; 25mg.ml^{-1} etp, 50mM BES, 5mM EDTA, pH7.0; and 25mg.ml^{-1}, 50mM Tricine, 5mM EDTA, pH8.0. The central g-value for the radical peak/trough is shown above the spectra, the relative gain is shown to the right of each spectra. The peak/trough linewidth is 1.0mTesla. E.p.r. conditions were: microwave frequency, 9.46GHz; modulation frequency, 100kHz; modulation amplitude, 0.5mTesla; microwave power, 174μW; temperature, 64K.

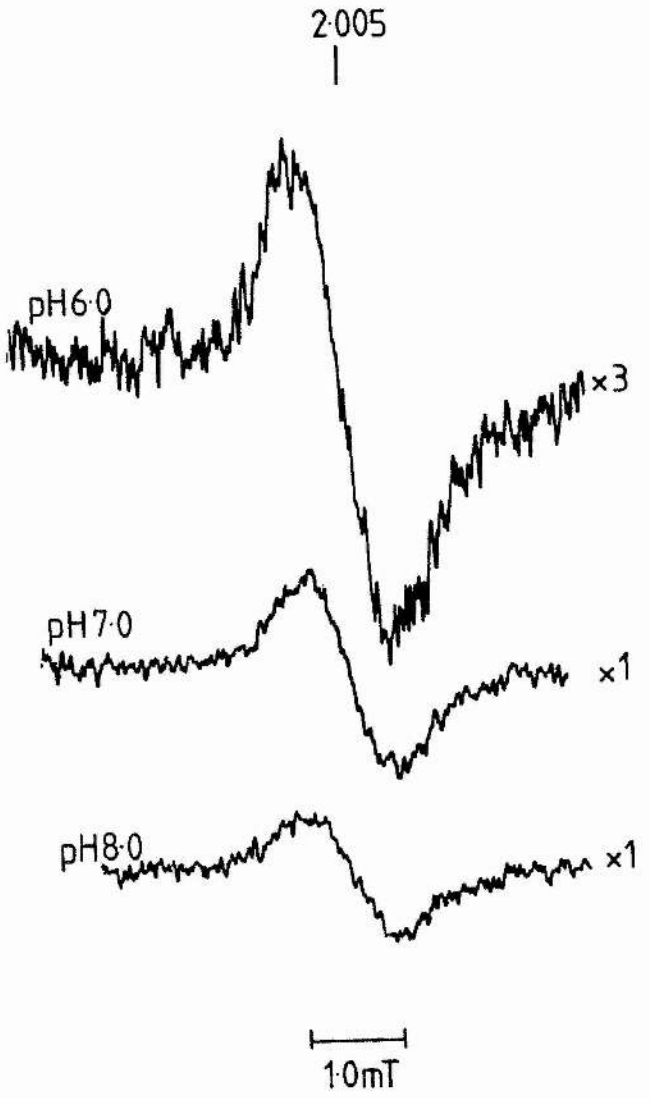
2·005
pH6·0
×3
pH7·0
×1
pH8·0
×1
1·0mT

membranes, suggests the free radical signal of Fig.6.6 can be assigned as a stabilized bound quinone site for the ubiquinol-oxygen oxido-reductase cytochrome-*bd*.

The free radical semiquinone intermediate must be highly stabilized, and therefore bound to the complex, if the two-electron carrier quinol is to sequentially transfer electrons to the single electron acceptor haem-b558. Haem-b558 of subunit I monitors the redox state of the quinone pool at the periplasmic aspect of cytochrome-*bd* and is thought to be the direct electron acceptor for quinol (Kranz and Gennis, 1984; Yang *et al.*, 1986; Green *et al.*, 1986; Lorence *et al.*, 1987).

The microwave power profiles of the free radical peak-trough at pH6.0, pH7.0 and pH8.0, 1 minute after nitrite addition are shown in Fig.6.7. To observe saturation of the free radical e.p.r. signal the P1/2 values were determined at low temperature (12K) when most radical signals are fully saturated (slow relaxation rate). The radical signal must be relaxed by an interacting centre which is paramagnetic and in close proximity to the quinol binding site. This centre is oxidized haem-b558 which will be in thermodynamic equilibrium with quinol (similar midpoint potentials, see below). The P1/2 values for pH6.0, 7.0 and 8.0 are 2.76mW, 1.74mW and 1.38mW, respectively, suggesting the radical is relaxed further at lower pH, this is discussed below in relation to a thermodynamic equilibrium between haem-b558 and quinol.

Further time courses of haem-NO formation were

Figure 6.7

Microwave power profile for the free radical signals of Fig.6.6.

The microwave power saturation profiles of the free radical signals at pH6.0, pH7.0 and pH8.0 of Fig.6.6 are shown. The arbitrary units for signal height are not equivalent for the three plots. The power profiles were determined at 12K. The P1/2 values for pH6.0 (●), pH7.0 (○) and pH8.0 (◆) were 2.76mW, 1.74mW and 1.38mW, respectively.

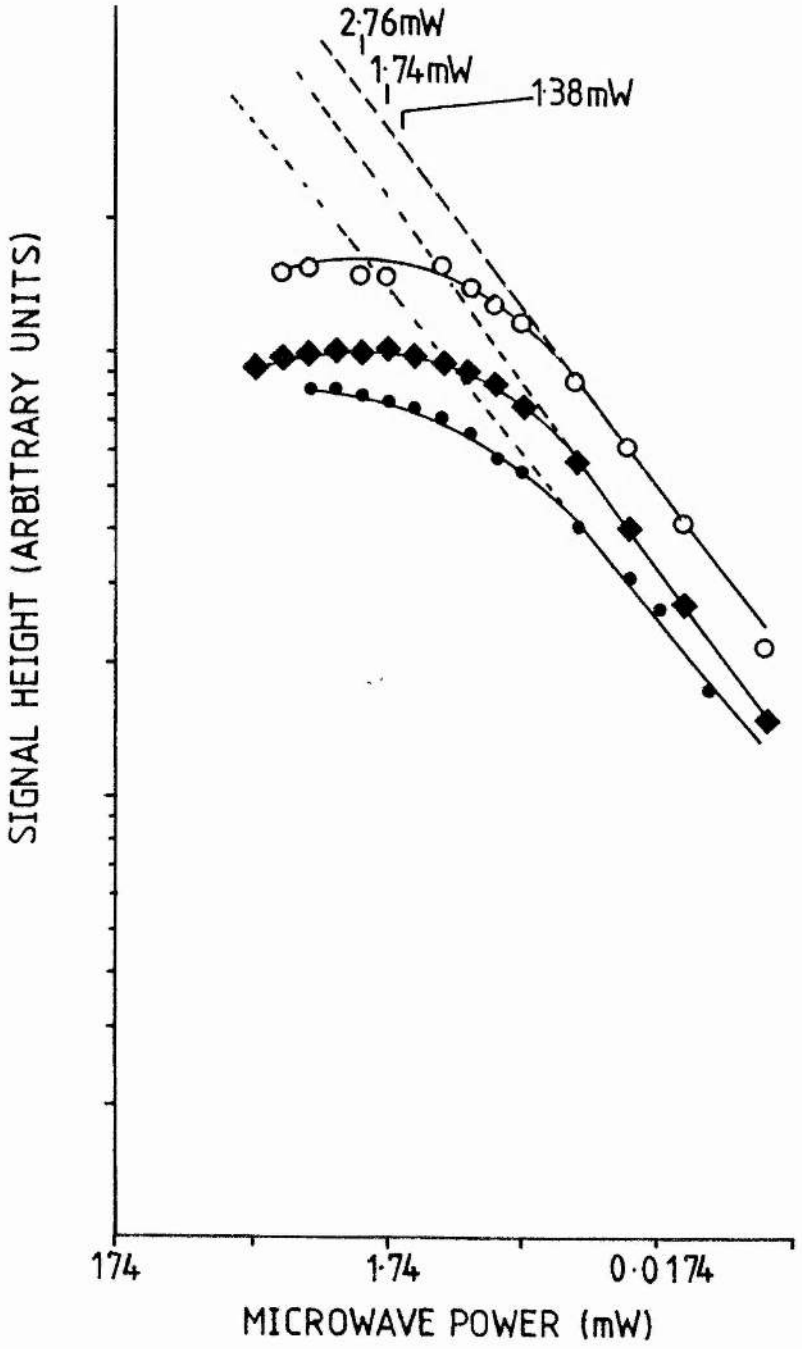
2·76mW
1·74mW
1·38mW
SIGNAL HEIGHT (ARBITRARY UNITS)
174
1·74
0·0174
MICROWAVE POWER (mW)

performed at pH6.0 and pH8.0 (Fig.6.8). The binding of NO to haem-d and haem-b595, from optical studies (Rothery *et al.*, 1987), is faster at lower pH (6.0) and much slower, with respect to haem-b595, at higher pH (8.0). This is because the reactive species for nitrite reduction is nitrous acid (pKa=3.37) and an ionizable group in the haem pocket (pKa=7.3) is required for reduction of nitrous acid and b595-NO formation (Rothery *et al.*, 1989). The basic requirement for an ionizable group, in the protonated form, may be related to the low affinity of haem-b595 for this ligand. If haem-d requires an ionizable group for functional catalysis then, from the data of Rothery *et al.* (1987), it must have a pKa value greater than 9.0. These differences in functional catalysis for nitrite reduction suggest different roles for the two centres within the haem pocket. Rothery (1989) has presented models for nitrous acid reduction based on the pH dependence of optical spectra. An ionizable group in the haem pocket may be related to proton transfer reactions and water formation for dioxygen reduction.

Comparing the pH6.0 (25mg.ml^{-1} etp, 50mM MES, 5mM EDTA) and pH8.0 (25mg.ml^{-1} etp, 50mM Tricine, 5mM EDTA) time courses of Fig.6.8 the g=2.032 peak of b595-NO forms at a slower rate at high pH (Fig.6.8c). The high-field trough observed in the pH8.0 spectra is attributable to reduced iron-sulphur centre, S1, of succinate dehydrogenase. Experimental conditions were similar to Fig.6.2 and the baseline spectra (b1) were not subtracted from subsequent haem-NO spectra. The free radical signal (around g=2.003) is

Figure 6.8

E.p.r. spectral time courses in the g=2.000 region for nitrite addition to reduced cytochrome-bd membranes, pH6.0 and pH8.0.

E.p.r. samples were prepared as in Fig.6.2 to show pH dependent time courses of haem-NO formation in FUN4/pNG2 membranes at 30°C. The baselines (bl) are 25mg.ml^{-1} etp, 50mM MES, 5mM EDTA, pH6.0 and 50mM Tricine, 5mM EDTA, pH8.0 reduced with 10mM sodium lactate (reaction vessel under anoxic conditions purged with Nilox scrubbed nitrogen gas, section 2.7.3). Baselines were not subtracted from subsequent spectra. After addition of 30mM sodium nitrite samples were extracted and frozen at set time intervals: a, 1 min; b, 3 mins; c, 7 mins; d, 12 mins; e, 25 mins; f, 60 mins. Spectral g-values are shown above the spectra. E.p.r. conditions were: microwave frequency, 9.47GHz; modulation frequency, 100kHz; modulation amplitude, 0.63mTesla; microwave power, 5.3mW; temperature, 30K. The gain was equivalent for all spectra. The high-field trough of the pH8.0 spectra is attributed to succinate dehydrogenase, S1.

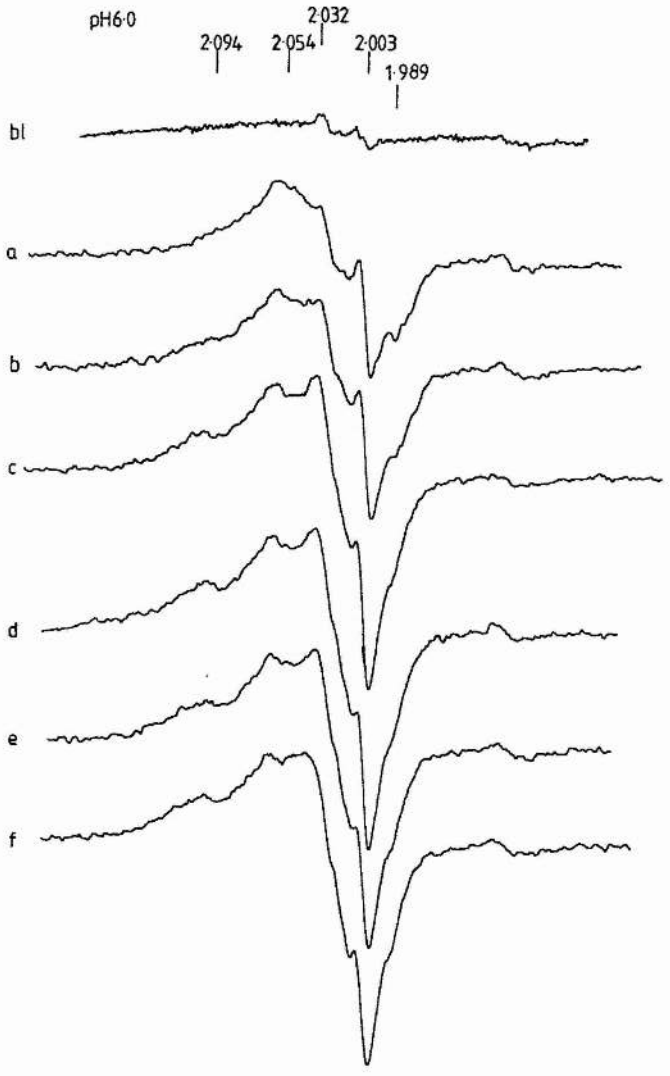
pH6·0
2·094
2·054
2·032
2·003
1·989
bl
a
b
c
d
e
f

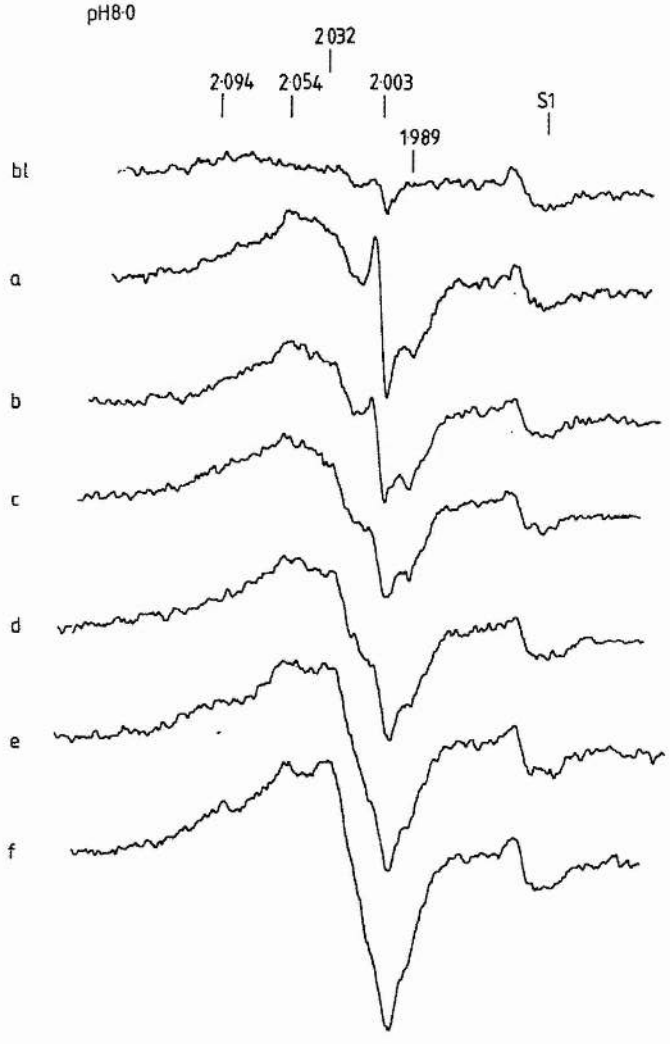
pH8·0
2·094
2·054
2·032
2·003
1989
S1
bl
a
b
c
d
e
f

observed 1 minute after nitrite addition, at pH6.0 and pH8.0, when d-NO has formed (Fig.6.8a). The g-value assignments are in accordance with Fig.6.2.

The radical signal is stabilized and remains throughout the pH6.0 time course to 60minutes (Fig.6.8f), although in the 8hr sample of Fig.6.3 it has diminished. In the pH8.0 time course the radical signal diminishes much faster and cannot be easily distinguish after 12-25 minutes (pH8.0, Fig.6.8 c,d,e). This intriguing time dependent diminution of the radical signal is difficult to assign to the kinetic mechanism of nitrite reduction.

The radical is formed upon formation of d-NO (single electron reduction of nitrite). Optical studies also demonstrated haem-b558 oxidation in the 1 minute time course (section 6.2). As only one electron is transferred, reducing nitrite to nitric oxide, an equilibrium must exist between the semiquinone and haem-b558. This explains the weak haem-558 optical signal in Fig.6.1 and is consistent with equilibrium for the similar midpoint potentials of quinone and haem-b558. The reduction of a second nitrite to form b595-NO at pH6.0 would suggest the radical signal would diminish at low pH whereas at pH8.0, when b595-NO formation is slower, the free radical would remain, this is obviously the reverse of what is observed in Fig.6.8. The diminution of the free radical is however related to the thermodynamic parameters for the haem centres and quinone. Fig.6.9 suggests a possible scheme for radical formation and diminution and is based on the thermodynamic limitations of

Figure 6.9

Models for radical formation and diminution during time dependent cytochrome-bd haem-NO formation.

Boxed representations of subunits I & II of cytochrome-*bd* are shown; quinol and haem-b558 are associated with subunit I and haem-b595 and haem-d are associated with subunit II. The midpoint potential values for haem are from Rothery and Ingledew (1989) and the quinol value is from Salerno and Ohnishi (1980).

a) pH6.0 (Fig.6.8). The box to the left gives the lactate reduced states of prosthetic groups before nitrite addition. Upon addition of nitrite oxidation of haem-b558 and quinol occurs (ΔE_h=10mV and at equilibrium) and NO ligates to reduced haem-d. The e.p.r. detectable haem-NO electron is shown at the N of nitric oxide although this electron is also delocalized over the haem centre and the oxygen atom. The unpaired electron of semiquinone is the e.p.r. detectable species of Fig.6.6. The nitric oxide ligand binds to Fe at an angle. As b595-NO is formed, and a further electron is transferred, the semiquinone/ferric haem-b558 concentration decreases. The semiquinone is highly stabilized by interaction with ferric haem-b558 and is only slowly re-reduced by the quinol pool. The strained binding angle for b595-NO is shown to suggest a small haem pocket which reduces a second nitrite (nitrous acid) with low affinity.

b) The same reaction as a) is shown for the 60mV/pH unit midpoint potential dependency of quinol at pH8.0 (Fig.6.8). The equilibrium betweem semiquinone and haem-b558 is now towards reduced haem-b558 (ΔE_h=130mV) and the free radical signal therefore diminishes faster than in a).

a) pH 6.0

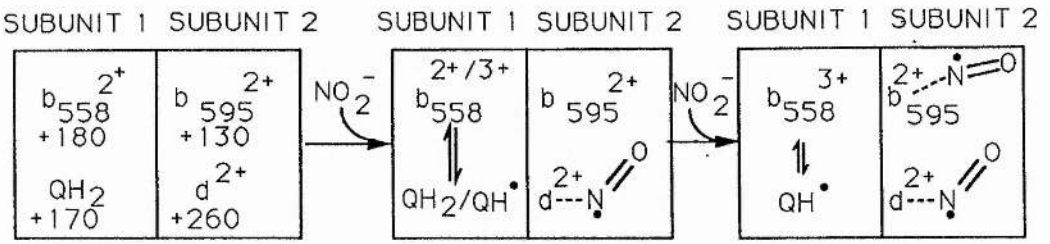
SUBUNIT 1
SUBUNIT 2
SUBUNIT 1
SUBUNIT 2
SUBUNIT 1
SUBUNIT 2
b558 2+
+180
QH2
+170
b 595 2+
+130
d 2+
+260
NO2 −
2+/3+
b558
QH2/QH•
b 595 2+
d2+---N=O
NO2 −
b558 3+
QH•
2+
b595 ---N=O
d2+---N=O

b) pH 8.0

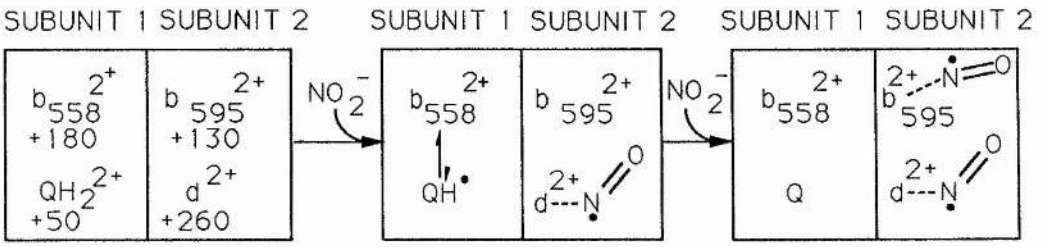
SUBUNIT 1
SUBUNIT 2
SUBUNIT 1
SUBUNIT 2
SUBUNIT 1
SUBUNIT 2
b558 2+
+180
QH2 2+
+50
b 595 2+
+130
d 2+
+260
NO2 −
b558 2+
QH•
b 595 2+
d2+---N=O
NO2 −
b558 2+
Q
2+
b595 ---N=O
d2+---N=O

the system at pH6.0 and pH8.0. The midpoint potentials of the haem centres are from Rothery and Ingledew (1989). The midpoint potential for the bound quinone of cytochrome-*bd* has not been determined and herein the E_{m7} value, +110mV, determined for bound quinone in complex II of mitochondria, is applied (Salerno and Ohnishi, 1980). The pH independent midpoint potentials of Rothery and Ingledew (1989) are shown in Fig.6.9 although the pH dependencies observed by Meindhart *et al.* (1989) are within the limits of the models presented. The quinone is assumed to have a 60mV/pH unit dependency in accordance with other two electron, two proton carriers; this also assumes the pK_R of the reaction is greater than pH8.0.

At pH6.0 (Fig.6.9a) the fully reduced enzyme can reduce nitrite to form d-NO and the semiquinone species is observed, from Fig.6.1 haem-b558 is also oxidized. An equilibrium exists between the semiquinone and haem-b558 due to the small ΔE_h value for the midpoint potentials (10mV). After the d-NO species has fully formed, the b595-NO species slowly forms, the single electron coming from the semiquinone species and haem-b558 which remain in equilibrium. Hence the radical signal remains until the semiquinone species is eventually reduced by the quinone pool and/or b595-NO has fully formed. At reaction completion all centres will again be fully reduced with haem-d and haem-b595 NO ligated. The NO is schematically shown bound at an angle to haem-d (see chapter 7) and the b595-NO species is shown at a strained angle to illustrate low affinity

haem-b595 nitrite reduction. Fig.6.9b shows the same reaction at pH8.0, where the ΔE_h value for haem-b558 and quinone is 130mV and the equilibrium for the semiquinone/b558 interaction is towards ferrous haem-b558. Therefore, at higher pH the radical signal diminishes much faster because haem-b558 has a much higher potential than the quinol.

6.4. Conclusion.

Both haem-d and haem-b595 reduce nitrite to ligate nitric oxide. Haem-d has a high NO affinity and haem-b595 affinity is low (much lower than haem-b595 CO affinity, chapter 5). No spin-spin coupling was observed between the two haem-NO species but this may be related to the slow relaxation rate of b595-NO and a small affect on d-NO T_2 rather than a large haem pocket with centres spatially far apart. The haem pocket is small enough to hinder the second nitrite reduction at haem-b595 suggesting haem-d and haem-b595 are in close proximity. The haem-d-NO e.p.r. spectra has a type I rhombic signal observed at low temperatures and high power and is assigned g_x=2.094, g_z=2.000, g_y=1.989 with a type II $g_?$=2.054, pH7.0, 30K. Haem-b595-NO is axial (type II) with a peak-trough at g=2.032 and g=1.997, this signal is more easily saturated than d-NO. A radical signal observed in the g_z region of haem-NO spectra was assigned to a cytochrome-*bd* bound semi-ubiquinone and related, thermodynamically, to the optically detectable oxidation of haem-b558 (section 6.3.5). No obvious superhyperfine splitting was observed in the g_z region suggesting the proximal ligands of haem-d and haem-b595 are not nitrogenous. These data are related to dioxygen binding at the active site by comparing the binding chemistries for NO and dioxygen ligation.

Nitrosyl haem ligands ligate at an angle to Fe in a similar fashion to the bent ligation of dioxygen (see

chapter 7 for chemistry; c.f. CO linear binding, chapter 5). If the oxygen atom of NO is held towards haem-b595 it is difficult for the second nitrite molecule (nitrous acid) to enter the active site to be reduced at haem-b595. Reduction of nitrite at haem-b595 can occur (although slowly) because the NO held by haem-d is not further reduced in a bridged reaction (c.f. dioxygen, chapter 7) and both haems are, therefore, available to bind ligands.

During catalytic turnover and dioxygen reduction, haem-b595 can ligate dioxygen as a centre in a bimetallic site and, with haem-d, directly reduce dioxygen to form peroxide. Under steady-state conditions of dioxygen reduction, and in the presence of nitrite, haem-b595 would not bind NO and nitrite would compete with dioxygen for haem-d only (Fig.6.10). Relating this to equilibrium analysis the enzyme/inhibitor/substrate complex of Fig.6.10 predicts competitive inhibition for cytochrome-*bd*. Competitive inhibition was observed for nitrite inhibition in the oxygen electrode studies of Rothery *et al.* (1987); Km varied and V_{max} remained constant for variable nitrite concentrations. Haem-b595 has a higher affinity for CO (although not as high as haem-d) because CO ligates in a linear conformation. From the CO data of chapter 5 and the NO data presented herein, haem-b595 only appears to bind ligands under extreme conditions. This agrees with the data of Lorence and Gennis (1989) where haem-b595 was ligated by peroxide while haem-d was dioxygen ligated, but only under conditions of excess peroxide.

Figure 6.10

Enzyme/inhibitor/substrate complex for Escherichia coli cytochrome-bd: nitric oxide binding.

The equilibrium complex for nitrite (NO) inhibition of cytochrome-*bd* during steady state dioxygen reduction is shown. The active site spatial arrangement of haem-d and haem-b595 is from Fig.5.10. Michaelis-Menten equilibrium analysis predicts competitive inhibition for dioxygen reduction in the presence of nitrite. The bent NO ligation to haem-d is similar to the bent configuration for dioxygen. The low affinity of haem-b595 for nitrite is due to steric hinderance within the active site. Haem-b595 will bind NO only under anoxic conditions when the 4e- reduction of dioxygen is not catalysed at the active site and haem-d is inhibited.

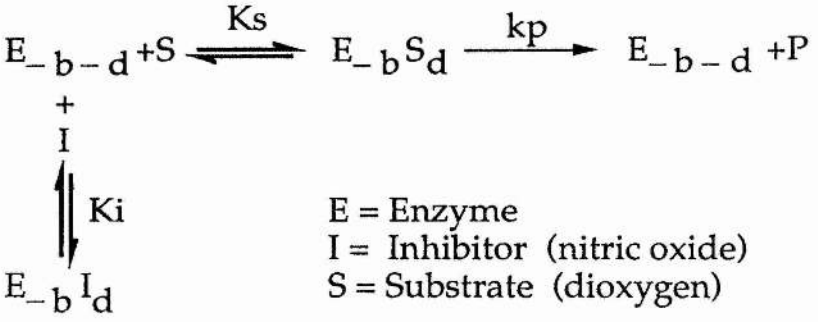

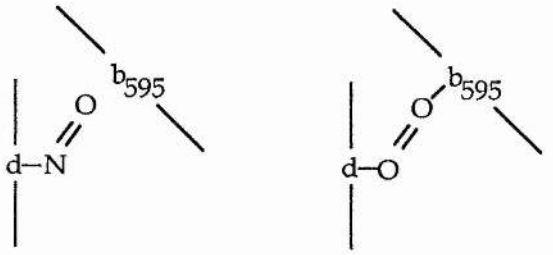

When

$$\frac{v^-}{[E]_t} = \frac{kp\,[E_{-b}S_d]}{[E_{-b-d}] + [E_{-b}I_d] + [E_{-b}S_d]}$$

Then

$$\frac{v^-}{V_{max}} = \frac{[S]}{K_s\left(1 + \frac{[I]}{Ki}\right) + [S]}$$

Cooperativity for dioxygen reduction in the presence of nitrite, as observed by Rothery *et al.* (1987) for polarographic studies, is not compatible with this analysis. Cooperativity was suggested to be a function of dioxygen binding to both haem-b595 and haem-d with subsequent reduction to peroxide and disproportionation to form water, leaving a single dioxygen bound (Fig.5.9). This cooperative affect may however be a facet of nitrite inhibition and analysis of the single progress curve (not initial rate). An Eadie-Hofstee plot of v versus v/s (v, rate; s, substrate) will be non-linear because v decreases faster than s due to inhibitor. To show this *E. coli* strain GO103, which is deleted in cytochrome-*bd* and has wild-type levels of cytochrome-*bo* (as a comparison to the EMG2 used by Rothery *et al.*, 1987), was tested for "cooperativity" in the presence of nitrite. Cytochrome-*bo* has one high-spin ligand binding haem and copper at the active site to give a similar bimetallic site to mitochondrial cytochrome oxidase (aa_3) which ligates only one dioxygen.

Fig.6.11a shows the oxygen electrode progress curve for nitrite inhibition of cytochrome-bo, experimental conditions were: air saturated 50mM MES, pH6.0; 1.1mg.ml^{-1} etp; 5.9mM sodium nitrite incubated for 5 minutes and the reaction was initiated by addition of 30mM sodium lactate; temperature 30°C. Fig.6.11b shows the integrated Eadie-Hofstee plot for the collected points of Fig.6.11a. A curved plot was obtained giving apparent "cooperative" kinetics. These data are consistent with cooperative-type

Figure 6.11

Nitrite inhibited progress curve for cytochrome-bo dioxygen reduction (and subsequent application to the integrated Eadie-Hofstee equation).

a) Oxygen electrode progress curve for nitrite inhibited cytochrome-bo activity. Points were collected with a BBC microcomputer. 1.1mg.ml^{-1} *E. coli* GO103 etp in air saturated 50mM MES pH6.0 were incubated for 5mins with 5.9mM sodium nitrite. The oxidase reaction was initiated by addition of 30mM sodium lactate; temperature, 30°C.

b) The points collected for Fig.6.11a were applied to the integrated Eadie-Hofstee equation (section 2.5.2). s_0, starting oxygen concentration (0.22mM); s, oxygen concentration (mM); time in seconds.

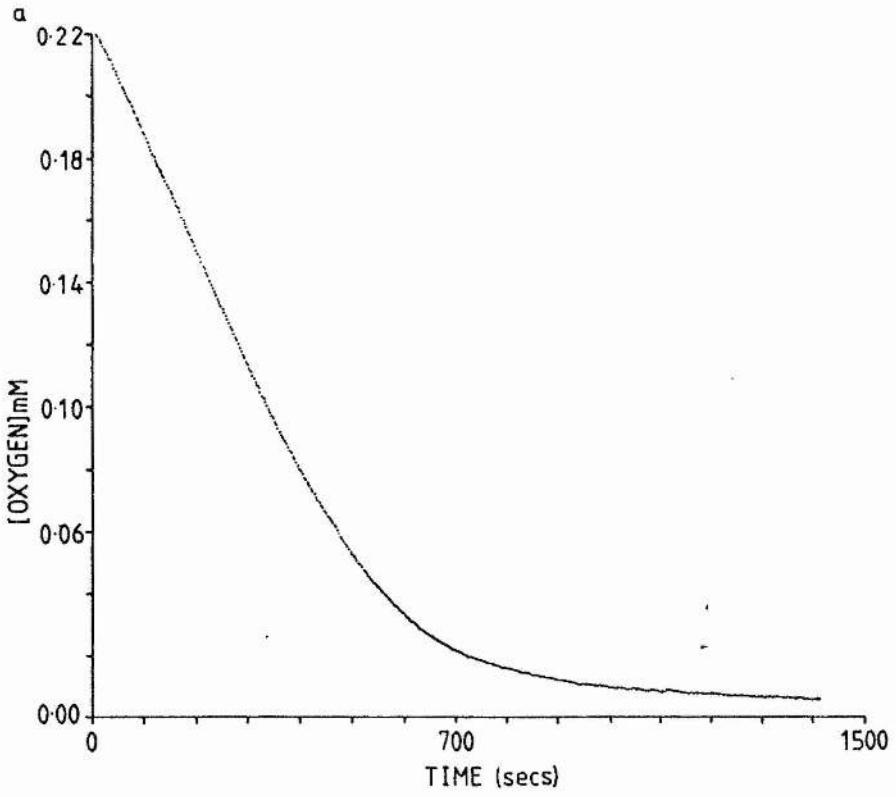
a
0·22
0·18
0·14
0·10
0·06
0·00
[OXYGEN]mM
0
700
1500
TIME (secs)

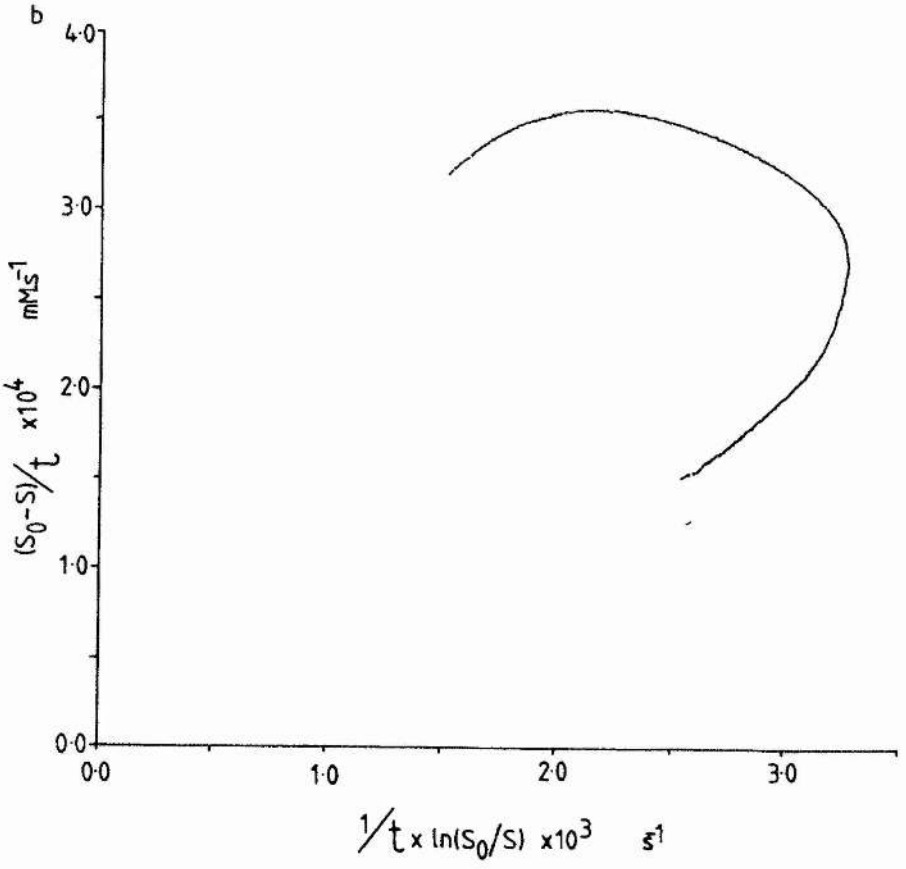
b
4·0
3·0
2·0
1·0
0·0
$(S_0-S)/t$ x10^4 mMs^{-1}
0·0
1·0
2·0
3·0
$1/t \times \ln(S_0/S)$ x10^3 s^{-1}

kinetics being a facet of inhibition and analysis of the single progress curve. The differentiated equation of Rothery *et al.* (1987) gave similar curved plots for these data. True cooperativity for dioxygen binding may be a function of "opening" the haem pocket for subsequent dioxygen binding (to haem-d only) but this would not be detected polarographically ("resting" state and "pulsed" states). A double dioxygen binding haem pocket for cytochrome-*bd* is not envisaged.

Further experimentation with NO ligated cytochrome-*bd* should determine the angle of binding for NO at the haem centres. Nitrogen-15 N.M.R. of nitrosyl ligands will characterize the binding angle from the large chemical shift for bent versus linear conformations (Mason *et al.*, 1985). Ligand binding with NO gas (not nitrite reduction) should determine e.p.r. detectable states for both the reduced and the oxidized forms of the haem centres and may further distinguish the functions of haem-d and haem-b595. Experimentation should be carried out with care as direct mixing of haemoproteins with NO gas is a relatively harsh treatment. Also the use of purified enzyme, and reconstitution experiments, will further confirm the haem-NO and free radical signals, the midpoint potential of the bound quinone of cytochrome-*bd* may then also be determined.

From these data chapter 7 presents model systems for a bimetallic dioxygen reduction site in cytochrome-*bd*.

Chapter 7

CONCLUSIONS

Chapter 7

7.1. Rapid-freeze quench / continuous flow apparatus used in conjunction with e.p.r spectroscopy.

Chapter 3 outlined the development of a rapid-freeze quench apparatus to be used in pre-steady state discontinuous spectral analysis. Test reactions determined the efficiency and limitations of the apparatus and a cryostat was constructed to a more compact and safer design than previous freeze-quench cryostats (Moodie *et al.*, 1990). A continuous-flow cell, for application to e.p.r. species detectable at room-temperature, was also constructed.

7.2. Internal electron transfers for Escherichia coli menaquinol-fumarate oxido-reductase.

Chapter 1 reviewed the biophysical data for fumarate reductase and herein only a summary of the conclusions drawn from chapter 4 and chapter 1 are given. Section 1.2.1 presented the high potential/low potential pathway proposed for electron transfer in fumarate reductase. To obtain kinetic data for internal electron transfers fumarate reductase was studied by rapid-freeze quenching (chapter 4). Internal equilibration of electrons at FR1 and FR3 are faster than can be kinetically resolved in the low millisecond range. From the data obtained, FR1 and FR3 are oxidized at a rate which is consistent with the predicted maximal turnover for fumarate reduction (benzyl viologen, $30s^{-1}$; Simpkin, 1985). No FR2 e.p.r. signal was observed

during turnover and no b-type cytochrome was detected. From the data of Simpkin and Ingledew (1985) and Simpkin,D.S., Moodie,A.D., Salerno,J.C. and Ingledew,W.J. (1990, submitted) the prosthetic groups of *E. coli* fumarate reductase are flavin and iron-sulphur centres FR1, FR2 and FR3 with a single menaquinol binding site at the anchor subunits (see also section 1.2.1). The midpoint potential values for these centres are; flavin, E_{m7}=-12mV; FR1, E_{m7}=-50mV; FR2, E_{m7}=-285mV; FR3, E_{m7}=-50mV; menaquinol, E_{m7}=-70mV-->-90mV.

The role of FR2 remains ambiguous but is unlikely to be vestigial as low potential iron-sulphur centres have been identified in all of the presently studied succinate-fumarate oxido-reductases. FR2 may not be low potential during turnover (as discussed in section 1.2.1) and a more likely role for FR2 would be to stabilize the n=1/n=2 transfers from menaquinol to FR3 and from FR1 to flavin. Spin-spin interactions are observed between all three iron-sulphur centres showing close spatial proximity and to divide these centres into independent electron transfer pathways would be a misrepresentation. From available data a high potential/low potential pathway cannot be supported and a sequential transfer of electrons from menaquinol to FR3, FR1, flavin and fumarate is consistent with the data presented herein and elsewhere. Fig.7.1 shows the proposed sequential transfer of electrons in *E. coli* fumarate reductase. The prosthetic groups are boxed to specify known subunits; flavin in subunit A, the

Figure 7.1

Model for sequential electron transfer in Escherichia coli menaquinol-fumarate oxido-reductase.

Fumarate reductase is schematically represented with the prosthetic groups in different subunits and a menaquinol binding site at the anchor subunits close to iron-sulphur centre, FR3 (see Fig.1.1). FAD, flavin; FR1, FR2, FR3, iron-sulphur centres; MQH, menaquinol binding site shown as the neutral semiquinone. The role of FR2 is ambiguous. Proton uptake/release is shown as either cytoplasmic (c) or periplasmic (p). The dots at each centre represent electron reduced centres.

Menaquinol reduces FR3, leaving bound semiquinone and releasing protons either into the cytoplasm or periplasm (stage 1). FR3 reduces FR1 at stage 2 and FR3 is re-reduced by semiquinone (stage 3). FR1 and FR3 then reduce the flavin (stages 4 to 6) and fumarate is reduced to succinate at stage 7. The enzyme is then fully oxidized and can be further reduced by menaquinol.

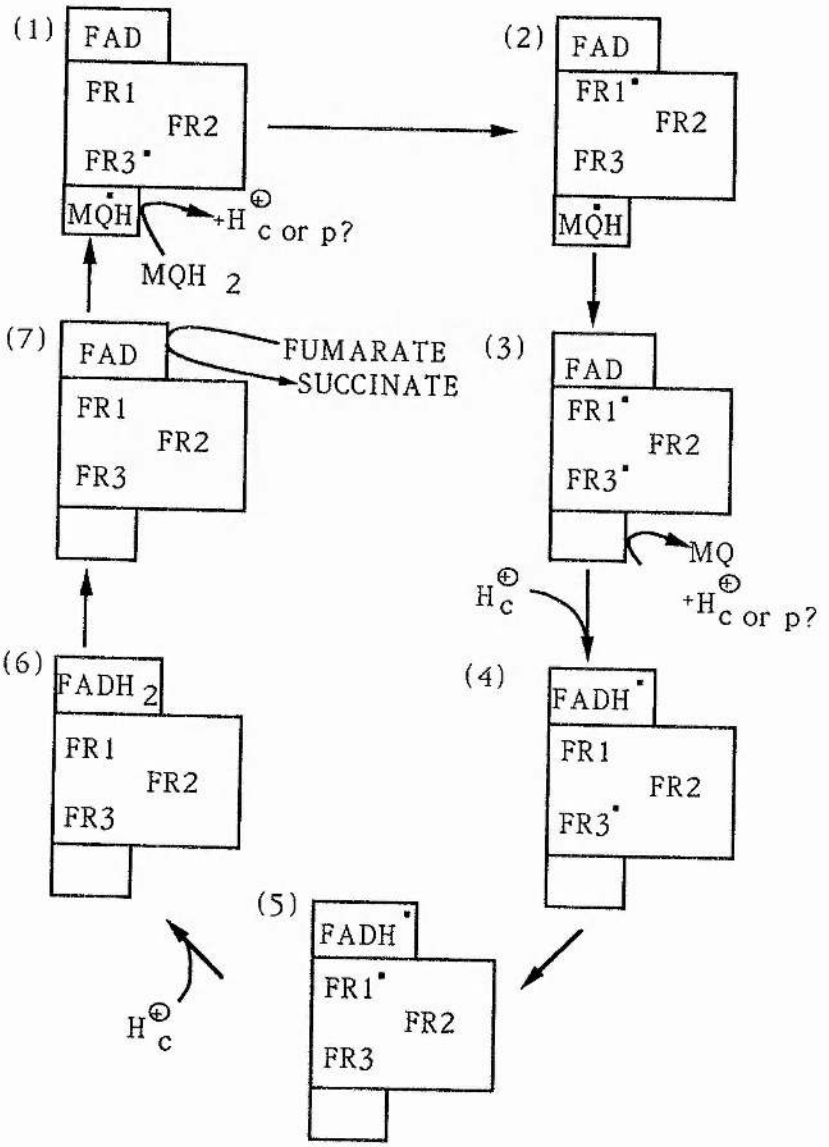
(1)
FAD
FR1
FR2
FR3
MQH
+H c or p?
MQH 2
(2)
FAD
FR1
FR2
FR3
MQH
(3)
FAD
FR1
FR2
FR3
MQ
+H c or p?
H c
(4)
FADH
FR1
FR2
FR3
(5)
FADH
FR1
FR2
FR3
H c
(6)
FADH 2
FR1
FR2
FR3
(7)
FAD
FUMARATE
SUCCINATE
FR1
FR2
FR3

iron-sulphur centres in subunit B and the menaquinol binding site at either subunit C or D. Flavin is shown as the pH7.0 neutral form (Simpkin,D.S., Moodie,A.D., Salerno,J.C. and Ingledew,W.J., 1990, submitted). Proton uptake by flavin is cytoplasmic but the release of protons from quinol has not been identified as cytoplasmic or periplasmic. To contribute to the proton-electrochemical gradient a proton-well arrangement for the anchor subunits would be required for periplasmic release of protons. This would be consistent with menaquinol binding at the cytoplasmic side of the anchor subunits for FR3 interaction. The high stability of both the flavin and the menaquinol free radicals suggest sequential transfer for n=2/n=1 transfers (Simpkin,D.S., Moodie,A.D., Salerno,J.C. and Ingledew,W.J., 1990, submitted). Cytochrome-*b* may be included between the quinone binding site and FR3 for sequential transfer in fumarate reductases' where haem content has been identified. Cytochrome-*b* may then give the chemi-osmotic advantage of quinol proton release at the periplasmic aspect of the membrane (section 1.2.1). The role of FR2 in Fig.7.1 is left ambiguous. Fig.7.1 is consistent with the biophysical data reviewed in chapter 1.

7.3. Catalytic mechanism of dioxygen reduction for Escherichia coli ubiquinol-oxygen oxido-reductase cytochrome-bd.

7.3.1. A bimetallic site.

Chapter 7

The four electron reduction of dioxygen to water is preferentially catalysed by two metallic centres in close proximity as found in the mitochondrial aa_3 centre, cytochrome oxidase. The peroxidases require only one ligand binding haem centre and possibly an ionizable group (amino acid) for reaction cycle intermediate stabilization (Vanngard, 1985; Edwards *et al.*, 1988). Cytochrome-*bd* of *Escherichia coli* reduces dioxygen in a four-electron transfer to form water (Minghetti and Gennis, 1988) but the active site catalytic mechanism for reduction is not known.

A basic requirement for a bimetallic reaction site during the four electron reduction of dioxygen to water can be related to the orbital chemistry of dioxygen: when two O atoms, with the electronic structure [$1s^2 2s^2 2p^4$], are brought together the electrostatic repulsions are overcome to form O=O, with the electron arrangement for the K and L shells of

[$(1s\sigma g)^2 (1s\sigma u)^2 (2s\sigma g)^2 (2s\sigma u)^2 (2p\sigma g)^2 (2p\pi u)^4 (2p\pi g)^2$]

where s and p are the named orbitals within each shell and sigma and pi are the bonding characteristics for the orbitals inphase (g) and out-of-phase (u) (Morse, 1976). From the correlation diagram for orbital overlap bonding orbitals are obtained for $1s\sigma g$, $2s\sigma g$, $2p\sigma g$ and $2p\pi u$ with the other orbitals being anti-bonding. This gives 10 bonding electrons and 6 anti-bonding electrons for dioxygen making formation highly favourable and the final molecule very stable. However, the two electrons in the $2p\pi g$ orbital,

which is only half full, will be unstable due to electrostatic repulsion and $2x(2p\pi g)^1$ orbitals exist. Dioxygen is therefore paramagnetic, a net spin S=1, with dioxygen in the triplet state when the number of wavefunctions (for angular momentum of zero between nuclei) is given as 2S + 1 (Morse, 1976). If the spins were paired then singlet dioxygen would be formed i.e. 2S + 1 = 1. Because the two electrons in triplet dioxygen have the same spin (parallel) it is more difficult, in a thermodynamic sense, for one centre to reduce dioxygen, the two electrons needed to form peroxide being anti-parallel in the single centre; i.e. $O\overline{1}\_$ + $O\overline{1}\_$ reduced by $Fe1\downarrow$ (ferrous) is thermodynamically difficult due to the angular momentum (spin) of the electrons but $O\overline{1}\_$ + $O\overline{1}\_$ reduced by $Fe1\downarrow$ + $Fe1\downarrow$ to form $O1\downarrow$ + $O1\downarrow$ (peroxide) is favourable, this leaves $Fe\overline{1}\_$ + $Fe\overline{1}\_$ (ferric haems). This is only a thermodynamic restraint when the reduced haem (ferrous) is in the low-spin configuration. It is not known if oxygen bound ferrous haem-d is high or low-spin although it will probably go through a high-spin to low-spin transition upon oxygen binding as found from magnetic circular dichroism and resonance Raman studies for haem-a_3 of cytochrome oxidase (Babcock *et al.*, 1976, 1981; Thomson *et al.*, 1976). Ferrous haem-d also shows little optical absorbance in the Soret region which is often an indication of low-spin haem. Resonance Raman spectra of oxycytochrome-*d* are electronically similar to the oxyglobins so haem-d is therefore probably low-spin in the dioxygen bound ferrous

state (d-650), unfortunately the wavelength regions associated with a ferryl haem-d intermediate were not studied (see later, Poole *et al.*, 1982b).

The initial, thermodynamically unfavourable, single electron reduction of dioxygen to superoxide (E_{m7}=-330mV) appears to be less negative when the intermediates are bound at a bimetallic centre (Malmstrom, 1982); this reaction may be side-stepped however by a two electron reduction to peroxide (E_{m7}=+270mV) which is more favourable, although when the overall reaction is favourable each individual step will be driven forward. If two centres, haem-a_3 and Cu_B in cytochrome oxidase and haem-d and haem-b595 in *E. coli* cytochrome-*bd*, each donated a single electron, of the same spin, then peroxide would be formed. Haem-b595 may act to donate an electron to the already oxidized haem-d which then further reduces superoxide to peroxide or haem-b595 may reduce the dioxygen directly. The potentially damaging superoxide intermediate would be tightly bound and quickly further reduced to peroxide; this probably accounts for the lack of positive identification of superoxide as an intermediate in other oxidases (although cytochrome oxidase may have a superoxide dismutase function; Markossian *et al.*, 1978). The peroxide formed is also potentially damaging and would be stabilized by ligating between oxidized haem-d and oxidized haem-b595 (the unpaired electron of Fe^{3+} pairing with the peroxy electron). However, stopped-flow data suggests haem-b595 remains reduced during catalytic turnover (Haddock *et al.*, 1976) and would not therefore stabilize

peroxide. An ionizable group (amino acid) would then be required at the haem pocket to stabilize peroxide via hydrogen bonding; such a group, with a pKa value of 7.3, is closely associated with haem-b595 (Rothery *et al.*, 1987). The ionizable group would then be involved in hydrogen transfer for water formation.

The peroxidases do not require a bimetallic site for catalysis because the substrate peroxide is not constrained by the limitations presented above for reduction of triplet state dioxygen. The peroxidases have an ionizable group (amino acid) in close proximity to the single haem centre to stabilize peroxide before cleavage to form bound hydroxyl and then water, via a ferryl (Fe^{4+}) intermediate (Vanngard, 1985). Cytochrome-*bd* has often been compared to the peroxidases because haem-b595 has both optical and e.p.r. spectral characteristics which are similar to the peroxidases (Bolscher *et al.*, 1984; Lorence *et al.*, 1986; Lukat *et al.*, 1988) but as outlined above this is probably due to the close association of this haem with an ionizable group for peroxide stabilization.

The conclusions reached in chapter 5 & 6 suggest haem-b595 is not an oxidase in its own right (see Ingledew, 1978) and does not independently bind and reduce dioxygen, but is part of a bimetallic site. A second haem centre at a bimetallic site (not Cu as in aa_3) may be an evolutionary link between the functional peroxidases and cytochrome oxidase.

Available data demonstrated CO ligation by both

reduced haem-b595 and haem-d, haem-d with a higher affinity (Chapter 5; Rothery, 1989). This is related to the electronic structure of CO

$$[(1s\sigma g)^2(1s\sigma u)^2(2s\sigma g)^2(2s\sigma u)^2(2p\sigma g)^2(2p\pi u)^4]$$

which shows no unpaired electrons and CO ligates to haem in a linear configuration, thus two CO molecules can be ligated in the haem pocket as shown in Fig.5.10. Both reduced haem-d and haem-b595 bind NO but haem-b595 has a very low NO affinity (chapter 6); this is also related to the electronic structure of NO

$$[(1s\sigma g)^2(1s\sigma u)^2(2s\sigma g)^2(2s\sigma u)^2(2p\sigma g)^2(2p\pi u)^4(2p\pi g)^1]$$

where the unpaired electron in the outer orbital causes the NO molecule to bind to haem at an angle, as depicted in Fig.6.10. When haem-d ligates NO the O atom is held towards the second haem in the bimetallic site (haem-b595), in a similar fashion to the bent configuration of dioxygen (dioxygen in the triplet state with unpaired electrons on each O atom). The binding of a second NO to haem-b595 is then hindered but can occur slowly because the NO bound to haem-d is not further reduced (c.f. dioxygen reduction later). Haem-d and haem-b595 can therefore independently bind CO and NO but cannot be assigned independent dioxygen binding roles (bimetallic site).

To confirm the bent configuration of NO, X-ray diffraction data of enzyme crystal structures in haemoproteins have shown NO to be held at an angle to the haem (Edwards *et al.*, 1988). This further confirms the bound ligand in haemoproteins as nitrosyl (NO) and not the

nitrosonium ion (NO^+) which would bind straight in a similar fashion to CO. The bent versus linear binding of CO, NO, O_2 or NO^+ being related to the orbital chemistry of the bonding with CO and NO^+ isoelectronic and binding straight and NO and O_2 also isoelectronic (when bound) and binding in a bent fashion (Huheey, 1975). The haem plane of haem-b595 is at 45° and haem-d is perpendicular to the membrane plane (R.A.Rothery, J.C.Salerno and W.J.Ingledew, unpublished data) and if dioxygen and peroxide are ligated between the two centres the haem pocket arrangement of Fig.5.10 and Fig.6.10 can be envisaged.

Cytochrome-*bd* is also a form of nitrite reductase (c.f. cytochrome-cd_1 of *Pseudomonas*; Ingledew and Saraste, 1979) reducing nitrite but not releasing the NO formed. If two NO molecules are held in close proximity in the haem pocket (not in the presence of dioxygen) a nitric oxide reductase activity may be detectable.

$$2NO + 2e^- + 2H^+ \longrightarrow N_2O + H_2O \quad E_{m\,7}=+1175mV$$

This reaction will be very slow because of the high activation energy in forming the N-N bond but has been shown to occur for reduced cytochrome oxidase in the presence of nitrite (mass spectrometry, Brudvig *et al.*, 1980).

The low Km for dioxygen reduction observed for cytochrome-*bd* may be a function of stabilization of intermediates with haem-b595, as the second centre at the bimetallic site, increasing the overall affinity of the complex for dioxygen. Cytochrome-*bd* has not been identified as a proton pump (Miller and Gennis, 1985) and if copper, as

the second centre in the bimetallic site of cytochrome oxidase, is necessary for proton-pumping (Wikstrom, 1989) cytochrome-*bd* may lose the chemi-osmotic advantage of proton pumping at the cost of increased dioxygen affinity (R.A.Rothery, personal communications). Even in the absence of proton pumping the utilization of dioxygen as a terminal electron sink gives a thermodynamic advantage over other terminal electron acceptors, such as nitrate and fumarate, for the large redox drop to oxygen (E_{m7}=+820mV) (Moodie and Ingledew, 1990). The electrons in cytochrome oxidase would do more work than in cytochrome-*bd* to pump protons across the membrane. Proton-pumping has been tentatively assigned to *E. coli* cytochrome-*bo* (Puustinen *et al.*, 1989) which has a haem-copper bimetallic site (Salerno *et al.*, 1989, 1990). The reduction of dioxygen cytoplasmically will contribute to the proton electrochemical gradient by scalar chemistry when electron transfer is vectorial, quinol releasing protons at the periplasm and water formation consuming protons in the cytoplasm (Miller and Gennis, 1985).

7.3.2. A model for dioxygen reduction at cytochrome-bd.

Fig.7.2 proposes a bimetallic site for *E. coli* cytochrome-*bd* dioxygen reduction. The model is based on the ligand binding data of chapters 5 & 6 and available triple trapping data for cytochrome-*bd* (Poole and Chance, 1981; Poole *et al.*, 1981; Poole *et al.*, 1982a; Poole *et al.*,

Figure 7.2

Model for Escherichia coli cytochrome-bd dioxygen reduction (a bimetallic site).

Haem-b595 and haem-d of the cytochrome-*bd* active site are shown with a catalytic mechanism for dioxygen reduction. Haem-b558 and the quinol binding site have been omitted for clarity. The major optical absorbance states of haem-d are shown boxed. The formation of d630--->d650--->d680 are consistent with time dependent triple trapping data as discussed in the text. Stage 1 is the fully reduced enzyme which ligates with dioxygen at stage 2 to form d650. Stage 2 can then either reduce dioxygen to superoxide, or, directly reduce dioxygen in a two-electron transfer to peroxide (stage 4). With the addition of protons at stage 5, followed by a single electron reduction, a ferryl haem-d intermediate is formed with water at stage 6. A further electron and proton addition gives hydroxyl haem-d (stage 7) which is further protonated to form water. The enzyme is then re-reduced by two quinols to form stage 1. The electrons added at stage 5 to 6 and 6 to 7 are from haem-b558 and quinol.

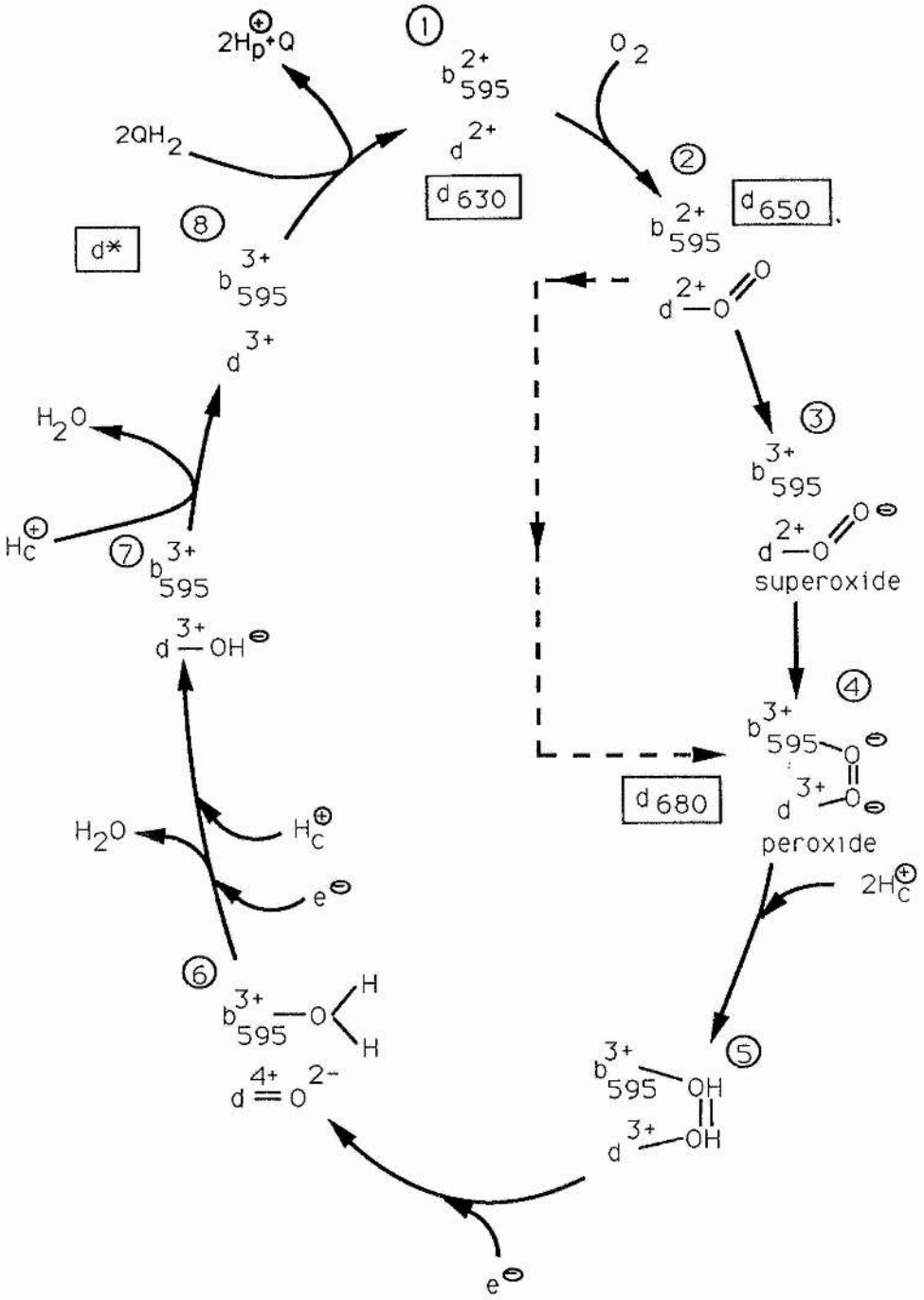
①
b^{2+}_{595}
d^{2+}
d630
$2H^{\oplus}_{p}+Q$
$2QH_2$
⑧
b^{3+}_{595}
d^{3+}
d*
O_2
②
b^{2+}_{595}
$d^{2+}-O-O$
d650
③
b^{3+}_{595}
$d^{2+}-O-O^{\ominus}$
superoxide
④
$b^{3+}_{595}-O^{\ominus}$
$d^{3+}-O^{\ominus}$
peroxide
d680
$2H^{\oplus}_{c}$
⑤
$b^{3+}_{595}-OH$
$d^{3+}-OH$
$e^{\ominus}$
⑥
$b^{3+}_{595}-O(H)H$
$d^{4+}=O^{2-}$
H_2O
$H^{\oplus}_{c}$
$e^{\ominus}$
$d^{3+}-OH^{\ominus}$
⑦
b^{3+}_{595}
H_2O
$H^{\oplus}_{c}$

1983a,b; Kumar *et al.*, 1985; Poole and Williams, 1987). Under conditions of high oxygen concentration the same intermediates will not necessarily be detected. A ferryl haem-d intermediate is included although this has not been identified in cytochrome-*bd*. Transient ferryl species have been identified in all peroxidases and oxidases studied to-date (Chance *et al.*, 1975; Karlsson *et al.*, 1981; Ellfolk *et al.*, 1983; Vanngard, 1985; Thomson *et al.*, 1988). This model is hypothesised as a testing model for future experimentation, especially for magnetic circular dichroism and Raman identification of the ferryl haem-d intermediate. Previous models for cytochrome-*bd* (not a bimetallic site) have not included an oxidized form of haem-d (Hata-Tanaka *et al.*, 1987) which, from stopped-flow data is one of the first species observed upon mixing with oxygen (Haddock *et al.*, 1976; Wariabharaj and Ingledew, 1987).

The fully reduced enzyme (stage 1, refer to Fig.7.2) has five electron holes (two quinone electrons, haem-b558, haem-b595 and haem-d) which is one more than mitochondrial cytochrome oxidase (two coppers and two haems) and one more than required for the four-electron reduction of dioxygen to water. The cycle of dioxygen reduction in cytochrome-*bd* will therefore not present the fully oxidized enzyme as an intermediate. The similar midpoint potentials of haem-b558, quinone and haem-b595 at pH7.0 will result in an equilibrium of oxidized/reduced forms of these centres (see chapter 6). The quinol binding site and haem-b558 are not shown in Fig.7.2 to simplify the reduction scheme. The reduction

sequence for cytochrome-*bd* is envisaged as:-

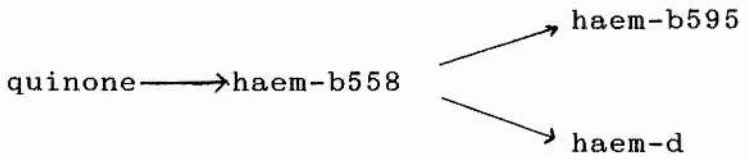

Stage 1 is the reduced form of the enzyme designated 'd630' from the optical absorbance of reduced haem-d at 630nm (see, Poole *et al.*, 1983a). From triple trapping data the first species to form upon mixing with oxygen is ferrous haem-d ligated by dioxygen, absorbing at 650nm (d650) (Poole *et al.*, 1983a,b). Dioxygen is then reduced either to stage 3 as superoxide and then to peroxide (stage 4) or directly to stage 4 from stage 2 in a two electron reduction from haem-d amd haem-b595 as discussed in section 7.3.1. Poole and Williams (1987) have suggested haem-b595 can directly reduce haem-d (or dioxygen?) and the e.p.r. triple trapping data of Kumar *et al.* (1985), reanalysed with the high-spin rhombic/axial assignments of Rothery and Ingledew (1989), show haem-b595 oxidation preceding haem-d oxidation. This is not however consistent with stopped-flow data where haem-b595 is not oxidized during catalytic turnover (Haddock *et al.*, 1976; Warhiabaraj and Ingledew, 1987); however at the higher temperatures used in stopped-flow haem-b595 may be rapidly re-reduced by haem-b558 (which from stopped-flow data becomes oxidized). If haem-b595 remained in the reduced ferrous state (acting as an electron sink) throughout the reaction cycle of Fig.7.2 the chemistry of dioxygen reduction would not change. The peroxy form of cytochrome-*bd* (stage 4) is the optically detectable species 'd680'

absorbing at 680nm (see Fig.1.5) (Poole *et al.*, 1983b; Poole and Williams, 1987). Peroxide is shown ligated between oxidized haem-d and oxidized haem-b595 although haem-b595 may be reduced and the peroxide stabilized by an ionizable group in the haem pocket (as discussed in section 7.3.1). At stage 5 uptake of two cytoplasmic protons is shown although this may involve ionizable groups (amino acids) in the haem pocket which are subsequently re-protonated. At stage 6 a single electron from haem-b558 (in equilibrium with quinol) forms one water and a ferryl haem-d intermediate bound to an oxygen atom. At stage 7 the uptake of a single proton and a further electron (from haem-b558/quinol) forms a hydroxyl ligated haem-d species which is then protonated to form a further water leaving oxidized haem-d, the optically undetectable d* (Pudek and Bragg, 1974, 1975), stage 8. To re-reduce the enzyme two quinols are oxidized to leave bound quinol and reduced haems b558, b595 and d at stage 1.

The detection of a ferryl intermediate for haem-d will lend support to stages 5 to 8 and, as mentioned above, haem-b595 may be quickly re-reduced during any of the stages, indeed haem-b595 may remain reduced throughout the cycle (rapid internal electron transfer). The cycle is therefore consistent with low temperature triple trapping data and can be easily modified to incorporate stopped-flow data.

To summarise, Fig.7.2 presents a bimetallic site four-electron reduction of dioxygen to water for *E. coli* ubiquinol-oxygen oxido-reductase cytochrome-*bd*.

7.3.3 Cytochrome-bd rapid freeze-quench studies?

To further observe electron transfer kinetics in cytochrome-*bd* (or cytochrome-*bo*) the enzyme may be studied by rapid-freeze quenching. The oxidase reactions are very fast and outwith the resolution of flow techniques but multi-phase kinetics and percentage oxidation/reduction may be observed. Freeze-quench samples can be studied by e.p.r. spectroscopy and low-temperature reflectance spectroscopy. Reduction of purified and reconstituted cytochrome-*bd* by stoichiometric amounts of quinol should show reduction kinetics for the haem centres. Oxidation of the reduced enzyme may assign the oxidation state of haem-b595 during turnover as a percentage of the total haem-b595 present and the intramolecular electron transfer rate may also be determined, i.e. is haem-b595 rapidly re-reduced by haem-b558 as stopped-flow data suggests (and as discussed in section 7.3.2). Kinetic studies in the presence of other ligands (CO and NO) will further characterize the functional differences between haem-d and haem-b595 and their dioxygen binding ability.

APPENDIX I

```
10 REM $$$$$$$$$$$$$$$$$$$$$$$$$$$$$$$$$$$$$$$$$
20 REM $  Alan D. Moodie.  1990                 $
30 REM $  Rapid Freeze Quench/Continuous Flow   $
40 REM $  BBC BASIC Ram System Control Program $
50 REM $$$$$$$$$$$$$$$$$$$$$$$$$$$$$$$$$$$$$$$$$
60 ?&FE62 = &FF
70 ?&FE6C = ?&FE6C OR &A0
80 ?&FE60 = &00
100 ON ERROR ?&FE60=&00:PROCvalues
110 S=S
120 value$="R"
130 T=T
140 value=0
150 MODE4
160 PROCvalues
170 PROCcontinue
180 ENDPROC
190 END
200 DEFPROCstart
210 ?&FE60=&00
220 ?&FE60 = &08
230 T%=TIME
235 A%=0
240 REPEAT
250 PRINT TAB(30,1);TIME-T%;
253 IF TIME-T%>5 AND A%=0 THEN A%=1: ?&FE60=&88:PRINT
    TAB(0,0);"T"
254 IF TIME-T%>55 AND A%=1 THEN A%=2:?&FE60=&08:PRINT
    TAB(0,0);" "
260 X$=INKEY$(0)
270 UNTIL TIME-T%>=T*100 OR ASC(X$) <>-1
275 ?&FE60=&31:?&FE60=&15:?&FE60=&2F
276 REPEAT UNTIL INKEY(100)
280 ?&FE60=&00
285 PROCinput
290 ENDPROC
300 DEF PROCvalues
310 CLS
320 PRINT "CONTINUOUS FLOW / RAPID FREEZE QUENCH-"
330 PRINT "-------------------------------------"
340 PRINT "RAM SYSTEM COMPUTER CONTROL"
350 PRINT "---------------------------"
360 PRINT TAB(0,10);"Motor Speed"
370 PRINT TAB(16,10);"[      ]"
380 PRINT TAB(19,10);S
390 PRINT TAB(0,15);"Forward/Reverse"
400 PRINT TAB(16,15);"[      ]"
410 PRINT TAB(19,15);value$
420 PRINT TAB(0,20);"Duration of Run"
430 PRINT TAB(16,20);"[      ]"
440 PRINT TAB(19,20);T
450 REPEAT
460 REPEAT
465 PRINT TAB(37,10);SPC(40)
```

```
470 INPUT TAB(24,10);"RTN to Enter "test$
480 IF ASC(test$)<>-1 THEN value=EVAL(test$)
490 UNTIL value >=0 AND value <251
500 S=value
510 PRINT TAB(24,10);SPC(25)
520 PRINT TAB(17,10);SPC(5)
530 PRINT TAB(19,10);S
540 REPEAT
545 PRINT TAB(37,15);SPC(40)
550 INPUT TAB(24,15);"RTN to Enter "test$
560 IF ASC(test$)<>-1 THEN value$=test$
570 UNTIL value$ = "F" OR value$ ="R"
580 PRINT TAB(24,15);SPC(25)
590 PRINT TAB(17,15);SPC(4)
600 PRINT TAB(19,15);value$
610 REPEAT
615 PRINT TAB(37,20);SPC(40)
620 INPUT TAB(24,20);"RTN to Enter "test$
630 IF ASC(test$)<>-1 THEN T=EVAL(test$)
640 UNTIL T >= 0 AND T< 100
650 PRINT TAB(24,20);SPC(25)
660 PRINT TAB(17,20);SPC(5)
670 PRINT TAB(19,20);T
680 PRINTTAB(0,26);"Press I to input values to
    controller"
690 PRINT TAB(0,28);"or RTN to change
    again.(Q=quit).....";
700 ANS$=GET$
710 PRINT TAB(0,28);SPC(40)
720 PRINT TAB(0,26);SPC(40)
730 IF ANS$="Q" THEN CLS:PRINT"You have left the
    program":END
740 UNTIL ANS$ = "I" OR ANS$ = "i"
750 PROCinput
760 ENDPROC
770 DEFPROCinput
780 IF S>=0ANDS<=15 THEN ?&FE60=16+S:?&FE60 = &20
790 IF S>15ANDS<=31 THEN ?&FE60=16+(S-16):?&FE60 = &21
800 IF S>31ANDS<=47 THEN ?&FE60=16+(S-32):?&FE60 = &22
810 IF S>47ANDS<=63 THEN ?&FE60=16+(S-48):?&FE60 = &23
820 IF S>63ANDS<=79 THEN ?&FE60=16+(S-64):?&FE60 = &24
830 IF S>79ANDS<=95 THEN ?&FE60=16+(S-80):?&FE60 = &25
840 IF S>95ANDS<=111THEN ?&FE60=16+(S-96):?&FE60 = &26
850 IF S>111ANDS<=127THEN ?&FE60=16+(S-112):?&FE60 = &27
860 IF S>127ANDS<=143THEN ?&FE60=16+(S-128):?&FE60 = &28
870 IF S>143ANDS<=159THEN ?&FE60=16+(S-144):?&FE60 = &29
880 IF S>159ANDS<=175THEN ?&FE60=16+(S-160):?&FE60 = &2A
890 IF S>175ANDS<=191THEN ?&FE60=16+(S-176):?&FE60 = &2B
900 IF S>191ANDS<=207THEN ?&FE60=16+(S-192):?&FE60 = &2C
910 IF S>207ANDS<=223THEN ?&FE60=16+(S-208):?&FE60 = &2D
920 IF S>223ANDS<=239THEN ?&FE60=16+(S-224):?&FE60 = &2E
930 IF S>239ANDS<=255THEN ?&FE60=16+(S-240):?&FE60 = &2F
940 IF value$ = "F" THEN ?&FE60 = &30
950 IF value$ = "R" THEN ?&FE60 = &31
```

```
 960 ENDPROC
 970 DEF PROCcontinue
 980 REPEAT
 990 REPEAT
1000 CLS
1010 MOVE 620,610:DRAW 620,895:DRAW 930,895:DRAW 930,610:
     DRAW 620,610
1020 MOVE 950,955:DRAW 950,1000:DRAW 1090,1000:DRAW
     1090,955:DRAW 950,955
1030 PRINT TAB(2,5);"Motor Speed"
1040 PRINT TAB(21,5);S
1050 PRINT TAB(2,8);"Forward/Reverse"
1060 IF value$ = "F" THEN PRINT TAB(21,8);"Forward"
1070 IF value$ = "R" THEN PRINT TAB(21,8);"Reverse"
1080 PRINT TAB(2,11);"Duration of Run "
1090 PRINT TAB(21,11);T
1100 PRINT TAB(24,11);"secs"
1110 PRINT TAB(24,1);"TIMER"
1120 PRINT TAB(30,1);"000"
1130 PRINT TAB(2,17);"Press R to recycle values"
1140 INPUT TAB(2,19);"or C to continue  ";
1150 recycle$ = GET$
1160 IF recycle$ = "R" OR recycle$ = "r" THEN PROCvalues
1170 UNTIL recycle$ ="C" OR recycle$ = "c"
1180 PRINT TAB(2,17);SPC(26)
1190 PRINT TAB(2,19);SPC(20)
1200 REPEAT
1210 VDU 23,1,0;0;0;0;
1220 PRINT TAB(5,25);"TO SET USER KEYS PRESS ANY KEY"
1230 press = GET
1240 UNTIL press
1250 PRINT TAB(0,25);SPC(40)
1260 REPEAT
1270 VDU 23,1,0;0;0;0;
1280 PRINT TAB(0,18);"THE FOLLOWING KEYS ARE NOW IN
     OPERATION"
1290 PRINT TAB(0,22);"PRESS SPACE BAR TO STOP MOTOR "
1300 MOVE 730,0 :DRAW 830,0 : DRAW 830,100 : DRAW 730,100
     :DRAW 730,0
1310 MOVE90,0 : DRAW 190,0:DRAW 190,100 :DRAW 90,100: DRAW
     90,0
1320 MOVE410,0 : DRAW 510,0 : DRAW 510,100 : DRAW 410,100
     : DRAW 410,0
1330 MOVE 1050,0 : DRAW 1150,0 : DRAW 1150,100 :DRAW
     1050,100 : DRAW 1050,0
1340 PRINT TAB(11,27);"CHANGE"
1350 PRINT TAB(14,30);"C"
1360 PRINT TAB(21,27);"REVERSE"
1370 PRINT TAB(24,30);"R"
1375 PRINT TAB(32,26);" FAST"
1380 PRINT TAB(32,27);"PICKUP"
1390 PRINT TAB(34,30);"L"
1400 PRINT TAB(2,27);"START"
1410 PRINT TAB(4,30);"S"
```

```
1420 v$ = GET$
1430 IF v$ = "R" OR v$ = "r" PROCreverse
1440 IF v$ = "S" OR v$ = "s" PROCstart
1450 IF v$ = "p" OR v$ = "P" PROCpickup
1455 IF v$ = "L" OR v$ = "l" PROCfast
1460 UNTIL v$ = "C" OR v$ = "c"
     :VDU23,1,1;0;0;0;:PROCvalues
1480 UNTIL FALSE
1490 ENDPROC
1500 DEF PROCreverse
1510 ?&FE60=&31
1515 ?&FE60=&1F
1520 ?&FE60=&2D
1530 ?&FE60=&08
1540 REPEAT UNTIL INKEY(5000)
1550 ?&FE60=&00
1560 PROCinput
1570 ENDPROC
1580 DEF PROCpickup
1590 ?&FE60 = &30
1600 ?&FE60 = &10
1610 ?&FE60 = &20
1620 ?&FE60 = &08
1630 REPEAT UNTIL INKEY(1000)
1640 ?&FE60 = &00
1650 PROCinput
1660 ENDPROC
1670 DEF PROCfast
1680 ?&FE60=&30
1690 ?&FE60=&1F
1700 ?&FE60=&2D
1710 ?&FE60=&08
1720 REPEAT UNTIL INKEY(300)
1730 ?&FE60 = &00
1740 PROCinput
1750 ENDPROC
```

BIBLIOGRAPHY

Ackrell,B.A.C., Kearney,E.B. and Edmondson,D. (1975) J. Biol. Chem. **250**, 7114-7119.

Ackrell,B.A.C., Cochran,B. and Cecchini,G. (1989) Arch. Biochem. Biophys. **268**, 26-34.

Alben,J.O., Moh,P.P., Fiamingo,F.G. and Altschuld,R.A. (1981) Proc. Natl. Acad. Sci. USA. **78**, 234-237.

Anni,H. and Yonetani,T. (1988) *In* Cytochrome Systems: Molecular Biology and Bioenergetics (Papa,S., Chance,B. & Ernster,L. eds.) pp371-375. Plenum Press, New York.

Anraku,Y. and Gennis,R.B. (1987) Trends Biochem. Sci. **12**, 262-264.

Babcock,G.T., Vickery,L.E. and Palmer,G. (1976) J. Biol. Chem. **251**, 7907-7919.

Babcock,G.T., Callahan,P.M., Ondrias,M.R. and Salmeen,I. (1981) Biochem. **20**, 959-966.

Ballou,D.P. (1971) PhD Thesis. University of Wisconsin, Madison, Wisconsin, USA.

Ballou,D.P. and Palmer,G.A. (1974) Anal. Chem. **46**, 1248-1252.

Bolscher,B.G.J.M., Plat,H. and Wever,R. (1984) Biochim. Biophys. Acta. **784**, 177-186.

Barlow,C. and Erecinska,M. (1979) FEBS Lett. **98**, 9-12.

Barman,T.E. and Gutfreund,H. (1964) *In* Rapid Mixing and Sampling Techniques in Biochemistry (Chance,B., Eisenhardt,R.H., Gibson,A.H. and Lonberg-Holm,K.K., eds.) pp339-343, Academic Press, New York.

Beinert,H., Hansen,R.E. and Hartzell,C.R. (1976) Biochim. Biophys. Acta. **423**, 339-355.

Beinert,H., Ackrell,B.A.C., Kearney,E.B. and Singer,T.P. (1975) Eur. J. Biochem. **54**, 185-194.

Blum,H., Leigh,J.S. and Ohnishi,T. (1980) Biochim. Biophys. Acta. **626**, 31-40.

Blum,H., Poole,R.K. and Ohnishi,T. (1980) Biochem. J. **190**, 385-393.

Borg,D.C. (1964) *In* Rapid Mixing and Sampling Techniques in Biochemistry (Chance,B., Eisenhardt,R.H., Gibson,A.H. and Lonberg-Holm,K.K., eds.) pp135-145, Academic Press, New York.

Bray,R.C. (1961) Biochem. J. **81**, 189-193.

Bray,R.C. and Petterson,R. (1961) Biochem. J. **81**, 194-195.

Bray,R.C. (1964) *In* Rapid Mixing and Sampling Techniques in Biochemistry (Chance,B., Eisenhardt,R.H., Gibson,A.H. and Lonberg-Holm,K.K., eds.) pp195-203, Academic Press, New York.

Bray,R.C. and George,G.N. (1985) Biochem. Soc. Trans. **13**, 560-567.

Brodie,A.F. (1963) Methods in Enzym. **6**, 295-308.

Brudvig,G.W., Stevens,T.H. and Chan,S.I. (1980) Biochem. **19**, 5275-5285.

Cammack,R., Crowe,B.A. and Cook,N.D. (1986a) Biochem. Soc. Trans. **14**, 1207-1208.

Cammack,R., Patil,D.S. and Weiner,J.H. (1986b) Biochim. Biophys. Acta. **870**, 545-551.

Cammack,R., Chapman,A., McCracken,J., Cornelius,J.B., Peisach,J. and Weiner,J.H. (1988) Biochim. Biophys. Acta. **956**, 307-312.

Castor,L.N. and Chance,B. (1955) J. Biol. Chem. **217**, 453-465.

Castor,L.N. and Chance,B. (1959) J. Biol. Chem. **234**, 1587-1592.

Cecchini,G., Thompson,C.R., Ackrell,B.A.C., Westenberg,D.J., Dean,N. and Gunsalus,R.P. (1986) Proc. Natl. Acad. Sci. USA. **83**, 8898-8902.

Cecchini,G., Ackrell,B.A.C., Deshler,J.O. and Gunsalus,R.P. (1986) J. Biol. Chem. **261**, 1808-1814.

Chance,B., Saronio,C. and Leigh,J.S. (1975) J. Biol. Chem. **250**, 9226-9237.

Cole,S.T. (1982) Eur. J. Biochem. **122**, 479-484.

Cole,S.T. (1987) Eur. J. Biochem. **167**, 481-488.

Cole,S.T. and Guest,J.R. (1979a) FEMS Microbiol. Lett. **5**, 65-67.

Cole,S.T. and Guest,J.R. (1979b) Eur. J. Biochem. **102**, 65-71.

Cole,S.T. and Guest,J.R. (1980a) Molec. Gen. Genet. **178**, 409-418.

Cole,S.T. and Guest,J.R. (1980b) Molec. Gen. Genet. **179**,

377-385.

Cole,S.T. and Guest,J.R. (1982) Biochem. Soc. Trans. **10**, 473-475.

Cole,S.T., Grundstrom,T., Jaurin,B., Robinson,J.J. and Weiner,J.H. (1982) Eur. J. Biochem. **126**, 211-216.

Cole,S.T., Condon,C., Lemire,B.D. and Weiner,J.H. (1985) Biochim. Biophys. Acta. **811**, 381-403.

Condon,C., Cammack,R., Patil,D.S. and Owen,P. (1985) J. Biol. Chem. **260**, 9427-9434.

Condon,C. and Weiner,J.H. (1988) Mol. Microbiol. **2**, 43-52.

Cornish-Bowden,A. (1976) *In* Principles of enzyme kinetics. Butterworth, London.

Crowe,B.A. and Owen,P. (1983) J. Bacteriol. **153**, 1493-1501.

Darlison,M.G. and Guest,J.R. (1984) Biochem. J. **223**, 507-517.

Degn,H. and Wohlrab,H. (1971) Biochim. Biophys. Acta. **245**, 347-355.

De Vries,S., Albracht,S.P.J. and Leeuwerik,F.J. (1979)

Biochim. Biophys. Acta. **546**, 316-333.

De Vries,S., Albracht,S.P.J., Berden,J.A. and Slater,E.C. (1982) Biochim. Biophys. Acta. **681**, 41-53.

De Vries,S., Albracht,S.P.J., Berden,J.A., Marres,C.A.M. and Slater,E.C. (1983) Biochim. Biophys. Acta. **723**, 91-103.

Dickie,P. and Weiner,J.H. (1979) Can. J. Biochem. **57**, 813-821.

Dutton,P.L. and Wilson,D.F. (1974) Biochim. Biophys. Acta. **346**, 165-212.

Edwards,C., Beer,S., Siviram,A. and Chance,B. (1981) FEBS Lett. **128**, 205-207.

Edwards,S.L., Kraut,J. and Poulos,T.L. (1988) Biochem. **27**, 8074-8081.

Ellfolk,N., Ronnberg,M., Aasa,R., Andreasson,L,E. and Vanngard,T. (1983) Biochim. Biophys. Acta. **743**, 23-30.

Elmes,M.L. Scraba,D.G. and Weiner,J.H. (1986) J. Gen. Microbiol. **132**, 1429-1439.

Fang,H., Lin,R-J. and Gennis,R.B. (1989) J. Biol. Chem. **264**, 8026-8032.

Fronticelli,C., Bucci,E., Zachary,A. and Rosen,B.P. (1986) Arch. Biochem. Biophys. **249**, 579-587.

Gennis,R.B. (1987) FEMS Microbiol. Revs. **46**, 387-399.

George,G.N., Bray,R.C. and Cramer,S.P. (1986) Biochem. Soc. Trans. **14**, 651-652.

George,G.N., Cramer,S.P., Frey,T.G. and Prince,R.C. (1987) *In* Advances in Membrane Biochemistry and Bioenergetics (Kim,C.H., Tedeschi,H., Diwan,J.J. and Salerno,J.C., eds.) pp429-438. Plenum Press, New York.

Georgiou,C.D., Fang,H. and Gennis,R.B. (1987) J. Bacteriol. **169**, 2107-2112.

Goldberg,I., Lonberg-Holm,K., Bagley,E.A. and Stieglitz,B. (1983) App. Environ. Microbiol. **45**, 1838-1847.

Gorren,A.C.F., de Boer,E. and Wever,R. (1987) Biochim. Biophys. Acta. **916**, 38-47.

Green,G.N., Kranz,J.E. and Gennis,R.B. (1984a) Gene **32**, 99-106.

Green,G.N., Kranz,R.G., Lorence,R.M. and Gennis,R.B. (1984b) J. Biol. Chem. **259**, 7994-7997.

Green,G.N., Lorence,R.M. and Gennis,R.B. (1986) Biochem. **25**, 2309-2314.

Grundsrom,T. and Jaurin,B. (1982) Proc. Natl. Acad. Sci. USA. **79**, 1111-1115.

Guest,J.R. and Nice,H.M. (1978) J. Gen. Microbiol. **109**, 329-333.

Guest,J.R. (1977) J. Bacteriol. **130**, 1038-1046.

Guest,J.R. (1981) J. Gen. Microbiol. **122**, 171-179.

Gutman,M., Bonomi,F., Pagani,S., Cerlti,P. and Kroneck,P. (1980) Biochim. Biophys. Acta. **591**, 400-408.

Gutowski,S.J. and Rosenberg,H. (1976) Biochem. J. **160**, 813-816.

Gutowski,S.J. and Rosenberg,H. (1977) Biochem. J. **164**, 265-267.

Gutteridge,S., Tanner,S.J. and Bray,R.C. (1978) Biochem. J. **175**, 869-878.

Haddock,B.A. and Schairer,H.U. (1973) Eur. J. Biochem. **35**, 34-45.

Haddock,B.A., Downie,J.A. and Garland,P.B. (1976) Biochem. J. **154**, 285-294.

Halliday,D. and Resnick,R. (1978) *In* Physics: parts 1 & 2. Third edition. John Wiley and Sons, New York.

Hansen,R.E., Kalal,T.T. and Beinert,H. (1967) Anal. Biochem. **20**, 40-50.

Hata-Tanaka,A., Matsuura,K., Itoh,S. and Anraku,Y. (1987) Biochim. Biophys. Acta. **893**, 289-295.

Hederstedt,L., Holmgren,E. and Rutberg,L. (1979) J. Bacteriol. **138**, 370-376.

Hederstedt,L. and Rutberg,L. (1981) Microbiol. Revs. **45**, 542-555.

Hederstedt,L. and Andersson,K.K. (1986) J. Bacteriol. **167**, 735-739.

Hederstedt,L., Bergman,T. and Jornvall,H. (1987) FEBS Lett. **213**, 385-390.

Hellingwerf,K.J., Bolscher,J.G.M. and Konings,W.N. (1981) Eur. J. Biochem. **113**, 369-374.

Henry,Y. and Banerjee,R. (1973) J. Mol. Biol. **73**, 469-482.

Hill,B.C., Greenwood,C. and Nicholls,P. (1986) Biochim. Biophys. Acta. **853**, 91-113.

Hirsch,C.A., Rasminsky,M., Davis,B.D. and Lin,E.C.C. (1963) J. Biol. Chem. **238**, 3770-3774.

Hoffman,P.S., Irwin,R.M., Carreira,L.A., Morgan,T.V., Ensley,B.D. and Dervartanian,D.V. (1980) Eur. J. Biochem. **105**, 177-185.

Huheey,J.E. (1975) *In* Inorganic Chemistry. Harper & Row, New York.

Ingledew,W.J. (1978) *In* Functions of alternative terminal oxidases (Degn,H., Lloyd,D. and Hill,G.C. eds.) pp79-87, Pergamon Press, Oxford.

Ingledew,W.J. (1983) J. Gen. Microbiol. **129**, 1651-1659.

Ingledew,W.J. and Ohnishi,T. (1975) FEBS Lett. **54**, 167-171.

Ingledew,W.J. and Ohnishi,T. (1977) Biochem. J. **164**, 617-620.

Ingledew,W.J. and Saraste,M. (1979) Biochem. Soc. Trans. **7**, 166-168.

Ingledew,W.J., Reid,G.A., Poole,R.K., Blum,H. and Ohnishi,T. (1980) FEBS Lett. **111**, 223-227.

Ingledew,W.J. and Poole,R.K. (1984) Microbiol. Revs. **48**, 222-271.

Iuchi,S., Kuritzkes,D.R. and Lin,E.C.C. (1986) J. Bacteriol. **168**, 1415-1421.

Johnson,M.K. Thomson,A.J., Walsh,T.A., Barber,D. and Greenwood,C. (1980) Biochem. J. **189**, 285-294.

Johnson,M.K., Morningstar,J.E., Cecchini,G. and Ackrell,B.A.C. (1985a) Biochem. Biophys. Res. Comm. **131**, 653-658.

Johnson,M.K., Morningstar,J.E., Cecchini,G. and Ackrell,B.A.C. (1985b) Biochem. Biophys. Res. Comm. **131**, 756-762.

Johnson,M.K. Thomson,A.J., Walsh,T.A., Barber,D. and Greenwood,C. (1980) Biochem. J. **189**, 285-294.

Johnson,M.K., Kowai,A.T., Morningstar,J.E., Oliver,M.E., Whittaker,K., Gunsalus,R.P., Ackrell,B.A.C. and Cecchini,G. (1988) J. Biol. Chem. **263**, 14732-14738.

Jones,R.W and Garland,P.B. (1977) Biochem J. **164**, 199-211.

Jones,H.M. and Gunsalus,R.P. (1987) J. Bacteriol. **169**, 3340-3349.

Karlsson,B., Aasa,R., Vanngard,T. and Malmstrom,B.G. (1981) FEBS Lett. **131**, 186-188.

Kay,W.W. and Kornberg,H.L. (1971) Eur. J. Biochem. **18**, 274-281.

Kita,K., Konishi,K. and Anraku,Y. (1984) J. Biol. Chem. **259**, 3375-3381.

Kita,K., Vibat,C.R.T., Meinhardt,S., Guest,J.R. and Gennis,R.B. (1989) J. Biol. Chem. **264**, 2672-2677.

Klimes,N., Lassman,G. and Ebert,B. (1980) J. Mag. Res. **37**, 53-59.

Knowles,P.F., Marsh,D. and Rattle,H.W.E. (1976) *In* Magnetic Resonance of Biomolecules. p245, John Willey & Sons Ltd.

Koland,J.G., Miller,M.J. and Gennis,R.B. (1984) Biochem. **23**, 1051-1056.

Kon,H. (1969) Biochem. Biophys. Res. Comm. **35**, 423-427.

Kon,H. and Kataoka,N. (1969) Biochem. **8**, 4757-4762.

Kranz,R.G. and Gennis,R.B. (1984) J. Biol. Chem. **259**, 7998-8003.

Kroger,A. and Klingenberg,M. (1973) Eur. J. Biochem. **34**, 358-368.

Kroger,A. (1978) Biochim. Biophys. Acta. **505**, 129-145.

Kroger,A. and Unden,G. (1985) *In* Coenzyme Q (Lenaz, G. ed.) p285-300, John Wiley & Sons Ltd.

Kumar,C., Poole,R.K., Salmon,I. and Chance,B. (1985) FEBS Lett. **190**, 227-231.

Lambden,P.R. and Guest,J.R. (1976) J. Gen. Microbiol. **97**, 145-160.

Latour,D.J. and Weiner,J.H. (1987) J. Gen. Microbiol. **133**, 597-607.

Leigh,J.S. (1970) J. Chem. Phys. **52**, 2608-2612.

Lemire,B.D., Robinson,J.J., Bradley,R.D., Scraba,D.G. and Weiner,J.H. (1983) J. Bacteriol. **155**, 391-397.

Lemire,B.D. and Weiner,J.H. (1986) Methods Enzym. **126**,

377-386.

Lemire,B.D., Robinson,J.J. and Weiner,J.H. (1982) J. Bacteriol. **152**, 1126-1131.

Lloyd,D. and Scott,R.I. (1983) Anal. Biochem. **128**, 21-25.

Lloyd,D. and Scott,R.I. (1987) *In* Spectrophotometry and spectrofluorimetry: a practical approach (Harris,D.A. and Bashford,C.L., eds.) pp165-172. IRL Press Ltd.

Lohmeier,E., Hagen,D.S., Dickie,P. and Weiner,J.H. (1981) Can. J. Biochem. **59**, 158-164.

Lorence,R.M., Miller,M.J., Borochov,A., Faiman-Weinberg,R. and Gennis,R.B. (1984) Biochim. Biophys. Acta. **790**, 148-153.

Lorence,R.M., Koland,J.G. and Gennis,R.B. (1986) Biochem. **25**, 2314-2321.

Lorence,R.M., Carter,K., Green,G.N. and Gennis,R.B. (1987) J. Biol. Chem. **262**, 10532-10536.

Lorence,R.M. and Gennis,R.B. (1989) J. Biol. Chem. **264**, 7135-7140.

Lowry,O.H., Rosebrough,N.J., Farr,A.L. and Randall,R.J. (1951) J. Biol. Chem. **193**, 265-275.

Lukat,G.S., Jabro,M.N., Rodgers,K.R. and Goff,H.M. (1988) Biochim. Biophys. Acta. **954**, 265-270.

Macy,J., Probst,I. and Gottschalk,G. (1975) J. Bacteriol. **123**, 436-442.

Malmstrom,B.G. (1982) Ann. Rev. Biochem. **51**, 21-59.

Markossian,K.A., Poghossian,A.A., Paitian,N.A. and Nalbandyan,R.M. (1978) Biochem. Biophys. Res. Comm. **81**, 1336-1343.

Mason,J., Mingos,D.M.P., Schaefer,J., Sherman,D. and Stejskal,E.O. (1985) J. Chem. Soc. Chem. Commun. pp444-446.

McConville,M.L. and Charles,H.P. (1979a) J. Gen. Microbiol. **113**, 155-164.

McConville,M.L. and Charles,H.P. (1979b) J. Gen. Microbiol. **113**, 165-168.

Meinhardt,S.W., Gennis,R.B. and Ohnishi,T. (1986) Biophys. J. **49**, 205.

Meinhardt,S.W., Gennis,R.B. and Ohnishi,T. (1989) Biochim. Biophys. Acta. **975**, 175-184.

Mell,H., Wellnitz,C. and Kroger,A. (1986) Biochim. Biophys. Acta. **852**, 212-221.

Miki,K. and Lin,E.C.C. (1973) J.Bacteriol. **114**, 767-771.

Miki,K. and Lin,E.C.C. (1975) J.Bacteriol. **124**, 1282-1287.

Miller,M.J. and Gennis,R.B. (1983) J. Biol. Chem. **258**, 9159-9165.

Miller,M.J. and Gennis,R.B. (1985) J. Biol. Chem. **260**, 14003-14008.

Miller,M.J., Hermodson,M. and Gennis,R.B. (1988) J. Biol. Chem. **263**, 5235-5240.

Minghetti,K.C. and Gennis,R.B. (1988) Biochem. Biophys. Res. Comm. **155**, 243-248.

Mitchell,R.H., Riedi,P.C. and Robertson,M. (1973) Cryogenics **13**, 492-494.

Mitchell,P. (1976) J. Theor. Biol. **62**, 327-367.

Moodie,A.D. and Ingledew,W.J. (1988) *In* Fifth European Bioenergetics Conference Short Reports, p97. IUB-IUPAB Bioenergetics Groups.

Moodie,A.D. and Ingledew,W.J. (1990) Adv. Micro. Physiol. **31**, in press.

Moodie,A.D., Mitchell,R.H. and Ingledew,W.J. (1990) Anal. Biochem. in press.

Moore,W.J. (1976) *In* Physical Chemistry. Longman, London.

Morningstar,J.E., Johnson,M.K., Cecchini,G., Ackrell,B.A.C. and Kearney,E.B. (1985) J. Biol. Chem. **260**, 13631-13638.

Morse,R.H. and Chan,S.I. (1980) J. Biol. Chem. **255**, 7876-7882.

Muhoberac,B.B. and Wharton,D.C. (1980) J. Biol. Chem. **255**, 8437-8442.

Murakami,H., Kita,K., Oya,H. and Anraku,Y. (1985) FEMS Microbiol. Lett. **30**, 307-311.

Naqui,A., Chance,B. and Cadenas,E. (1986) Ann. Rev. Biochem. **55**, 137-166.

Ohnishi,T., Salerno,J.C., Winter,D.B., Lim,J., Yu,C.A., Yu,L. and King,T.E. (1976a) J. Biol. Chem. **251**, 2094-2104.

Ohnishi,T., Lim,J., Winter,D.B. and King,T.E. (1976b) J. Biol. Chem. **251**, 2105-2109.

Ohnishi,T., Salerno,J.C., Blum,H., Leigh,J.S. and Ingledew,W.J. (1977) *In* Bioenergetics of Membranes (Packer,L., ed.) pp209-216. Elsevier North-Holland Biomedical Press.

Ohnishi,T., King,T.E., Salerno,J.C., Blum,H., Bowyer,J.R. and Maida,T. (1981) J. Biol. Chem. **256**, 5577-5582.

Ohnishi,T. and Salerno,J.C. (1982) *In* Iron-sulfur proteins (Spiro,T.G., ed.) pp285-328, John Wiley & Sons, New York.

Ohnishi,T. (1987) Current Topics in Bioenergetics **15**, 37-65.

Olson,J.S., Ballou,D.P., Palmer,G. and Massey,V. (1974) J. Biol. Chem. **249**, 4363-4382.

Palmer,G. and Beinert,H. (1964) *In* Rapid Mixing and Sampling Techniques in Biochemistry (Chance,B., Eisenhardt,R.H., Gibson,A.H. and Lonberg-Holm,K.K., eds.) pp205-218, Academic Press, New York.

Palmer,G. (1985) Biochem. Soc. Trans. **13**, 548-560.

Poole,R.K. and Chance,B. (1981) J. Gen. Microbiol. **126**, 277-287.

Poole,R.K., Scott,R.I. and Chance,B. (1981) J. Gen.

Microbiol. **125**, 431-438.

Poole,R.K., Sivaram,A., Salmon,I. and Chance,B. (1982a) FEBS Lett. **141**, 237-241.

Poole,R.K., Baines,B.S., Hubbard,J.A.M., Hughes,M.N. and Campbell,N.J. (1982b) FEBS Lett. **150**, 147-150.

Poole,R.K. (1983) Biochim. Biophys. Acta. **726**, 205-243.

Poole,R.K., Kumar,C., Salmon,I. and Chance,B. (1983a) J. Gen. Microbiol. **129**, 1335-1344.

Poole,R.K., Salmon,I. and Chance,B. (1983b) J. Gen. Microbiol. **129**, 1345-1355.

Poole,R.K., Baines,B.S. and Appleby,C.A. (1986) J. Gen. Microbiol. **132**, 1525-1539.

Poole, R.K. and Williams,H.D. (1987) FEBS Lett. **217**, 49-52.

Poole,R.K. and Ingledew,W.J. (1987) In *Escherichia coli* and *Salmonella typhimurium*: Cellular and Molecular Biology (Heidhardt,F.C., Ingraham,J.L., Low,K.B., Magasanik,B., Schaechter,M. and Umbarger,H.E. eds.), Vol.1; pp170-200. American Society of Microbiology. Washington D.C.

Poole,R.K. and Williams,H.D. (1988) FEBS Lett. **231**, 243-246.

Pudek,M.R. and Bragg,P.D. (1974) Arch. Biochem. Biophys. **164**, 682-693.

Pudek,M.R. and Bragg,P.D. (1975) FEBS Lett. **50**, 111-113.

Puustinen,A., Finel,M., Virkki,M. and Wikstrom,M. (1989) FEBS Lett. **249**, 163-167.

Reddy,D., Lancaster,J.R. and Cornforth,D.P. (1983) Science **221**, 769-770.

Reid,G.A. and Ingledew,W.J. (1979) Biochem. J. **182**, 465-472.

Reid,G.A., Haddock,B.A. and Ingledew,W.J. (1981) FEBS Lett. **131**, 346-350.

Rice,C.W. and Hempfling,W.P. (1978) J. Bacteriol. **134**, 115-124.

Robinson,J.J. and Weiner,J.H. (1981) Biochem. J. **199**, 473-477.

Robinson,J.J. and Weiner,J.H. (1982) Can. J. Biochem. **60**, 811-816.

Rothery,R.A., Houston,A.M. and Ingledew,W.J. (1987) J. Gen. Microbiol. **133**, 3247-3255.

Rothery,R.A. (1989) PhD Thesis, University of St.Andrews, U.K.

Rothery,R.A. and Ingledew,W.J. (1989) Biochem. J. **261**, 437-443.

Ruzicka,F.J., Beinert,H., Schepler,K.L., Dunham,W.R. and Sands,R.H. (1975) Proc. Nat. Acad. Sci. USA. **72**, 2886-2890.

Salerno,J.C. and Ohnishi,T. (1976) Biochem. Biophys. Res. Comm. **73**, 833-840.

Salerno,J.C., Harmon,H.J., Blum,H., Leigh,J.S. and Ohnishi,T. (1977) FEBS Lett. **82**, 179-182.

Salerno,J.C. and Ohnishi,T. (1980) Biochem. J. **192**, 769-781.

Salerno,J.C., Bolgiano,B. and Ingledew,W.J. (1989) FEBS Lett. **247**, 101-105.

Salerno,J.C., Bolgiano,B., Poole,R.K., Gennis,R.B. and Ingledew,W.J. (1990) J. Biol. Chem. **265**, 4364-4368.

Sasarman,A., Surdeanu,M., Szegli,G., Horodniceanu,T., Greceanu,V. and Dumitrescu,A. (1968) J. Bacteriol. **96**, 570-572.

Shaw,R.W., Hansen,R.E. and Beinert,H. (1978) Biochim. Biophys. Acta. **504**, 187-199.

Shunk,C.H., Linn,B.O., Wong,E.L., Wittreich,P.E., Robinson,F.M. and Folkers,K. (1958) J. Am. Chem. Soc. **80**, 4752-4753.

Simpkin,D. (1985) PhD Thesis. University of St.Andrews, U.K.

Simpkin,D. and Ingledew,W.J. (1984) J. Gen. Microbiol. **130**, 2851-2855.

Simpkin,D. and Ingledew,W.J. (1985) Biochem. Soc. Trans. **13**, 603-607.

Spain,J.D. (1982) *In* BASIC Microcomputer Models in Biology. Addison-Wesley, London.

Spencer,M.E. and Guest,J.R. (1973) J. Bacteriol. **114**, 563-570.

Spencer,M.E. and Guest,J.R. (1982) J. Bacteriol. **151**, 542-552.

Stevens,T.H. and Chan,S.I. (1981) J. Biol. Chem. **256**, 1069-1071.

Thomson,A.J., Brittain,T., Greenwood,C. and Springall,J.

(1976) FEBS Lett. **67**, 94-98.

Thomson,A.J., Greenwood,C., Gadsby,P.M.A. and Foote,N. (1988) *In* Cytochrome Systems: Molecular Biology and Bioenergetics (Papa,S., Chance,B. & Ernster,L. eds.) pp349-360. Plenum Press, New York.

Timkovich,R., Cork,M.S., Gennis,R.B. and Johnson,P.Y. (1985) J. Am. Chem. Soc. **107**, 6069-6075.

Tsubaki,M., Hiwatashi,A., Ichikawa,Y. and Hori,H. (1987) Biochem. **26**, 4527-4534.

Turner,N.A., Bray,R.C. and Diakun,G.P. (1989) Biochem. J. **260**, 563-571.

Unden,G. and Kroger,A. (1981) Eur. J. Biochem. **120**, 577-584.

Unden,G. and Kroger,A. (1986) Methods Enzym. **126**, 387-399.

Van der Plas,J., Hellingwerf,K.J., Seijen,H.G., Guest,J.R., Weiner,J.H. and Konings,W.N. (1983) J. Bacteriol. **153**, 1027-1037.

Van Hoek,A.N., Van Gaalen,M.C.M., De Vries,S. and Berden,J.A. (1987) Biochim. Biophys. Acta. **892**, 152-161.

Vanngard,T. (1985) Biochem. Soc. Trans. **13**, 619-622.

Von Jagow,G. and Link,T.A. (1986) Methods Enzym. **126**, 253-271.

Wariabharaj,D.S. and Ingledew,W.J. (1987) Biochem. Soc. Trans. **15**, 931-932.

Weiner,J.H. and Dickie,P. (1979) J. Biol. Chem. **254**, 8590-8593.

Weiner,J.H., Lemire,B.D., Elmes,M.L., Bradley,R.D. and Scraba,D.G. (1984) J.Bacteriol. **158**, 590-596.

Weiner,J.H., Cammack,R., Cole,S.T., Condon,C., Honore,N., Lemire,B.D. and Shaw,G. (1986) Proc. Natl. Acad. Sci. USA. **83**, 2056-2060.

Wever,R. and Van Gelder,B.F. (1974) Biochim. Biophys. Acta. **368**, 311-317.

Wever,R., Van Gelder,B.F. and Dervartanian,D.V. (1975) Biochim. Biophys. Acta. **387**, 189-193.

Wikstrom,M., Krab,K. and Saraste,M. (1981) *In* Cytochrome Oxidase, a Synthesis. Academic Press, London.

Wikstrom,M. (1988) *In* Fifth European Bioenergetics Conference Short Reports, pp36-37, IUB-IUPAB Bioenergetics

Group.

Wikstrom,M. (1989) Nature **338**, 776-778.

Williams,R.J.P. (1987) FEBS Lett. **226**, 1-7.

Wilson,D.F., Erecinska,M. and Owen,C.S. (1976) Arch. Biochem. Biophys. **175**, 160-172.

Wong,J.T-F. (1975) *In* Kinetics of Enzyme Mechanisms. Academic Press, London.

Wood,D., Darlison,M.G., Wilde,R.J. and Guest,J.R. (1984) Biochem. J. **222**, 519-534.

Yang,F-D, Yu,L, Yu,C-A, Lorence,R.M. and Gennis,R.B. (1986) J. Biol. Chem. **261**, 14987-14990.

Yonani,T., Yamamoto,H., Erman,J.E., Leigh,J.S. and Reed,G.H. (1972) J. Biol. Chem. **247**, 2447-2455.

Yoshimura,T., Ozaki,T., Shintani,Y. and Watanabe,H. (1979) Arch. Biochem. Biophys. **193**, 301-313.

Yu,C.A. and Yu,L. (1982), Biochem. **21**, 4096-4101.

Yu,L., Xu,J-X., Haley,P.E. and Yu,C-A. (1987) J. Biol. Chem. **262**, 1137-1143.